Theory and Application of Nonlocal Hillslope Sediment Transport

By

Tyler Hill Doane

Dissertation

Submitted to the Faculty of the

Graduate School of Vanderbilt University

in partial fulfillment of the requirements

for the degree of

DOCTOR OF PHILOSOPHY

in

Earth and Environmental Sciences

August 10, 2018

Nashville, Tennessee

Approved:

David J. Furbish, Ph.D

George M. Hornberger, Ph.D.

Erin C. Rericha, Ph.D.

Guilherme A.R. Gualda, Ph.D

DEDICATION

This dissertation is dedicated to all of the unnamed hills.

ACKNOWLEDGMENTS

I first and foremost want to sincerely thank my adviser, David Furbish, for the guidance and support that he provided to me during my graduate career. The ideas presented in this dissertation represent six years of extensive discussions with David and a dramatic evolution of my own thoughts, abilities, and goals. Two particularly important elements of David's advising have been instrumental; the patience with which he advised me and the freedom that he afforded to me for exploration. I am proud of the ideas that I present here, but getting to these ideas required that I open many doors that led very indirectly to this ultimate product. I very much appreciate David's effective mentorship and now I will always consider him a friend and a colleague.

I would like to thank my committee members, Dr. George Hornberger, Dr. Erin Rericha, and Dr. Guilherme Gualda, for constructive advice and encouragement. Courses with Dr. Hornberger and Dr. Gualda were particularly formative for me and have led to interesting discussions over the years. Dr. Rericha provided a valuable opinion from a different perspective than the common foundation of the Earth Sciences.

There are many colleagues, peers, and friends that helped in field work, discussion, experiments, or papers that I wish to recognize. I highly value the opportunities that I had to work with Dr. Josh Roering and Dr. Danica Roth at the University of Oregon and I look forward to continuing collaboration with them. I have been lucky to work closely with Dr. Rina Schumer, whose work I admire. I am grateful to Dr. Amanda Keen-Zebert for help during our field work in California, obtaining OSL dates, and continued support and discussions. I also thank Timothy Watkins, Sarah Sams, and Aiden and Jesse Emilo for helping with data collection that is central to this dissertation.

I sincerely thank all of my peers at Vanderbilt who have become dear friends. The group of people that make up the Vanderbilt EES department and close affiliates have made my time here intellectually rewarding, and equally important, very fun. It was truly a pleasure

to come to work every day largely because of the people. There are too many folks to name all of them individually, but I want to highlight several here. Chris Myers, Scott Worland, Siobhan Fathel, Will Frazier, Austin Royer, Ayla Pamukcu, Moyo Ajayi, Leland Cohen, Michelle Foley, Heather Bemis, Chris Tasich and Chelsea Peters were all central figures in my social and academic life here and made it a very special time for me. I know I am lucky to have such friends.

I want to thank my family for encouraging me to follow this path. For over ten years, they have supported me on this path, humored me by asking questions, and made me proud of my work.

Last I want to thank my partner, Lindsey Grubbs, for being such a constant source of support, the jokes, and giving me the confidence to explore weird and fun ideas.

TABLE OF CONTENTS

LIST OF TABLES

LIST OF FIGURES

Chapter 1

Introduction

Unconsolidated sediment commonly mantles Earth's surface. Steep mechanical, biological, and chemical gradients at the boundary between the geosphere and atmosphere break rock into granular material which forms a soil mantle. The histories, trajectories, and characteristics of soil/sediment particles contain clues to processes of Earth's surface and are the subject of many geological studies. Namely, the soil mantle and the dynamic processes that occur within it are important for atmospheric carbon levels, ground-water hydrology, ecology, and biology. The motion of these sediment/soil particles is one major focus of geomorphology and in this dissertation I explore the characteristics and consequences of quantitative descriptions of sediment transport.

Consider a single grain of sand. One grain of sediment likely has an irregular shape (*Brantley et al.*, 1999) (Figure 1.1A), a number of crystallographic defects, and is composed of a range of elements– some of which are replacement ions. Now consider dropping said grain onto a flat surface. We are concerned with the motion of the particle through time and the final position after one drop. On impact with the surface, the particle will rebound with some velocity according to the coefficient of restitution, at some trajectory and with some angular velocity according to the details of the impulse with the surface. In principle, we could solve Newton's second law for the motion of the particle through time and nearly capture the trajectory of the single grain. However, now consider the trajectories of many particles and over a great number of drops (Figure 1.1B). The complexity of the problem very quickly makes this approach laborious and of limited practical value. A probabilistic approach can be much more productive. That is, a few simple physical constraints can inform a probability distribution of positions that particles are likely to occupy. In this way, we can describe the essence of particle behavior without attempting to describe the details

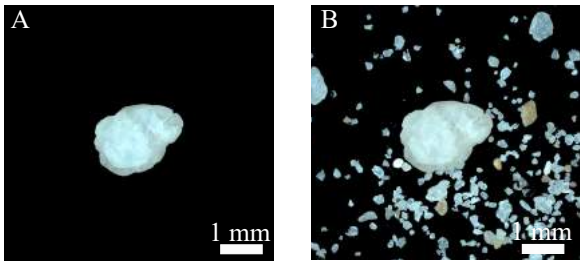

Figure 1.1: Microscope images of a single grain of quartz (A) and multiple grains (B) to highlight the complexity involved in the description of many grains of sediment.

of the trajectories of all particles.

There is a legacy of probabilistic approaches in geomorphology (*Einstein*, 1937; *Sayre and Hubbell*, 1965; *Furbish et al.*, 2009a; *Ancey*, 2010; *Fathel et al.*, 2015, 2016). However, most of these approaches apply to sediment transport in a fluvial setting, where the periods of particle motion and rest occur at timescales short enough for humans to record a great number of observations. Work with regard to hillslopes, where we rarely observe particles in motion, typically does not explicitly involve probabilistic descriptions. Instead, there is a long legacy of transport models that are inherently temporally and spatially averaged formulations (*Ganti et al.*, 2012) that are functions of macroscopic land-surface variables, namely slope (*Culling*, 1963; *Fernandes and Dietrich*, 1997; *Roering et al.*, 1999, 2007). Whereas such models are physically-based and are capable of simulating observed landscape behaviors, the necessary averaging required by such models obscures the details of the transport process (*Furbish et al.*, 2017).

There are many scales at which we can investigate aspects of particle motion. Grain-scale dynamics consider the physics of grain-to-grain interactions (*Furbish et al.*, 2009a; *Ferdowsi et al.*, 2018). The evolution of a cohort of particles reveals the statistical characteristics of particle motions through time (*Schumer et al.*, 2009; *Voepel et al.*, 2013; *Fathel et al.*, 2016; *Furbish et al.*, 2017). Hillslope form and evolution result from the macroscopic relationships between hillslope properties and bulk sediment motion (*Fernandes and Dietrich*, 1997; *Roering et al.*, 1999, 2007). The dynamics of these three different scales

must relate to each other. Here, I explore a range of the scales associated with particle transport and land-surface evolution. Namely, beginning with distributions of single-grain displacements informed by grain-to-grain interactions, the work below explores the consequences of different transport descriptions and behaviors that span scales from particle travel distances to landform and hillslope evolution.

Within the last decade, a growing number of researchers have embraced a nonlocal approach to hillslope sediment transport (*Schumer et al.*, 2009; *Furbish and Haff*, 2010; *Foufoula-Georgiou et al.*, 2010; *Tucker and Bradley*, 2010; *Gabet and Mendoza*, 2012; *Ganti et al.*, 2012; *DiBiase et al.*, 2017). A nonlocal class of models explicitly includes a treatment of sediment particle travel distances, and by doing so allows for particles that began motions "far" away from a position x to pass by position x thereby contributing to the flux. There are several different ways to include nonlocality in a mathematical description; however, perhaps the simplest and most common relies on the probability distribution of particle travel distance. Nonlocal models differ from more common local models, which require the spatial and temporal averaging mentioned above, and state that the flux of sediment beyond a position x is solely dependent on the slope at the position x. It is important to note that the difference between nonlocal and local models is strictly mathematical. There is no physical distinction between the two models because sediment transport demands that particles in transport travel a finite distance – a requirement that nonlocal models explicitly include but is averaged over in local models (*Ganti et al.*, 2012). This is not to diminish the value of local models, which are effective tools for coarse applications of landscape evolution and of the sediment flux, but instead to highlight the mathematical differences that represent the same processes.

The value of a nonlocal formulation lies in the explicit treatment of the transport process while remaining a relatively simple concept – a certain volume of sediment is set in motion over a given area and is subsequently distributed according to a distribution of travel distance. These elements are, in principle, measurable and therefore growing interest in

research is aimed at exploring mathematical expressions of nonlocal transport (*Foufoula-Georgiou et al.*, 2010; *Furbish and Haff*, 2010; *Tucker and Bradley*, 2010; *Ganti et al.*, 2012; *Furbish and Roering*, 2013; *Gabet and Mendoza*, 2012; *Shelef and Hilley*, 2016). However, demonstrating nonlocal transport using natural examples has largely lagged behind the theoretical advances. Two primary goals that motivated the work for this dissertation are to (1) demonstrate nonlocal transport in a natural setting, and (2) identify signatures of nonlocal transport.

1.1 Structure of the Dissertation

I wrote the chapters of this disseratation as stand-alone journal manuscripts. Each chapter has an introduction that sets up the particular relevance of the problem. However, I briefly summarize and connect the chapters here.

The arc of the work presented below begins with a demonstration of nonlocal transport in a natural setting. Because of the inherent difficulty involved with observing a great number of natural sediment particle travel distances on hillslopes, I rely on the long-term evolution of a well-constrained landform to evaluate the performance of a nonlocal model. A suite of moraines that emerge from the eastern front of the Sierra Nevada satisfy this description. I numerically simulate the evolution of moraines according to different mathematical descriptions of transport and evaluate their ability to recreate the observed land-surface form. This chapter reveals three items with regard to hillslope sediment transport. First, I demonstrate that nonlocal transport can match or exceed the performance of local formulations, which had not previously been demonstrated. Second, demonstrating nonlocal transport required that I more thoroughly develop functional forms for the relevant parameters that control sediment transport. We discover that the volumetric entrainment rate may be nonlinearly related to the land-surface slope and a dominant transport process is intermittent release of sediment that is trapped behind sage brush. Last, demonstrating nonlocal transport demands a comparison to local formulations. We are able to show that

mathematical approximations of local and nonlocal formulations can lead to remarkably similar forms and therefore we expect equally similar paths of land-surface evolution. A challenge then is to determine signatures of nonlocal transport, which we suggest are highlighted in a Fourier wavenumber domain representation of land-surface evolution. This finding is reported in the second chapter, but a full treatment of land-surface evolution in wavenumber domain is presented in the third chapter.

Signatures of different hillslope sediment transport models contained in land-surface evolution are subtle. All common hillslope sediment transport formulations contain land-surface slope as a central element and therefore tend to degrade topographic highs and aggrade topographic lows. The details of land-surface evolution, however, do reveal differences. To explore the details, we study land-surface evolution in wavenumber domain via the Fourier transform. We do this for two reasons. First, wavenumber domain effectively highlights coarse and detailed elements of a function, which allows us to focus on only the detailed elements. Second, a nonlocal formulation contains information about characteristic length-scales. The Fourier transform discretizes a signal based on scales and so we suspected that wavenumber domain might reveal unique signatures of nonlocal transport. However, our analysis shows that although a nonlocal formulation results in different wavenumber domain evolution, the major signature that is highlighted in wavenumber domain is the linearity or nonlinearity of the sediment transport model. This chapter reviews theory supporting transport formulations and properties of the Fourier transform, and then applies theory to different well-constrained landforms. We show that, in wavenumber domain, linear diffusion is manifest as vertical decay of the spectrum whereas nonlinear diffusion is represented by compression of the spectrum towards the origin. These are two end-member ways to reduce topographic variance, and land-surface evolution may be composed of both linear and nonlinear processes. The degree of spectral decay or compression reflects the relative magnitude of linear or nonlinear processes respectively.

One of the simplest statements one can make with regard to sediment transport is that

particles are either in a state of motion or rest. A nonlocal formulation explicitly includes a description of the particle travel distance but omits a description of the particle rest times – although it does involve a rate constant that is, in principle, related to the rest time distribution of the ensemble of all particles. The particle-independent quantities of sediment flux and land-surface elevation are insensitive to the quantities that represent individual particles. A description, however, of particle rest times allows for a complete probabilistic description of *particle* transport. When combined, the distributions of particle rest times and travel distances can describe the drift and spread of a cohort of particles (*Voepel et al.*, 2013). A cohort of particles are often referred to as tracer particles and the evolution of a plume of them is a common problem in fluvial settings (*Einstein*, 1937; *Sayre and Hubbell*, 1965; *Nikora et al.*, 2001; *Schumer et al.*, 2009; *Voepel et al.*, 2013; *Bradley*, 2017). However the evolution of tracer particles on hillslopes had not previously been addressed, largely because we are unable to observe natural rest times on hillslopes. This chapter provides a preliminary approach to describing the distribution of particle rest times on hillslopes. The theory builds on that for fluvial settings but makes necessary adjustments. The major contribution of this chapter is to address the impact of temporary dams on the distribution of particle rest times. These dams can be anything that hinder the downslope motion of particles such as shrubs, down trees, or boulders. As they hinder particle motion, wedges of sediment build up behind the dam and particle rest times become longer than they would have otherwise been. This chapter highlights the role of these dams in particle rest time distributions and suggests that they effectively lengthen particle rest times and may cause anomalous particle behavior.

I conducted the work for this dissertation over the past four years. It is by no means comprehensive, but we are able to make some important conclusions and suggestions for future work. I close the dissertation with a look forward. My, oh my! It has been and will be fun!

Chapter 2

Nonlocal sediment transport on steep lateral moraines, eastern Sierra Nevada, California, USA

2.1 Introduction

Recent work on hillslope sediment transport has highlighted the idea that sediment particle travel distance is an important component of the flux (*Michaelides et al.*, 2010; *Lamb et al.*, 2011; *Shelef and Hilley*, 2016; *Carretier et al.*, 2016). In certain settings, transport processes may redistribute sediment over length scales that are long relative to hillslope topographic (e.g., slope) length scales. These situations require nonlocal formulations for the hillslope sediment flux. That is, the flux at a position x [L] is a weighted function of the conditions around x. This class of nonlocal models differs significantly from more common local models that assume particle motions are much smaller than the length scales over which hillslope properties change. Local models suggest that the flux may be described as a function of local conditions at x whereas nonlocal models stipulate that distal conditions contribute to the flux at x. Previous research has focused on the theoretical development of nonlocal descriptions of flux that explicitly include the effect of long-distance particle motions (*Foufoula-Georgiou et al.*, 2010; *Tucker and Bradley*, 2010; *Furbish and Haff*, 2010; *Furbish and Roering*, 2013) and has highlighted the mathematical difference between local and nonlocal models. Existing literature presents compelling reasons to use nonlocal formulations for the hillslope sediment transport. It shows that nonlocal fomulations reproduce steady-state topographic profiles (*Foufoula-Georgiou et al.*, 2010; *Furbish and Haff*, 2010), are theoretically sound, and contain parameters that are physically based and potentially measurable (*Furbish and Roering*, 2013). We augment existing work by demonstrating nonlocal transport and its consequences in a field setting at the hillslope

scale. Demonstrating nonlocal transport requires that we first distinguish between nonlocal and local formulations.

The mathematical distinction between nonlocal and local sediment transport is well-defined. However, a physical distinction may be obscured by the presence of a suite of processes that transport sediment over various length scales (*Furbish and Roering*, 2013). For example, the lengths of disturbance-driven particle motions due to shrink-swell, freeze-thaw cycles and localized bioturbation are on the order of the pore diameters (or perhaps many pore diameters) within the soil column. The lengths of particle motions on the soil surface produced by rain splash are on the order of millimeters to decimeters. These quasi-random motions in the soil column or on its surface result in a bulk downslope motion whose rate is approximately proportional to the local land-surface slope (*Culling*, 1963; *Carson and Kirkby*, 1972; *Fernandes and Dietrich*, 1997; *Jyotsna and Haff*, 1997; *Furbish et al.*, 2009a). In contrast, processes such as dry ravel, shallow landslides, tree throw, patchy surface flows and the activity of fossorial animals may involve transport distances that are on the order of meters if not much longer. This is particularly true in steepland settings where particle transport distances increase (*Gabet et al.*, 2003; *Gabet and Mendoza*, 2012). On any given hillslope, a suite of individual transport mechanisms with different characteristic length scales may compose the aggregate sediment transport. Length scales of particle motions for these processes may blend smoothly or discretely from short (pore scale) to long (many meters), complicating a physical distinction between local and nonlocal transport. Thus, identifying behaviors and characteristics of transport formulations, and their veracity when applied to field conditions, is clouded by the variability of length scales of natural transport processes. In this paper, we overcome this difficulty by evaluating the long-term evolution of geomorphic features.

Directly observing natural sediment transport on hillslopes usually requires being in the right place at the right time, and, except for field-based plot-scale experiments or at instrument-deployed sites, direct measurements of transport are unusual if not impossible

over large areas and timescales. At climate-change and longer timescales, we have no choice but to consider how the time-integrated effects of transport are reflected in land-surface geometry, possibly including additional soil constituents whose behaviors are coupled with surface evolution (*Furbish*, 2003; *Roering et al.*, 2004; *Johnson et al.*, 2014; *Anderson*, 2015). In certain situations, the hillslope form and land-surface evolution may reflect the time-averaged characteristics of transport. We believe this to be the case for our descriptions below of transport and the post-depositional evolution of lateral moraines that emerge from the eastern front of the Sierra Nevada, California, USA. These moraines provide an ideal opportunity to evaluate different transport formulae because they have well-defined ages and initial conditions.

Specifically, we use local linear (*Fernandes and Dietrich*, 1997; *Mudd and Furbish*, 2007), local nonlinear (*Roering et al.*, 1999; *Ouimet et al.*, 2009; *DiBiase et al.*, 2010) and nonlocal (*Furbish and Haff*, 2010; *Furbish and Roering*, 2013) formulations of hillslope sediment transport to numerically simulate the evolution of these steep lateral moraines. The analysis reveals two significant items. First, based on numerical analyses we show that nonlocal models mimic moraine profile evolution with higher fidelity than local, linear diffusion. To our knowledge, this is the first demonstration that documents nonlocal hillslope sediment transport at the hillslope scale using the class of models described below. Nonlocal models match the performance of nonlinear models and we argue that these models share low-order mathematical form, and are therefore expected to perform similarly. We are able to make the first estimates of the numeric values of parameters that are central to the nonlocal formulation and reflect real physical and measurable components of sediment transport. The parametric values we extract are likely specific to the lateral moraines because glacial till contains such a wide range of grain sizes and moraines are entirely composed of unconsolidated sediment. However, so long as the landscape is transport-limited, similar values may apply to the region due to regional climate and ecology. Second, we are able to identify a distinct mathematical behavior of nonlocal and local

nonlinear formulations for sediment transport. In particular, we observe that the evolution of the Fourier transform of the land-surface elevation shows amplification in certain wavenumbers k ($k = 2\pi/L$ where L is the wavelength) for nonlocal and nonlinear models. This differs from the behavior associated with the linear "diffusive" description of the flux normally adopted for convenience in landform/landscape evolution models, which necessarily results in spectral decay of all wavenumbers. In addition we show that simplified versions of nonlocal and nonlinear flux models share mathematical similarities leading to similar behavior under certain conditions.

In section 2 we review the concepts of local linear, local nonlinear and nonlocal sediment transport and we present modifications to formulations suggested by previous authors. Section 3 describes the setting, glacial history and characteristics of the lateral moraines used in the study. In section 4 we focus on numerical methods. Results showing that nonlocal transport effectively accounts for the evolution of the land surface are presented in section 5. Here we also present a basic description of the time-evolution of the Fourier transform of the land-surface elevation. A full treatment of this spectral behavior is beyond the scope of this paper, but the results indicate value in using the evolution of Fourier transforms to clarify key elements of land-surface evolution.

2.2 Theory

2.2.1 Local Linear Transport

For disturbance-driven transport involving relatively short particle motions — whether due to the continual creation and collapse of porosity within the active soil thickness or to surface transport by rain splash — the volumetric flux $q(x)$ [$\mathrm{L}^2\ \mathrm{T}^{-1}$] often is described by a linear, slope-dependent transport model, namely (*Culling*, 1963; *Fernandes and Dietrich*,

1997; *Jyotsna and Haff*, 1997; *Carson and Kirkby*, 1972; *Tucker and Bras*, 1998),

$$q(x) = -D\frac{\mathrm{d}\zeta}{\mathrm{d}x} = -DS\,, \tag{2.1}$$

where ζ [L] is the land-surface elevation, D [$\mathrm{L}^2\ \mathrm{T}^{-1}$] is a diffusivity-like rate constant, and the land-surface slope $S = \mathrm{d}\zeta/\mathrm{d}x$. This is by definition a local formulation of transport. The surface slope S is defined locally at a scale larger than the disturbance-driven motions, and it is assumed that these motions (locally) are uninfluenced by variations in soil or land-surface conditions over distances longer than the scale used to define the slope. The linear slope dependency represents the lowest order effect of gravity in producing a downslope bias in motions of soil particles. Process oriented formulations have confirmed the slope dependency (*Furbish et al.*, 2009a,b; *Anderson*, 2002; *Dunne et al.*, 2010)

2.2.2 Local Nonlinear Transport

There is evidence that the volumetric sediment flux is nonlinearly related to the land-surface slope (*Ouimet et al.*, 2009; *DiBiase et al.*, 2010). For example, *Roering et al.* (1999) developed a nonlinear model with the form,

$$q(x) = -D\frac{S}{1-(|S|/S_c)^2}\,, \tag{2.2}$$

where S_c is a critical slope. As the magnitude of the land-surface slope approaches S_c, the flux q mathematically approaches infinity. The behavior of (2.2) at slopes below S_c is consistent with data of hillslope form (*Roering et al.*, 1999, 2007) and erosion rates. To create a nonlinearly slope-dependent flux, this model partially calls on increasing sediment transport distances involved with small landslides and ravel. However, given that (2.2) is a local function of x, the model does not explicitly include long-distance sediment motions.

Nonetheless, in relation to our comparison below of the nonlinear model (2.2) with non-local formulations of transport, we note that both are motivated by the same idea: on steep

slopes, long-distance motions become a significant component of the flux. As described in the next section, the difference between these models is the treatment of particle motions. In addition, whereas nonlocal models may in principle be adapted to short timescale problems, for example, sediment and nutrient delivery to channels, local nonlinear models effectively account for observed sediment fluxes and topographic configurations when averaged over much longer timescales, and necessarily require spatial averaging of the land-surface slope over scales of 7-10 meters (*Roering et al.*, 2010). We suggest that nonlocal and nonlinear models share key mathematical attributes, namely, that they combine terms that are nonlinear in slope and therefore behave similarly for long timescale applications.

2.2.3 Nonlocal Transport

Several formulations have been proposed to describe nonlocal sediment transport on hillslopes. First, nonlocality can be introduced with a fractional calculus model where a non-integer derivative of a quantity yields a nonlocal dependence (*Foufoula-Georgiou et al.*, 2010). Second, rule-based models that follow particles or parcels of sediment downslope and evaluate a probability of continuing motion based on the local slope conditions result in long-distance motions (*Tucker and Bradley*, 2010). A third model appeals to the sediment entrainment rate and the probability density function (pdf) of travel distance in order to describe the flux (*Furbish and Haff*, 2010; *Furbish and Roering*, 2013). The pdf of travel distance describes the probability that particles move to within a distance r to $r+dr$ from the starting position. In this case the flux at x is a convolution integral-like (*Gilad and Von Hardenberg*, 2006) expression of sediment entrained at all surrounding positions x' weighted by the probability that it travels at least a distance $x-x'=r$, thereby contributing to the flux at x. Mathematically this is expressed as,

$$q(x) = \int_{-\infty}^{x} E(x')R(x-x';x')\,\mathrm{d}x'\,, \tag{2.3}$$

where $E(x')$ [L^3 L^{-2} T^{-1}] is a volumetric entrainment rate, R is a kernel related to the probability density function of $f(r,x')$ of travel distances $r = x - x'$, and x' is an upslope position. On a hillslope where slopes vary as a function x', $R(x-x',x')$ should reflect the increasing probability of long distance motions on steeper slopes (*Gabet and Mendoza*, 2012). The flux then is a unique result of the particular configuration of slopes around x. We use (2.3) as the general formulation for the flux throughout this paper, because the volumetric entrainment rate and a probability density function of particle travel distance are two physically interpretable and potentially measurable components. This approach also complements research that focuses on estimating the particle travel distance of various transport processes (*Gabet*, 2003; *Furbish et al.*, 2009b; *Michaelides et al.*, 2010; *Gabet and Mendoza*, 2012; *DiBiase et al.*, 2017).

Nonlocal hillslope sediment transport models have been primarily developed for transport-limited conditions. However, a particularly appealing characteristic of a flux formulation like (2.3) is that it may be applied to detachment limited conditions as well. In this case, the entrainment rate, E, becomes the rate of detachment as opposed to the entrainment of unconsolidated regolith. In this situation, the functional form of $E(x')$ may be different from what is presented below. Nonetheless the mathematical framework would be the same. Furthermore, similar transport theories may apply to fluvial sediment transport (*Parker et al.*, 2000; *Furbish et al.*, 2012; *Martin et al.*, 2012; *Fathel et al.*, 2015; *Heyman et al.*, 2016). Therefore, this type of description of the flux opens opportunities to examine commonalities between transport on hillslopes and in rivers.

2.2.3.1 Entrainment Rate

The entrainment rate E [L^3 L^{-2} T^{-1}] represents a volume of sediment set in motion per unit area during a time interval dt. There are likely different and valid functional forms for $E(x')$ that reflect natural entrainment processes. For example, entrainment by rainsplash is uniform when averaged over long times relative to a shifting ground cover. In contrast, the

incidence of tree throw may increase with increasing slope (*Hellmer et al.*, 2015), which implies a slope dependency in the entrainment rate. A general functional description of the entrainment rate is

$$E(x') = E_0 + E_1|S|^{\alpha}, \tag{2.4}$$

where E_0 [L^3 L^{-2} T^{-1}] is a uniform background entrainment rate and E_1 [L^3 L^{-2} T^{-1} is a slope-modulated term. For simplicity, Furbish and Haff [2010] set $\alpha = 1$. Here, we explore the possibility that $\alpha \neq 1$.

For the analyses presented below, we set $E_0 = 0.001$ m yr^{-1} as a constant in order to limit the fitting of parameters, and then appeal to previous work suggesting that E_1 is larger (*Furbish and Haff*, 2010). Setting $E_0 = 0.001$ m yr^{-1} is based on the amount of degradation at the ridge top. Over the 40 ka of evolution, this value of E_0 suggests that 40 m of material has been entrained. However, the bulk of that material remains at the ridge. We expect that E_0 may vary from 0.001 m yr^{-1}, however, we think that we are within an order of magnitude of the actual value because lowering due to the divergence of the flux at the ridge is necessarily less than 40 m. If E_0 is too low, then the value of E_1 can largely make up the difference on sloped terrain. If the value of E_0 is too large, then E_1 can not counteract the excess flux. Therefore, we think a value of 0.001 m yr^{-1} is a conservative estimate. Furthermore, insofar as this paper is aimed at demonstrating nonlocal transport from land-surface form and E_0 is a constant regardless of profile form, fitting this quantity as a free parameter adds little or no insight to the behavior of the moraine surface. That is, the value of E_0 has little impact on the form of the evolving moraine, although it does influence the magnitude of the flux, and therefore will influence the magnitude of other parameters that we fit. We must interpret the parametric values as being influenced by our choice of values for E_0.

The motivation for a nonlinear functional form for $E(x')$ comes from the observation that obstacles on hillslopes both trap and route sediment downslope (*Furbish et al.*, 2009b; *DiBiase and Lamb*, 2013; *Lamb et al.*, 2013) (Figure 2.1). These are essentially no-flux

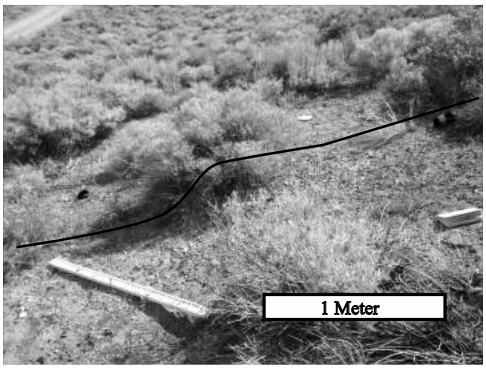

Figure 2.1: Image of shrub showing its behavior as a sediment capacitor with upslope sediment storage and over-steepened downslope side. The black line represents a trace of the land-surface.

obstacles where sediment accumulates on the upslope side and is eroded from the downslope side. This has the important effect of over-steepening the land-surface immediately downslope of the obstacle. We suggest that when the obstacles are removed, the trapped sediment is available for transport and ravels downslope (*DiBiase and Lamb*, 2013). The volume of sediment that is released depends on the volume of sediment that is trapped in a wedge upslope of the over-steepened portion (Figure 2.2). Immediately below an obstacle we typically observe a minor depression that would act to locally disentrain sediment. However, the depressions are often small in comparison to the mounds that form upslope. Furthermore, disentrainment does not bear on the volume of entrained sediment. This is only one mechanism for producing a nonlinear relationship between entrained sediment volume and land-surface slope and we expect that there are likely many processes (i.e. (*Michaelides and Martin*, 2012)) that share this type of relationship.

To obtain a functional form of E for this process we approximate the volume of the over-steepened wedge in relation to the land-surface slope. To do so, we approximate the flux near a downslope no-flux obstacle with linear diffusion, which produces an over-steepened surface. Linear diffusion is used here purely for illustration purposes to generate mounds that resemble those observed in the field. We do not suggest that sediment transport is en-

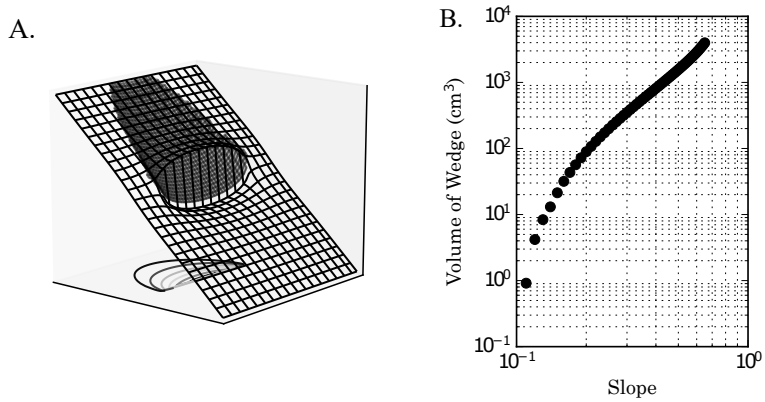

Figure 2.2: Schematic diagram showing how the volume of entrained material increases nonlinearly with slope. Contour lines (A) show the thickness of the wedge of sediment available for ravel, with calculations of the volume entrained as a function of slope (B).

tirely described by (2.1). We then define a three-dimensional wedge with a bottom surface that extends from the base of the over-steepened step up-slope to the land-surface and is inclined at the angle of repose (Figure 2.2A). Results from this simulation show a nonlinear relationship between the entrained volume and the land-surface slope (Figure 2.2B) (*Putkonen et al.*, 2012). The volume-slope relationship represents an idealized case whereas in reality mound geometry varies, and we expect some deviation from the relationship presented in Figure 2.2B. Nonetheless we suggest that this analysis captures the nonlinearity of the relationship, which is central in determining the functional form of $E(x)$. For slopes between 0.1 and 0.7, the entrained volume appears to be well-approximated by a power relationship somewhere between S^2 and S^3. For simplicity, we use a squared relationship,

$$E(x') = E_0 + E_1 |S(x')|^2 , \tag{2.5}$$

where E_1 represents effects of obstacle density and removal rate. E_0 represents the rate of entrainment due to slope independent processes such as rain-splash or lofting due to freeze-thaw. Here we assume that obstacles are uniformly distributed and their mean duration is constant. Therefore, obstacle removal rate in E_1 sets the time-scale and gives it the

dimensions [L T^{-1}].

Building sediment capacitors requires a sufficient amount of time for the obstacle to accumulate sediment. The early evolution of the moraine in this case, then, had some spin-up time during which the initial capacitors were constructed. The timescale for capacitor construction is much shorter than that for the moraine evolution and is insignificant in terms of land-surface morphology. The spin-up time may become significant for small landforms where capacitors are relatively large.

The capacitors at our field site are Sage brush. We note that the argument above is specific to the idea of storage and release of sediment by shrubs, while acknowledging the possibility of a changing ecology and climate during the period of moraine evolution (*Mensing*, 2001). Nonetheless, we speculate that this period, except immediately following glacier recession, likely involved the continuing occurrence of vegetation with similar effects on transport. Furthermore, we suggest that vegetative sediment capacitors is one mechanism for a nonlinear formulation of E with slope, although there may be other processes with nonlinearly slope-dependent entrainment rates. With this uncertainty, we must view the fitting of moraine profiles in relation to the nonlocal formulation of transport as an hypothesis, and we note that the model testing described below includes a linearly and nonlinearly slope-dependent form for E.

2.2.3.2 Travel Distance

The kernel-like term in (2.3), $R(x-x',x')$, is the survival function of the pdf $f(r,x')$, where $R = 1 - \int_0^r f(r,x')\,\mathrm{d}r$. Previous research (*Furbish and Haff*, 2010; *Furbish and Roering*, 2013) has used an exponential pdf for several reasons. First, comprehensive empirical data that reflects travel distances of the suite of processes that might occur on hillslopes is limited. However, we heuristically imagine that most particles move short distances while a few will travel far — a general behavior captured by exponential functions. We note that power-law functions share this behavior and we address this below. Second, exponential

distributions have simple expressions for their statistical moments, which has proven useful in approximating nonlocal behavior in advection-diffusion form (*Furbish and Haff*, 2010). In contrast, power-law distributions often have undefined statistical moments. Third, an exponential distribution reflects the notion that arresting a particle in motion is a Poisson process where over any interval of space, particles in motion have constant probability of stopping. Rock-drop experiments show that travel distances are distributed exponentially and that a friction model performs well in simplified conditions (*Kirkby and Statham*, 1975; *Gabet and Mendoza*, 2012; *DiBiase et al.*, 2017). This idea leads to the conceptualization of a decay constant (e.g., the mean of an exponential distribution) which we recast as a spatial disentrainment rate that describes the proportion of sediment that stops over a given distance. This allows us to begin with a physically based although simple conceptualization of the bulk motion of sediment.

Previous authors have suggested that kernels with exponential forms result in landscape evolution that is consistent with local linear diffusion (*Foufoula-Georgiou et al.*, 2010). Whereas this analysis is correct for uniform kernels, the flexibility offered in (2.3) can result in unique nonlocal behaviors while using exponential distributions of travel distance. Including the function $E(x')$ in (2.3) also leads to unique behavior. That is, the volumetric entrainment rate and the mean particle travel distance can vary as a function of land-surface conditions, which leads to unique behaviors using an exponential pdf for travel distance. The flux in this case becomes a linear combination (exponential weighting by $R(x-x',x')$) of surrounding values for the volumetric entrainment rate ($E(x')$). We also suggest that although under certain conditions exponential kernels lead to behaviors described by local transport, (2.3) explicitly relates sediment contributions from different locations on a hillslope and is inherently nonlocal.

The concept of disentrainment is treated in previous research (*Furbish and Roering*, 2013); however, we briefly outline the physical interpretation here. Generally, disentrainment describes the probability that a particle or portion of sediment set in motion at x' at

time t moves to an interval $r = x - x'$ to $r + \mathrm{d}r = x - x' + \mathrm{d}x$ at time $t + \mathrm{d}t$. This rate does not define the particular path taken by each particle or proportion of the entrained volume. Rather, particles may take any number of motions to get to $x = x' + r$ at $t + \mathrm{d}t$. This concept reflects the notion that there may be a suite of processes transporting particles downslope and that a single particle may experience motion due to any number of processes several times during the interval $\mathrm{d}t$. This simplifies the problem into a purely probabilistic one in which the pdf of travel distance simply represents the distribution of particle positions after a given time $\mathrm{d}t$. By allowing for the possibility of particle travel distance to be a result of multiple hops we are in effect considering a discrete process. However the mathematics that we use are continuous in time and space. For this reason the entrainment rate and pdf of particle travel distance must be time-averaged quantities (*Furbish and Haff*, 2010; *Furbish et al.*, 2012), such that the pdf of travel distances represents a distribution of transition probabilities associated with the interval $\mathrm{d}t$.

The development of a disentrainment rate is based on two ideas common in hillslope sediment transport. First, empirical data suggest that particle transport distances increase on steeper slopes for a host of processes (*Gabet et al.*, 2003; *Furbish et al.*, 2009b; *Dunne et al.*, 2010; *Gabet and Mendoza*, 2012). Second, hillslope sediment flux nonlinearly increases as land-surface slopes approach a critical slope, S_l (*Roering et al.*, 1999; *Ouimet et al.*, 2009; *DiBiase et al.*, 2010). This implies that the sediment particle travel distance nonlinearly increases with slope, or the spatial disentrainment rate nonlinearly approaches zero. Combining these constraints we can describe a disentrainment rate, $P(x')$ [L^{-1}], that is slope-dependent and goes to zero when $|S| \to S_l$,

$$P(x') = \frac{1}{\lambda_0}\left[\frac{2S_l}{S_l - S(x')} - 1\right] \quad -S_l < S < 0\,, \tag{2.6}$$

where λ_0 is a characteristic length scale and $S(x')$ is the local land-surface slope which carries sign. In this case, S_l represents the slope at which particle motions continue indefi-

nitely, and differs from the definition of the critical slope S_c which is the slope at which the flux becomes unbounded. When $S \to S_l$, the flux is simply the entirety of what is entrained, and therefore the flux does not approach infinity. So long as $S << S_l$, the actual value of S_l has little impact on the flux values calculated. The mean travel distance is $1/P(x')$, which has a nonlinear relationship with slope and is consistent with experimental results of particle travel distances (*Gabet and Mendoza*, 2012). For an exponential pdf of travel distances,

$$f(x-x',x') = \frac{1}{\lambda_0}\left[\frac{2S_l}{S_l - S(x')} - 1\right] e^{-\frac{x-x'}{\lambda_0}\left[\frac{2S_l}{S_l - S(x')} - 1\right]}. \tag{2.7}$$

Using the relationship between f and R we get

$$R(x-x',x') = 1 - \int_0^x f(x-x',x')\mathrm{d}x' = e^{-\frac{x-x'}{\lambda_0}\left[\frac{2S_l}{S_l - S(x')}\right]}, \tag{2.8}$$

which describes the probability of sediment traveling at least a distance $x - x'$ such that it contributes to the flux at x. Inserting (2.8) for $E(x')$ into (2.3), we obtain the flux in the positive x direction

$$q_p(x) = \int_{-\infty}^{x} \left[E_0 + E_1|S(x')|^{\alpha}\right] e^{-\frac{x-x'}{\lambda_0}\left[\frac{2S_l}{S_l - S(x')}\right]} \mathrm{d}x', \tag{2.9}$$

This expression represents the downslope component of the flux; however, there is a possibility that the net flux will involve an upslope component.

2.2.3.3 Bi-directional motions

Processes such as rainsplash (*Furbish et al.*, 2009b; *Dunne et al.*, 2010) and transport due to fossorial animals (*Gabet et al.*, 2000, 2003) distribute sediment both downslope and upslope. The proportion, p, of downslope transport and the proportion, n, of upslope

transport may be specified by

$$
\begin{aligned}
p(x') &= \tfrac{1}{2}\left[1 - \tfrac{S(x')}{S_p}\right] \qquad -S_p \le S \le S_p \\
p(x') &= 1 \qquad -S > S_p \\
p(x') &= 0 \qquad -S < -S_p \\
n(x') &= 1 - p(x'),
\end{aligned}
\tag{2.10}
$$

where S_p is a threshold slope magnitude above which all sediment moves in the same direction. The flux in the negative direction involves convolving the negative-bound portion of entrained sediment with the survival function,

$$
q_n(x) = \int_{\infty}^{x} n(x')E(x')e^{-\frac{x'-x}{\lambda_0}\left[\frac{2S_l}{S_l+S(x')}-1\right]}\,\mathrm{d}x'. \tag{2.11}
$$

The total flux is the sum of positive and negative contributions

$$
q(x) = \int_{-\infty}^{x} p(x')E(x')e^{-\frac{x-x'}{\lambda_0}\left[\frac{2S_l}{S_l-S(x')}-1\right]}\,\mathrm{d}x' + \int_{x}^{\infty} n(x')E(x')e^{\frac{x'-x}{\lambda_0}\left[\frac{2S_l}{S_l+S(x')}-1\right]}\,\mathrm{d}x'. \tag{2.12}
$$

The net flux according to (2.12) on a flat surface is zero as positive and negative motions cancel each other. As slopes steepen, downslope motions make up a larger component of the entrained volume and travel distances increase (Figure 2.3).

Although the downslope component of the flux is expected to dominate at our field site, the presence of an upslope component changes the slope-dependency. That is, the slope dependency of n and p, which contain $S(x')$, adds another slope-dependent term. Therefore, the impact of the upslope flux, although small, may be observed in hillslope form. We expect this to be particularly true on low-angle slopes, or at ridge-tops where the magnitude of concavity is large.

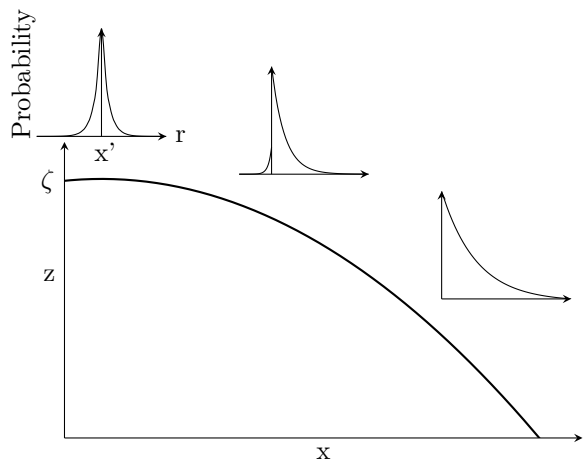

Figure 2.3: Schematic diagram of a hillslope profile $\zeta(x)$ showing the partitioning of positive and negative motions starting from a position x' and how the probability density function of particle travel distances r changes as a function of local slope.

2.3 Moraine Evolution

Moraines can be useful landforms for testing sediment transport formulations because they have a well-constrained initial condition (*Putkonen et al.*, 2008) and their depositional ages are estimated from exposure-age dating techniques. This allows us to use a specified model, starting from the initial condition, to simulate the evolution of the moraine over its age. The outputs of these numerical models can be compared with the observed condition to evaluate the performance of sediment transport formulations.

We focus on the evolution of the interior of lateral moraines because they are better preserved than terminal moraines which are often degraded by fluvial processes. Although there is some uncertainty with regard to the depositional age of moraines, typical age ranges of thousands of years (*Rood et al.*, 2011) do not significantly affect the results and implications presented below. The general evolution of a lateral moraine is as follows. While the associated glacier is active, the lateral moraine is buttressed by the ice that it contains, which allows for the interior side to oversteepen. Following the retreat of the glacier, the moraine quickly relaxes to the angle of repose, which for glacial till is ~ 0.67 (*Putkonen et al.*, 2008). We assign the exposure-age of the moraine to this condition and numeri-

cally simulate the subsequent evolution of the moraine by the proposed sediment transport formula.

The moraines on the east side of the Sierra Nevada, California, are particularly well-suited for this type of study for several reasons. First, they often emerge from the mountain front and are deposited in the adjacent basins. This configuration allows for moraines to be completely unconfined and the form is not conditioned by the geometry of valley walls or floors. Therefore, the form of the moraine is only a result of the initial condition, its age, and sediment transport. Second, the glacial chronology of this region is well studied (*Schaefer et al.*, 2006; *Phillips et al.*, 2009; *Rood et al.*, 2011), which provides estimates for the ages of deposition. Third, these moraines have large side-slope lengths of $\sim$120 m, which we may assume is much larger than typical sediment particle displacements. A great number of particle displacements are responsible for the observed moraine form; thus large moraines represent a greater "sampling" of particle motions than smaller landforms.

The moraines on the eastern side of the Sierra Nevada record a suite of glacial advances and retreats. Last Glacial Maximum advances are represented by the Tioga (14-25 ka) (*Kaufman et al.*, 2003) moraines and penultimate glaciations are represented by the Mono Basin (92-119 ka (*Phillips et al.*, 1990) or 60-80 ka (*Kaufman et al.*, 2003)) moraines. Between these two major glaciations is the Tahoe glaciation (42-50 ka) (*Kaufman et al.*, 2003). For the purpose of this paper we specify an age for the Tahoe glaciation as 40 ka. For simplicity, we present the results from the youngest age estimate. We recognize that many authors suggest older ages for the Tahoe glaciation. Modeling results using 40 ka and 50 ka for initial conditions do not change the fit of models nor do parameters change significantly. Here we look at the post-glacial evolution of Tioga 3 and Tahoe lateral moraines that emerge from Bloody Canyon. Both are well preserved (Figure 2.4). The late Pleistocene glaciers in Bloody Canyon sourced granites and metasedimentary rocks in the Sierra Nevada to the west. The glacial till composed of these materials, particularly the granite clasts, weather into residual sand and gravel (Figure 2.1). Such coarse materials

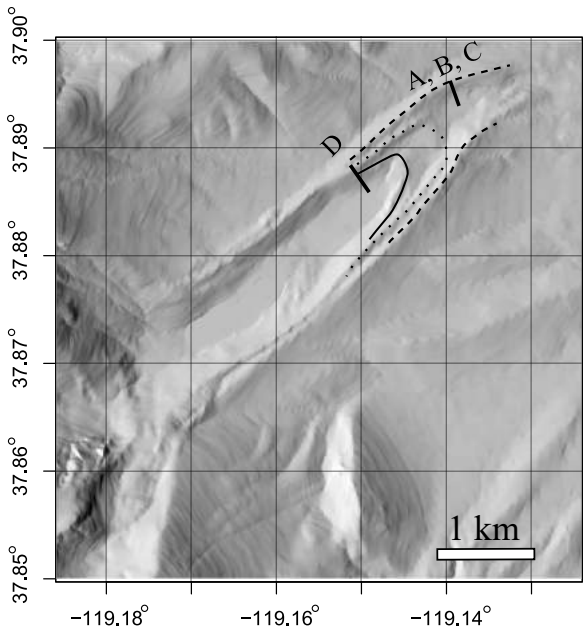

Figure 2.4: Hillshade image of Bloody Canyon, California with traces of Tahoe (40 ka, dashed line (*Schaefer et al.*, 2006; *Kaufman et al.*, 2003)), Tioga 1 (25 ka, dotted line (*Kaufman et al.*, 2003)), and Tioga 3 (18 ka, solid line (*Morgan and Putkonen*, 2012; *Rood et al.*, 2011)). Locations and orientations of profiles A, B, C and D are shown.

have high infiltration rates and concentrated overland flow and ponding of water on the surface is likely rare. Furthermore, because the moraines are composed entirely of porous unconsolidated sediment, there is no perched water table. These characteristics suggest that any localized surface flows are stochastic in space and time, thereby reducing the opportunity for concentrated rilling or incision. As such, the surfaces have remained relatively planar, which justifies a one-dimensional application of the numerical simulations. Planar surfaces are observed on all moraines, including those dated as Mono Basin (92-119 ka), which suggests that the moraines remain well-drained as they evolve.

A simple but significant observation is that the concentration of boulders changes as a function of position. Boulder concentration is high near the crest and approaches zero in the depositional apron of the moraine (Figure 2.5). In the apron we note that the surface is composed almost entirely of grusified gravels and sand that were presumably transported to the depositional apron. The boulders represent a coarse lag left behind as more mobile,

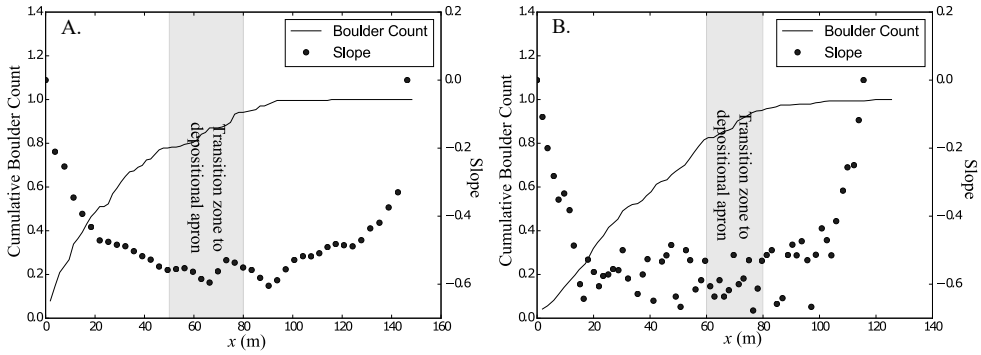

Figure 2.5: Plot of cumulative boulder count (lines) and surface slope slope (dots) as a function of horizontal position for profile C (A) and profile D (B). The depositional apron begins where the rate of boulder accumulation decreases.

finer-grained material moved downslope, such that with time the exposed boulder density increases at the crest and decreases near the toe (*Putkonen et al.*, 2008). The presence of this lag and accompanying apron provides evidence that sediment transport occurs primarily over the surface of the moraine. Particles at the surface move when a disturbance occurs with sufficient energy to displace them. Disturbances with energy sufficient to move grains of sand and gravel occur far more frequently than those capable of moving boulders, and as such, finer material is moved downslope quickly, leaving behind a boulder lag. Although surface motions do not imply a certain transport formula, such motions are a requirement for nonlocal transport, as long-distance motions only occur on the surface. Consequently, we would expect to see a signature of nonlocal transport in this setting. We note that this may suggest an armoring effect during the evolution of the moraine, and we address this in the discussion in the context of nonlocal transport.

2.4 Methods

2.4.1 Field Methods

Using a self-leveling transit, we collected a high-resolution (2-3 m) topographic profile along the path of steepest descent down the interior flanks of the lateral moraines. At two

to three meter intervals, we sampled at or above the typical spacing of sagebrush which dominates the ecology of the area. As described above, the shrubs act as sediment capacitors (*Furbish et al.*, 2009b; *Lamb et al.*, 2011, 2013) and locally add roughness elements to the land surface. Because our study is focused on the large-scale form of the moraine, we limited our sampling interval to the spacing of shrubs to avoid resolving roughness elements with greater detail. For each survey, we extended the profile from several meters down the exterior side of the crestline to several meters along the flat interior valley. In addition to collecting topographic data we also collected a count of boulders exposed on the surface as a function of downslope position. We conducted a high resolution count of boulders that were 25 cm or greater in diameter within 2×4 meter areas positioned along the profile. The boulder surveys were conducted along profile C (Tahoe) and D (Tioga 3). Profile C was collected for the purpose of a boulder survey so the resolution is coarser and the toe of the moraine is incompletely sampled. Nonetheless we include this profile in our analysis.

2.4.2 Numerical Methods

To evaluate local and nonlocal models of hillslope sediment transport, we have written three numerical procedures that simulate the evolution of moraines from their initial condition (slope at 0.67 (*Putkonen et al.*, 2008)) according to (2.1), (2.2), or (2.3). The models simulate the evolution of moraines over their specified ages and outputs are compared with observed moraine forms. Due to the mathematical distinction between local and nonlocal models, the numerical procedures differ significantly.

2.4.2.1 Surface evolution according to local linear transport

To evaluate the changing surface elevation, we substitute (2.1) into the Exner equation to obtain

$$\frac{\partial \zeta}{\partial t} = D \frac{\partial^2 \zeta}{\partial x^2} \,, \tag{2.13}$$

which is the familiar diffusion equation. Systems that evolve according to (2.13) are common in nature and the mathematical treatment of this problem is extensive (*Carslaw and Jaeger*, 1959; *Fernandes and Dietrich*, 1997; *Mudd and Furbish*, 2007; *Hornberger and Wiberg*, 2013). The evolution of a moraine is a transient problem with a no-flux boundary at the crest and a long flat run-out in the interior valley floor. This problem may be simulated in two ways. The evolution may be modeled by iteratively calculating the change in elevation according to (2.13) through finite-differencing with proper treatment at the boundaries. Alternatively, we may analytically solve the evolution of the land-surface in the wave number domain through time using a Fourier transform. The evolution of the Fourier transform of a linearly diffusing land-surface has an analytical solution (*Carslaw and Jaeger*, 1959; *Schumer et al.*, 2009),

$$Z(k,t) = Z(k,0)e^{-k^2Dt}, \tag{2.14}$$

where $Z(k)$ is the Fourier transform of the land-surface elevation, k is the wave number ($2\pi/L$ where L is wavelength), and t is time. Using this analytic expression allows us to compare modeled profiles and observed profiles directly with the specified moraine age without iterating through time steps. In order to satisfy the boundary conditions, we reflect the interior side of the moraine such that the slope at the crest remains zero.

We use (2.14) to find the value of D that produces the best fit between modeled and observed moraine forms. To quantify the fit, we define a cost function as the sum of squared differences between modeled and observed Fourier transforms of the moraine surface,

$$C_f(D) = \sum_{i=1}^{N} [Z_m(k) - Z_o(k)]^2, \tag{2.15}$$

where Z_m and Z_o are the Fourier transforms of the modeled and observed land surfaces respectively. We then use a Gauss-Newton iteration scheme to find the value of D that minimizes (2.15). Because (2.15) is a function of one variable and it is a quadratic, the

solution that we iteratively determine is a global minimum and is necessarily the best-fit solution.

We note that over timescales of 10 ka or more, values of D are likely to vary as climate changes (*Hughes et al.*, 2009; *McGuire et al.*, 2014; *Madoff and Putkonen*, 2016). At this time, however, we do not have information to justify choices of D through time. Furthermore, we demonstrate in Appendix 0.1 that, in the absence of external boundary forcing, the form of the land surface only reflects the time-averaged diffusivity. In this sense, the form of a moraine undergoing linear diffusion expresses no memory of changes in climate as might be reflected in changing diffusivity values.

2.4.2.2 Surface evolution according to local nonlinear transport

To numerically simulate the evolution of the moraine profiles according to a nonlinear flux formulation requires an iterative, finite-difference approach. To do so, we use Equation 9 in Roering et al. (1999), which places (2.2) into continuity. To identify the best-fit parameter, D, for this model, we simulate the evolution of the moraine profile over the specified age. We compare the modeled profile to the observed to obtain a misfit, which is used by a Gauss-Newton iteration scheme to pick a new value for D that minimizes the misfit. We note that S_c is also a tunable parameter, however, to avoid fitting too many parameters, we test $S_c = 0.8$ and $S_c = 1.2$, which represent two extreme possibilities.

2.4.2.3 Surface evolution according to nonlocal transport

The mathematical form of (2.3) is more complex than a local expression and we are unaware of an analytical solution such as (2.14). Therefore, modeling the evolution of a feature as a consequence of a convolution-like flux description is an iterative procedure. Note that the kernel in (2.3) varies with position so that the integral form of the flux is not a true convolution. This characteristic precludes us from making use of the convolution theorem for Fourier transforms which would significantly reduce the computational complexity.

To find the best-fit parameters for a nonlocal formulation we numerically simulate the complete evolution of the moraine many times until the solution approaches a minimum of a cost surface, $C(E_1, \lambda_0)$. To make this process reasonable in terms of computational time, we developed a rapid algorithm to calculate the flux. To numerically encode (2.3) can require integrating over the entire $2N$ domain if there are positive and negative components to the flux. This results in an algorithm whose complexity is $\mathscr{O}[2N^2]$ and is an inherently slow computational process. For large domains, this makes the brute-force method for calculating the flux slow. However, we follow a procedure (*Gilad and Von Hardenberg*, 2006) that can turn (2.3) into a true convolution by approximating the kernel.

The basic premise of the method is that the kernel function $R(x-x',x')$ is approximated by the sum of a series of N_l functions of the same form as $R(x-x',x')$, each weighted uniquely. The weights change as a function of position, thereby placing the spatial dependency of $R(x-x',x')$ on the weighting functions $w(x')$. This allows us to write

$$q(x) \approx \sum_{l=1}^{N_l} \int_0^x \kappa(x-x';\phi_l) w_l(x') E(x')\, \mathrm{d}x' \,, \tag{2.16}$$

where $w_l(\phi, x')$ is a function that weights the approximating kernel $\kappa(x-x';\phi_l)$, ϕ is the actual value of the parameter in the kernel, and ϕ_l is the value of the parameter in the approximating kernels. We can then divide (2.16) up into $h_l(x') = w_l(x')E(x')$ and $g_l = \kappa(x-x';\phi_l)$ so that

$$q(x) \approx \sum_{l=1}^{N_l} h_l * g_l \,. \tag{2.17}$$

The convolution theorem for Fourier transforms can be applied to (2.17), as this is now in the form of a proper convolution. Upon inspection, the approximation of the flux produces nearly identical results as when (2.3) is encoded directly. The computational complexity of this process is $\mathscr{O}[N_l N \log(N)]$, which for large domains is much smaller than the direct method.

An efficient algorithm that determines the surface evolution makes an iterative cost

function minimization procedure possible. To find the set of parameters that minimizes $C_N(E_1, \lambda_0) = \sum(\zeta_i - z_i)^2$, we use a Levenberg-Marquadt descent procedure which marches down the cost-function surface until it reaches a minimum (Figure 2.6). In this case, the cost function is a nonlinear function of two variables, E_1 and λ_0, which could create local minima that would incorrectly identify the best-fit set of parameters. However, from observation we see that, for a variety of initial values of parameters, the Levenberg-Marquadt algorithm consistently leads to a similar minimum, which suggests that it is a global minimum (Figure 2.6) and that the results represent the best-fit parameters. The Levenberg-Marquardt algorithm fit only values for E_1 and λ_0 and kept the choice of $E_0 = 0.001$ constant.

We also did not parameterize S_l, although it is a tunable parameter in P. For slopes significantly less than S_l, λ_0 is the dominant variable determining the mean particle travel distance, and therefore the flux. The presence of soil or regolith in transport-limited regimes suggests that the land-surface slope is well below the limiting slope, on which particles continue to travel indefinitely. Therefore, we may assume that S_l is significantly larger than slopes on the moraine surface such that errors associated with variations in the choice of S_l are relatively small.

We test three different nonlocal formulations against the surface evolution of lateral moraines. Case I is a nonlocal formulation with linearly slope-dependent entrainment and a downslope flux only. Case II has a linearly slope-dependent entrainment rate but with both upslope and downslope fluxes. Case III has a slope-squared dependency for entrainment and only downslope flux.

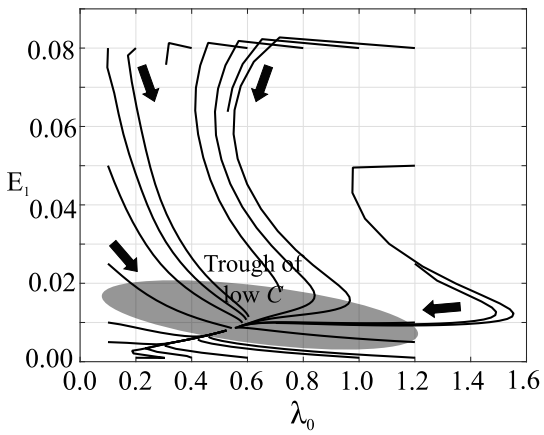

Figure 2.6: Two-dimensional plot showing the trajectory of parameters chosen by the Levenberg-Marquardt algorithm. All model runs started with initial parameteric values at the edge of the plot and iteratively march along the lines shown until the minimum is approached as denoted by the gray region. The common stopping place shared by all model runs suggests that the parameters presented here are the best-fit parameters and not a local minima.

2.5 Results

2.5.1 Model Performance

We have tested six different transport models here, three of which are members of the nonlocal class but have either different functional forms for $E_1(x')$ or contain upslope and downslope contributions to the flux. Each of these models has two adjustable parameters, E_1 and λ_0, which are determined by the Levenberg-Marquadt procedure outlined above. In contrast, linear and nonlinear diffusion have only one free parameter, D (recall we test two separate values for S_c for nonlinear models).

Results from numerical experiments are summarized in Table 2.1. Nonlocal models more accurately predict profile forms than local linear diffusion as measured by the cost function. In general, nonlocal transport results in a cost, C_f, that is at least half of that generated by local linear models; however there is quite a bit of variation within the performance of nonlocal models themselves. Nonlocal models that contain positive and negative components of the hillslope sediment flux (Case II) are the worst-performing of the three

Table 2.1: Table of best-fit parameters and sum of squared differences for each profile as a result of nonlocal, local linear diffusion, and local nonlinear diffusion.

Profile	**A**	**B**	**C**	**D**
Age (ka)	~ 40	~ 40	~ 40	18
Nonlocal Positive Flux Only				
$\sum(z-\zeta)^2$	129.00	64.99	127.33	83.22
E_1	0.005	0.0038	0.0042	0.0036
λ_0	0.65	0.75	0.57	0.61
Nonlocal Positive and Negative Flux				
$\sum(z-\zeta)^2$	184.81	115.63	199.16	121.50
E_1	0.0037	0.0028	0.0025	0.0022
λ_0	0.70	0.78	0.68	0.76
Nonlocal Positive Flux with $E = E_0 + E_1 S^2$				
$\sum(z-\zeta)^2$	39.44	10.64	52.80	63.92
E_1	0.014	0.011	0.01	0.01
λ_0	0.32	0.37	0.30	0.40

Profile	**A**	**B**	**C**	**D**
Age (ka)	$\sim$40	$\sim$40	$\sim$40	$\sim$18
Linear diffusion				
$\sum(z-\zeta)^2$	385.80	320.44	329.00	184.5
D	0.015	0.013	0.012	0.01
Nonlinear diffusion with $S_c = 1.2$				
$\sum(z-\zeta)^2$	179.27	119.70	157.27	99.27
D	0.01	0.0096	0.0081	0.0076
Nonlinear diffusion with $S_c = 0.8$				
$\sum(z-\zeta)^2$	41.63	15.69	48.68	52.98
D	0.0061	0.0055	0.0046	0.0041

tested here. A nonlocal flux model with linearly slope-dependent entrainment rate but only a downslope flux performs slightly better with a cost C that is about 40-60 points lower (Case I). Finally, a nonlocal formulation with nonlinear, slope-dependent entrainment rate and positive flux only (Case III) provides the best fit for all models. The cost C_f for this class of models is about an order of magnitude lower than local linear models on profiles *A*-*C*. In particular, consider profile *B* where case III results in $C \approx 10\ m^2$, more than an order of magnitude lower than linear diffusion (Figure 2.7). Note that C is a measure of the disagreement between the modeled topography, which is smooth and represents a time-averaged surface, and the observed topography which contains roughness elements and represents a moment in time. Because these roughness elements are not resolved in the numerical model, the cost C can never approach zero. Instead, the most successful model will approach some finite value of C that reflects the magnitude and spatial concentration of the roughness elements. Considering this, we suggest that these models are approaching the limit of C when the observed forms resolve the roughness elements and models do not.

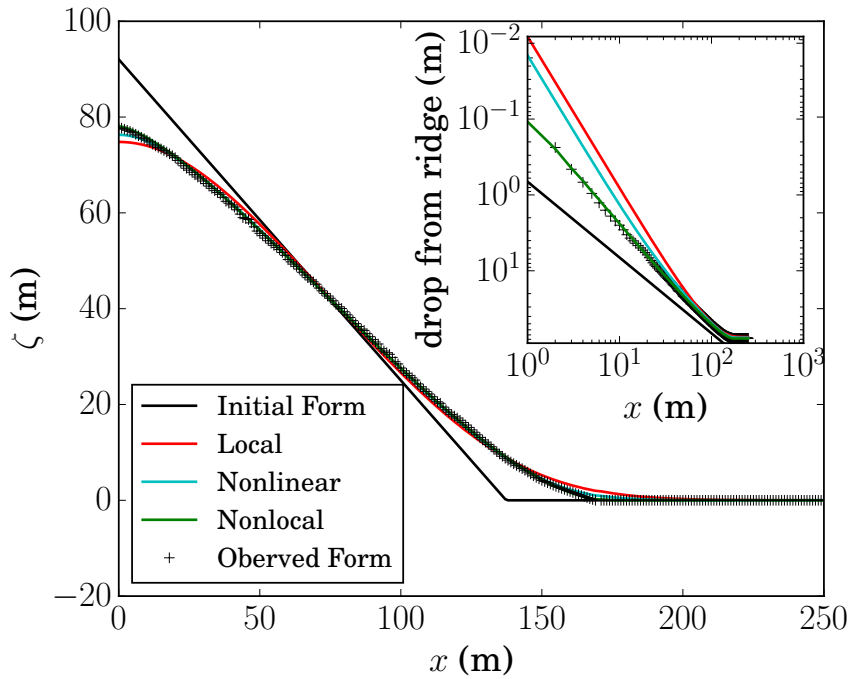

Figure 2.7: Plot of modeled (lines) and observed (crosses) land-surface elevation ζ versus horizontal position x. Drop-from-ridge plot (inset) highlights mismatch at the ridge of local models. The nonlinear model has $S_c = 0.8$ and the nonlocal model uses $E_0 + E_1|S|^2$.

All models were run on a domain that represents 250 meters of horizontal distance. The side-slopes of the moraines are all different lengths; therefore, direct comparison between C_f for different profiles can not be done.

Local nonlinear models are capable of matching the abilities of nonlocal models to reproduce the observed profile form (Table 1). However, these nonlinear models require that the critical slope be around 0.8, which is significantly lower than values for the Oregon Coast Range (*Roering et al.*, 2007). This value is not unreasonable, as S_c is thought to vary by a factor of 1.5. The sparse vegetation supported by the semi-arid climate of the Mono Basin lacks the vegetative anchors that are present in wetter areas which may contribute to lower critical slopes. Whereas these factors suggest that low S_c values may be expected, it is important to recognize that S_c is the slope at which the flux asymptotically becomes unbounded. Although critical slopes of 0.8 are possible, they are the lower limit of expected values. Furthermore, note that Figure 2.8A shows slopes that locally exceed 0.8, suggesting

this location would have an unrealistically large flux in the absence of averaging over some spatial (or temporal) interval. This concept is addressed in the discussion.

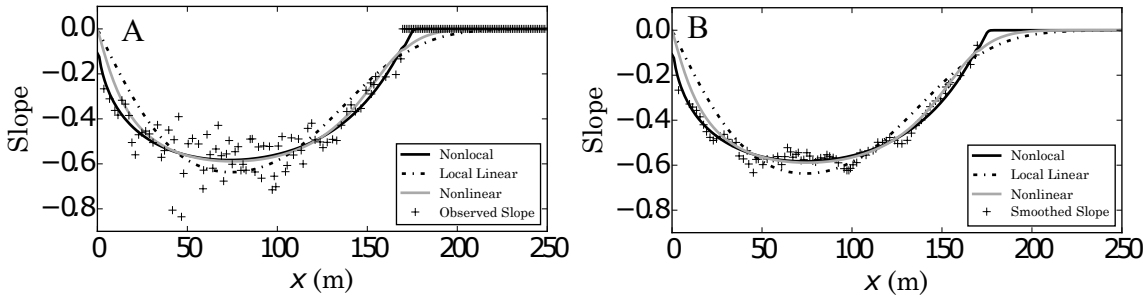

Figure 2.8: Plots of observed (crosses) and modeled (lines) land-surface slopes versus horizontal position for raw slope values (A) and smoothed values (B) using a 5-point moving average.

The difference in model ability is highlighted by the residuals between modeled and observed profiles (Figure 2.9). At most locations on the moraine, the residual resulting from a nonlocal model is smaller than that of the linear model. In particular, nonlocal models perform better at the ridge and toes of the moraines. For example, in every model run, linear diffusion over-predicts erosion at the crest and extends the depositional toe further out. In some cases, linear diffusion over-predicts over 2.5 meters of erosion where nonlocal models fit quite well with residuals on the order of decimeters or less. The numerical fits are also highlighted in plots of land-surface slope from modeled and observed forms (Figure 2.8). These represent a more demanding fit than elevation residuals, and show that, relative to the local linear model, the nonlocal and local nonlinear models more closely fit the raw and smoothed values of slope, particularly near the crest (0 – 50 m), the mid-slope (70–80 m) and over the sediment apron (120 – 170 m).

The Levenberg-Marquardt algorithm that converges to a set of parameters that produce the best-fit topographic profile yields reasonable parametric values for nonlocal transport formulations. The most consistent estimates of parameters across profiles are generated by a slope-squared entrainment relationship (Case III). These values suggest that a slice of sediment from zero to one cm thick, depending on the slope, is entrained annually in this

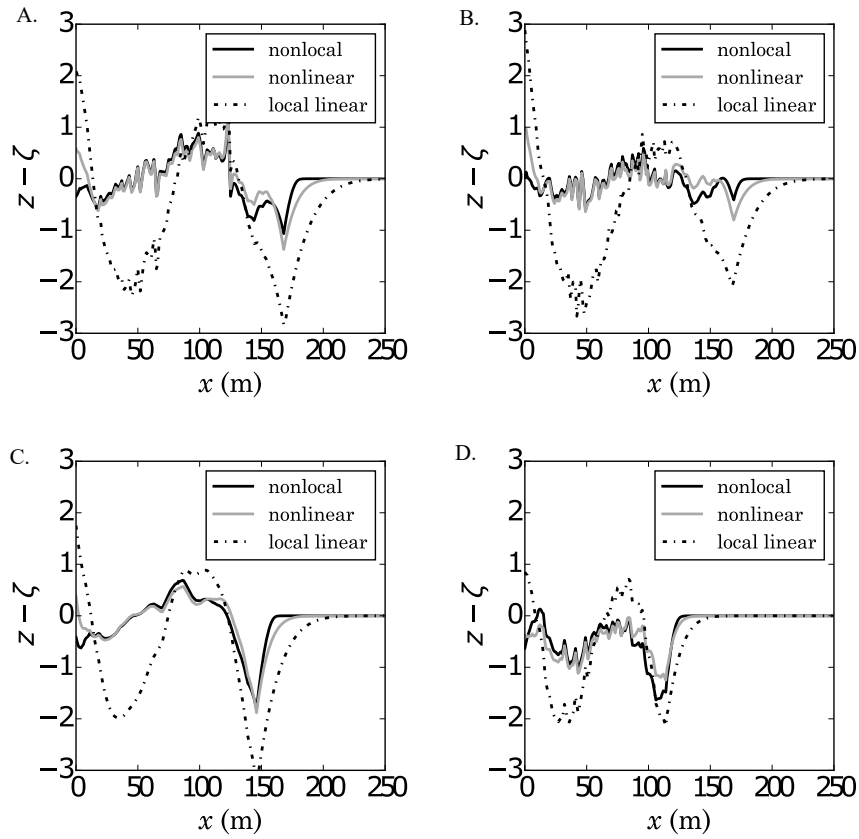

Figure 2.9: Plots of residuals between observed z and modeled ζ elevations versus horizontal distance x for moraine profiles A, B, C and D.

setting. This is a time-averaged value, and at short timescales, we may observe isolated events that stochastically entrain far more (or less). Values for λ_0 are also consistent across profiles and suggest that mean travel distances $\mu_\lambda \approx 0.35/\left[2S_l/(S_l - S) - 1\right]$, or for $S \approx 0.6$, $\mu_\lambda \approx 1.2$ m.

2.5.2 Fourier Transforms

The application of Fourier transforms and their time evolution highlights distinct characteristics of nonlocal and linear processes. On inspection of (2.14) we note that there is only one possibility for the time evolution of the Fourier transform of a linearly diffusing medium. That is, the amplitude, $Z(k)$, of all wavenumbers can only decrease at a rate proportional to k and $Z(k)$. The amplitude at larger k decays faster than for smaller k, or in

terms of wavelength, longer wavelength features persist for longer time. Whereas we see this behavior in the Fourier transform of the observed land surface for some wavenumbers, there are others that either grow or do not decay (Figure 2.10). Furthermore, linear diffusion predicts a much larger decrease in spectral amplitude in many wavenumbers, most notably, larger wavenumbers. Taken together, these observations simply and definitively illustrate that linear diffusion does not accurately account for the evolution of the moraine.

Whereas linear diffusion overestimates decay and is incapable of increasing spectral amplitude, nonlocal models can actually add spectral amplitude (Figure 2.10) in certain wavenumbers. That nonlocal models are capable of growing wavenumbers is consistent with the observed behavior. Furthermore, nonlocal models lead to growth in the same wavenumbers that have grown during the evolution of the moraine. Namely, the initial spectrum (gray) is shifted towards lower wavenumbers in both the observed and nonlocal spectra (black). To be clear, whereas we observe an increase in spectral amplitude in certain wavenumbers, this is not to say that the system has added variance. Indeed, the variance of the land surface has decreased, but it is distributed differently among wavenumbers which results in select wavenumbers increasing in spectral amplitude. Spectra for profiles $B-D$ show a similar behavior, we have shown only one here for simplicity.

We emphasize that the finite spectral amplitudes over wavenumbers $0.007 < k < 0.02$ and $0.015 < k < 0.02$ in Figure 2.10 are part of the evolving basic structure of the moraine form. These local maxima represent the spectral amplitude that accounts for the large concavities at the ridge and toe of the moraine. The Fourier transform of a triangle contains local maxima and minima at wavenumbers that are related to the width of the triangle (*Poularikas*, 1998). Therefore, local maxima not simply attributable to "noise" in the transform, and they are not at the high wavenumbers associated with localized roughness on the moraine surface (e.g., due to the roughness created by shrub mounds). As the spectrum of the land surface is shifted to lower wavenumber, it is like a triangle that is laterally stretched and vertically diminished. As such, the local maxima that remain in the spectrum represent

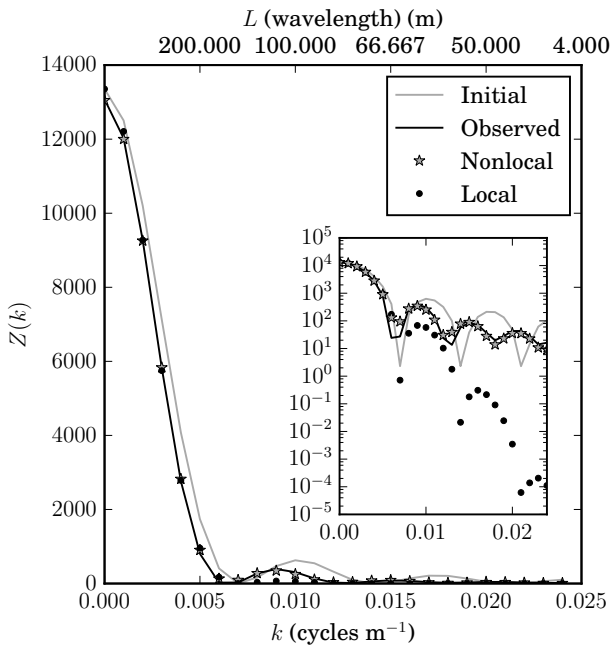

Figure 2.10: Fourier transforms of the observed (black line), modeled (circles and stars) and initial condition (gray line) of moraine profile A. Note that the wavenumber k has been divided by 2π. The inset is a semilog plot of the transform that highlights the transform at higher wavenumbers.

an important, but relatively small portion of the variance that maintains a quasi-triangular form.

We pursue a full treatment of this spectral behavior separately; here we provide a summary of key elements relevant to our treatment of moraine evolution. The time-evolution of the growth rates of the Fourier spectrum is of particular interest as it may provide a tool to decipher the roles of nonlocal/nonlinear versus local, linear transport. Figure 2.11 shows how positive growth rates of the spectrum change as the simulated moraine evolves according to nonlocal transport. Early evolution is marked by fast growth rates in high wavenumbers (short wavelength) for short periods of time that give way to more persistent but slower growth in lower wavenumbers (longer wavelength). This is not surprising as low wavenumber (long wavelength) features simply represent more mass. This type of transfer of spectral amplitude is known of as an inverse spectral cascade (*Domaradzki and Rogallo*,

1990). With continued evolution, the positive growth rates asymptotically approach zero, and the temporal evolution of the Fourier spectrum then is close to what is expected for linear diffusion. Note that spectral growth rates co-evolve with the land-surface slope and concavity, and in particular as slopes and concavities are reduced, positive growth rates are reduced. Therefore, certain topographic configurations (e.g., those with steep slopes and sharp concavities), nonlocal and local, nonlinear formulations lead to fundamentally different Fourier evolution, but for others (e.g., those with low slopes and small concavities), their Fourier behaviors may be similar. We hypothesize that the temporal evolution of the Fourier transform might be a useful tool to decipher the roles of nonlocal versus local, linear transport in other settings.

The reader will note that we have not offered a comparison between nonlinear diffusion and nonlocal transport. The nonlinearities in a nonlinear and nonlocal formulation result in similar behavior in wavenumber domain. There are some subtle differences in behavior; however, a discussion of these is beyond the scope of this paper. Insofar as the modeled land-surface profiles for nonlinear and nonlocal formulations are similar, so too are their spectral evolution. We address these similarities in the following section.

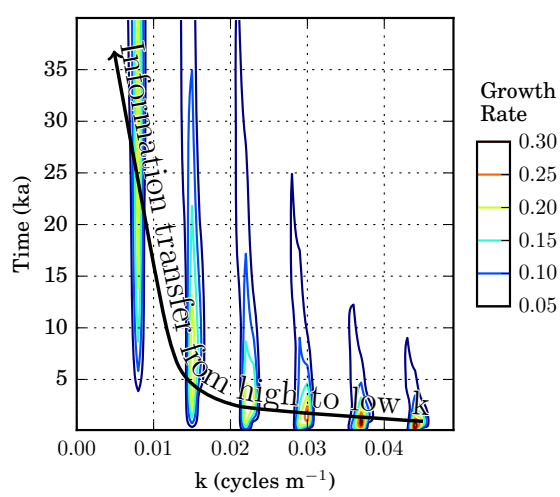

Figure 2.11: Plot of time versus spectral wavenumber k showing the temporal evolution of the growth rates of wavenumbers. Note that only positive growth rates are shown here for simplicity.

2.6 Discussion

2.6.1 Performance of nonlocal models

The results summarized in Table 2.1 show that the nonlocal flux formulation with only a positive, or downslope, component mimics the topographic evolution of the moraine better than other nonlocal models. Such models are consistent with the notion that a majority of transport is accomplished by dry ravel, which only mobilizes sediment in the downslope direction. That downslope-only flux models (nonlocal Case III) perform better may reflect that we use similar mathematics to describe upslope and downslope flux components in bi-directional flux models. It is likely, however, that the bulk downslope and upslope processes differ and may be better represented by different mathematics or parameters. For example, on these moraines most downslope motion may be due to dry ravel, whereas a smaller, but persistent upslope contribution may come from rainsplash. We expect that both entrainment rates and travel distance for rainsplash are functionally different from dry ravel. To test this scenario would require adding another set of parameters for the negative flux. To avoid being unnecessarily heuristic, we instead suggest that the downslope flux is much larger than the upslope component. This assumption may have an impact on the flux at locations with low slopes, where the positive and negative flux contributions can be similar in magnitude. As such, this may partly explain the deviations we observe between observed and modeled profile forms for nonlocal transport at the crests and toes of moraines.

The spatial variation in grain size illustrated in Figure 2.5 could affect transport parameters in nonlocal and local formulations of transport. Recognizing that entrainment of particles requires a disturbance of sufficient energy to dislodge them, we suggest that smaller particles will be entrained by smaller disturbances which occur more frequently than the large ones required to move large particles. Therefore, a higher density of boulders might reduce entrainment E. However, we have somewhat arbitrarily determined boulders to be those greater than 25 cm in diameter whereas the impact on entrainment may be more ac-

curately addressed by the distribution of grain sizes as opposed to the concentration of a single grain-size fraction. In addition, although the density of boulders is greater near the ridge, it may not be great enough to significantly alter the values for E. Further work might address the impact of grain size on either the entrainment rate or the pdf of travel distances (*DiBiase et al.*, 2017).

2.6.2 Comparison with local nonlinear flux description

The nonlinear transport model, (2.2), is a physically based model and is capable of capturing the essential behaviors of hillslope evolution and flux values. The success of (2.2) serves as motivation for the class of nonlocal models discussed here. That is, recognition of nonlinear dynamics brought attention to the idea that long-distance motions can contribute significantly to the hillslope sediment flux. Both classes of models are based on the notion that sediment particle travel distance is a key component of the flux yet they differ in their treatment of it. Given this similarity, nonlocal models ought to subsume nonlinear ones. There are, however, noteworthy differences between nonlocal and nonlinear models.

Recall that a nonlinear model is capable of nearly matching the result of a nonlocal model (Table 2.1), but to do so, $S_c = 0.8$. We have noted that locally, slopes exceed 0.8, meaning that the sediment flux at this location would be unrealistically large for a nonlinear model such as (2.2). However, a nonlinear model is not intended to be applied at scales smaller than the biogeomorphic scale of roughness present on hillslopes (*Roering et al.*, 2010). Local formulations such as (2.2) and (2.13) require a spatial average of slope (window of 7-10 m according to *Roering et al.* (2010)), or alternatively, a time-averaged value at a location such that land-surface slope used in the models smoothly varies downslope. In contrast, nonlocal models remove this scale-dependence of slope (*Ganti et al.*, 2012) and do not explicitly require averaging. In this contribution we do use time-averaged values for slope; however, the mathematical development of the entrainment rate, $E(x')$ is based on the presence of biogeomorphic roughness creating locally over-steepened faces.

In this sense, the formulation is acknowledging the presence of roughness in an implicit manner. Whereas a nonlocal model can in principle incorporate the biogeomorphic roughness present on hillslopes, we have not advanced the application at the relevant timescales or spatial resolution. However, now that we have demonstrated nonlocal transport at geomorphic timescales, future work might be well-suited to address shorter timescales and applying a nonlocal theory that explicitly includes the biogeomorphic roughness. Last, although we use a time-averaged slope here, the local slopes that we calculated do not exceed the limiting slope S_l, as they do in the nonlinear case.

In the case where $|S| > S_l$, a nonlocal formulation does not imply that the flux becomes infinite. The critical slope S_c in (2.2) represents a limiting situation where the flux nominally becomes very large, assuming sediment is available to be transported (in a time-averaged sense). In contrast, the critical slope S_c in the nonlocal formulation is to be interpreted as the slope at which sediment, once mobilized, does not become disentrained. In this situation where particle motions are not arrested, the flux is set by the upslope convolution of the entrainment volume, as in detachment-limited conditions (*Lamb et al.*, 2011).

2.6.3 Mapping Nonlocal to Nonlinear Flux Models

The different mathematics of nonlocal and nonlinear flux models prevent a straightforward comparison of the two. However, approximations of these models lead to identification of the essential behaviors which may be shared. To do so, we simplify both nonlinear and nonlocal flux models. For the simplification of nonlocal transport, we follow the steps of Furbish and Haff (2010) and approximate (2.3) with an advection-diffusion equation,

$$q(x)_{ad} = E(x)\mu_\lambda - \frac{\partial}{\partial x}\left[E(x)\sigma_\lambda\right], \tag{2.18}$$

where μ_λ and σ_λ^2 are the first and second moments of $f(r;x)$. Furthermore, Furbish and Haff (2010) show that the first term of (2.18) dominates, such that we can neglect the

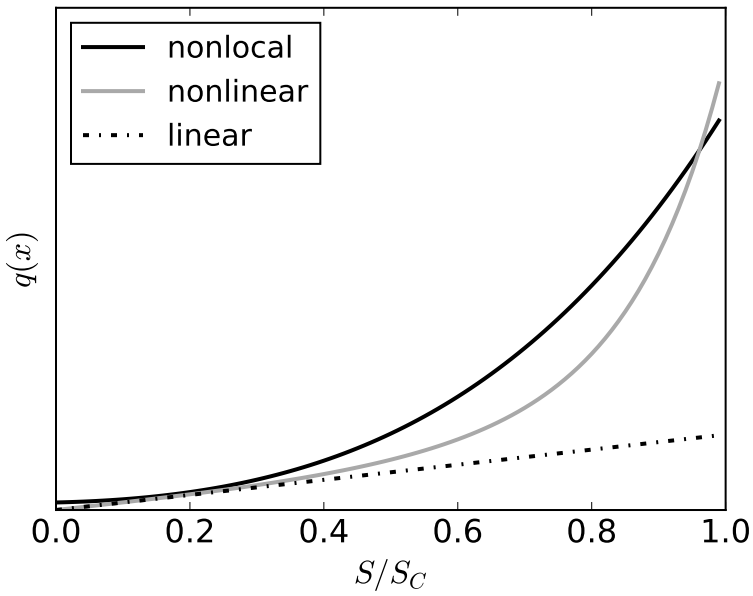

Figure 2.12: Plot of flux versus slope S/S_c based on the simplified versions of the nonlocal and nonlinear flux models together with the linear flux model. The flux values (y-axis) are only relative quantities depending on the choice of parameters. The nonlinear model here is approximated out to five terms.

diffusive term. The expression for μ_λ is determined from a binomial expansion of $R(x - x', x')$. For a negative slope and with only downslope motions, the mean travel distance is

$$\mu_\lambda = \lambda_0 \left(1 - \frac{S}{S_l}\right)^2. \tag{2.19}$$

Using a nonlinear form for $E(x')$, the advective term of (2.18) is

$$q_a = E_0\lambda_0 - E_0\lambda_0\frac{2S}{S_l} + \left(\frac{E_0\lambda_0}{S_l^2} + E_1\lambda_0\right)S^2 - E_1\lambda_0\frac{2S^3}{S_l^2} + E_1\lambda_0\frac{S^4}{S_l^2}. \tag{2.20}$$

In comparison, the binomial expansion of the local nonlinear formulation leads to,

$$q_a = -D\left(S + \frac{S^3}{S_c^2} + \frac{S^5}{S_c^4} + \frac{S^7}{S_c^6} + \ldots\right). \tag{2.21}$$

Note that (2.21) contains only odd powers of S, whereas (2.20) contains consecutive integer

powers of S. However, (2.20) and (2.21) do share a fundamental property in that they are both linear combinations of local nonlinear slope terms. Furthermore, we note that $E\lambda_0$ [L^2 T^{-1}] carries dimensions consistent with a hillslope diffusivity D, which suggests then that (2.20) can be mapped to a term of the same power in (2.21). Although there is a mismatch between approximated flux values (Figure 2.12), the basic form is the same. That these curves are approximations based on expansions, yet share the same form, provides an explanation for why nonlinear and nonlocal formulations lead to similar behaviors. Both the entrainment rate, E, and the disentrainment rate, P, are nonlinear functions of slope and both contribute to the nonlinear behavior of the sediment flux. However, we suggest that the key part of the nonlinearity appears to come from E. The shared behavior holds for $S \ll S_c$ and $S \ll S_l$. When $S \to S_c$ and $S \to S_l$ higher order terms in (2.21) become significant and (2.20) and (2.21) diverge.

2.6.4 Sensitivity to E and λ_0

The two central parameters for the nonlocal convolution integral flux formulation, E and λ_0, set the magnitude of sediment transport. These parameters hold real physical meaning that can be measured or modeled. This provides an opportunity to hypothesize about the impact of changing ecological or climatological conditions. For example, imagine a substantial shift in climate which drives an ecologic change from a grassland to a shrubland (*Pelletier et al.*, 2016). Under these new conditions, long-distance transport events may become more common as there are fewer vegetative anchors for the soil which reflects an increase in E. Furthermore, this may increase the travel distance if patchy surface flows become a more prominent process, and which is represented by an increase in λ_0. Whereas the result of both changes is an increase in the flux, the response of the flux to each is not necessarily equal. Therefore, we question which parameters hold the most weight for a flux formulation as written in (2.3).

To investigate this we perform a sensitivity analysis. We make use of the Leibniz inte-

gral rule and take the derivative of the flux (2.9) with respect to E_1 and λ_0. To make this problem tractable, we must simplify the topography and imagine a hillslope with uniform slope, S, such that the spatial dependency of $E(x')$ and $R(x-x';x')$ on x is removed. Furthermore, we conduct this analysis at a position beyond the saturation length of sediment transport. This represents a sensitivity analysis of the sediment flux some finite distance from the crest of a hillslope. We note that this is inherently a transient condition; however, it provides a simple and first-order estimate on the impact of key parametric values. We also point out that many slopes like the interior of a moraine are highly linear, thereby lending merit to this approach. Making these assumptions, the derivatives of (2.9) are

$$\frac{\mathrm{d}q(x)}{\mathrm{d}E_1} = \int_0^x S e^{-\frac{x-x'}{\lambda_0}\left(\frac{S_l+S}{S_l-S}\right)} \mathrm{d}x' \tag{2.22}$$

$$\frac{\mathrm{d}q(x)}{\mathrm{d}\lambda_0} = -\int_0^x \frac{E_1 S}{\lambda_0^2}\left(\frac{S_l+S}{S_l-S}\right)(x-x')e^{-\frac{x-x'}{\lambda_0}\left(\frac{S_l+S}{S_l-S}\right)} \mathrm{d}x'. \tag{2.23}$$

We can integrate (2.22) and (2.23) and neglect exponential terms that involve $\exp(-x/\lambda_0) \approx 0$, because we are sufficiently far downslope. This results in two, nearly identical nonlinear functional forms,

$$\frac{\mathrm{d}q(x)}{\mathrm{d}E_1} = \lambda_0 |S| \left(\frac{S_l-S}{S_l+S}\right) \quad S<0 \tag{2.24}$$

$$\frac{\mathrm{d}q(x)}{\mathrm{d}\lambda_0} = E_1 |S| \left(\frac{S_l-S}{S_l+S}\right) \quad S<0 \tag{2.25}$$

The flux is nonlinearly sensitive to both variables as slopes approach S_l. However, sensitivities differ based on the magnitude of the other variable in question. We should note the different units of (2.24) [L] and (2.25) [L T^{-1}], although a timescale is tied to (2.24), as λ_0 is the characteristic travel distance after a given time $\mathrm{d}t$. Insofar as lateral displacements, λ_0, are greater than the depth of entrained sediment per year, we see that the flux is more sensitive to E_1 than λ_0. For systems with higher E_1, the distribution of sediment becomes more significant in calculations of the flux. That is, if there is a lot of sediment in motion, emphasis should be placed on keeping track of it spatially; and if it travels far, then

emphasis is placed on how much is in motion.

High sensitivity of the flux to E_1 is supported by the result presented in Figure 2.6, where surface of the cost function $C(E_1, \lambda_0)$ can be inferred from the paths taken by iterative choices of parameters. In particular, we emphasize that all paths converge to the same orientation before approaching the minimum of $C(E_1, \lambda_0)$. Furthermore, the orientation of that path is close to parallel with the λ_0 axis. These paths suggest that the cost surface contains a trough oriented along the λ_0 axis (denoted in Figure 2.6). This trough suggests that so long as the value of E_1 is correct, changes in λ_0 over up to an order of magnitude do little to change the form of the moraine. Although this indicates that the modeled hillslope form (not the flux) is more sensitive to changes in E_1, in order to correctly model the evolution of the land surface, one must first correctly describe the flux. Therefore, we interpret the geometry of $C(E_1, \lambda_0)$ as a reflection of the sensitivity of flux formulations to various transport parameters.

Consider a system with relatively small E_1 and a numerically larger λ_0. Now consider a significant but not large change in climate, namely, a shift that does not result in dramatic ecological changes. According to (2.24), depending on the value of λ_0 and on steep slopes, a slight shift in E_1 can lead to quite large increases in the flux. More specifically, the changes in the flux can be many times greater than the change in E_1. This type of analysis is similar to efforts that explore what values of the diffusivity-like rate constant D might take on in different settings. It is largely suggested that it varies as a function of climate and ecology (*Tucker and Bras*, 1998; *Istanbulluoglu and Bras*, 2005; *Hughes et al.*, 2009; *Pelletier et al.*, 2016). However, this problem is a complex one that involves the specifics of ecology, geology, and climatology. The convolution integral forms of the nonlocal flux deconstruct rate constants like D into two physically interpretable parameters which are capable of addressing some of these specifics. This may provide an opportunity to theoretically address the impact of climate on hillslope sediment transport and erosion rates.

Through estimating a value of D for local linear diffusion, we show that, in this setting, the form of a moraine reflects only the time-averaged value of D (Appendix 0.1). Previous work has demonstrated this concept (Figure 6, *Madoff and Putkonen*, 2016), although it has not addressed the mathematical basis. This is easily proven when the diffusion equation is examined in the wavenumber domain and is a point that may be significant in efforts to unfold the record of climate in hillslope form. To be clear, this concept only applies to topographic configurations that lack a boundary condition that reflects tectonic conditions (i.e. channel). There are numerous landforms for which there is no external forcing other than climate. For example, river terraces, faults scarps, and paleo-shorelines are all topographic features that lack externally forced boundary conditions, and therefore their evolution is driven only by climate. In such settings, under linear diffusion, their form would be expected to reflect a single value for D and contain no information about changing conditions. It remains unclear if a nonlinear formulation for sediment transport shares this property or not.

2.7 Conclusions

We have provided field-based evidence that demonstrates nonlocal sediment transport operating at the hillslope scale. By a measure of sum-of-squared differences, nonlocal hillslope sediment transport formulations reproduce observed profile forms with greater fidelity than local, linear diffusion. In particular we note that nonlocal formulations better describe the evolution of locations with large concavity. Nonlocal, convolution integral-based formulations match the performance of local nonlinear ones. We have shown that nonlinear and nonlocal formulations are expected to perform similarly as they are both motivated by the same theory, and mathematical simplifications highlight that the formulations share an underlying mathematical form.

In demonstrating the presence nonlocal sediment transport, we have obtained the first estimates of the parameters in the convolution integral-like flux formulation for sediment

transport. Throughout this paper we have attempted to highlight that nonlocal formulations offer physically clear parameters that can potentially be measured in the field. Here we have estimated the values for the time-averaged volumetric entrainment rate and a characteristic length-scale of particle travel distance. We find that time-averaged values for $E_1 \approx 0.01$ m/yr and $\lambda_0 \approx 0.35$ m. This implies that, on average, the thickness of the slice of sediment that is entrained annually in this setting goes from zero to one cm as slopes go from zero to one. The interpretation of λ_0 is that this nominally represents the average total (unidirectional) displacement of particles entrained (perhaps multiple times) on a horizontal surface during one year.

We have questioned which parameter is most influential for the volumetric sediment flux. A sensitivity analysis reveals that the flux depends most heavily on the slope-dependent term of the entrainment rate. That the entrainment dominates the flux is consistent with research on bedload sediment transport where changes in particle activity primarily control changes in the sediment flux, not hop distance lengths (*Ancey et al.*, 2008; *Radice et al.*, 2009; *Ancey*, 2010; *Roseberry et al.*, 2012). Insofar as the entrainment rate, E, dominates the flux at our field site, we expect that future efforts aimed at empirically or theoretically determining values for E would be worthwhile.

We have identified behaviors in wavenumber domain that distinguish between local linear diffusion and nonlocal/nonlinear formulations. Whereas all transport models result in an overall decay of topographic variance, the way in which this decay occurs differs. Linear diffusion shows that spectral amplitude contained in every wave-number must decrease. Nonlinear and nonlocal models destroy topographic variance by concentrating spectral amplitude to low wavenumbers. In doing so, spectral amplitude in certain wavenumbers can temporarily grow, thereby providing a unique signature. These signatures have some potential as being tools to identify the style of sediment transport that has occurred during a landform or landscape's history.

Chapter 3

Compression and decay of hillslope topographic variance in Fourier wavenumber domain

3.1 Introduction

Mathematical descriptions of hillslope sediment transport are a central component of geomorphology. Formulations for sediment transport provide a tool to analyze the form of landscapes (*Roering et al.*, 2007), identify relationships between tectonics and climate(*Perron et al.*, 2012; *Fernandes and Dietrich*, 1997; *Hurst et al.*, 2012; *Hughes et al.*, 2009; *McGuire et al.*, 2014), and understand the motion and spatial distribution of nutrients and organic carbon (*Reneau and Dietrich*, 1991; *Hales et al.*, 2012). Three hillslope sediment transport models are common, namely, local linear diffusion, local nonlinear diffusion, and nonlocal transport. Each of these is supported by a different theory; however, they share a common foundation in that the rate of sediment transport is a function of the land-surface slope. Linear and nonlinear models describe the hillslope sediment flux as linear or nonlinear functions of the local slope. Nonlocal models describe the flux as a weighted function of surrounding slopes. Whereas mathematical distinctions between these three formulae are clear, their physical manifestations are not easily distinguished. This work is aimed at identifying clear and fundamental consequences of these three transport formulae that are observable in land-surface evolution.

At a large scale, the slope-dependencies of local linear, nonlinear, and nonlocal transport lead to an elastic evolution of topography (*Schumer et al.*, 2017). That is, in the absence of tectonic forcing, topographic highs tend to degrade and lows tend to fill. With reference to landscape-scale applications then, all models effectively produce the same low-order morphology. If a question is aimed at a low order description of transport, the simplest transport model is appropriate. However, these models definitively differ in their

theoretical underpinnings and therefore the meaning of central parameters or the magnitude of parameters themselves may change. Generally, however, parameters of transport formulations are rate constants that reflect the magnitude of regolith churning or the activity of particles. To obtain values for these, it is common to numerically simulate land-surface evolution and back-calculate a value that results in the best-fit modeled land-surface profile (*Fernandes and Dietrich*, 1997; *Nash and Beaujon*, 2006; *DiBiase et al.*, 2010; *Madoff and Putkonen*, 2016; *Doane et al.*, 2018). However, fitting linear and nonlinear models will result in different estimates of the hillslope diffusivity, and will imply different magnitudes of soil churning (*Doane et al.*, 2018). Therefore, we must rely on signatures of linear, nonlinear, and/or nonlocal processes in land-surface form if we are to correctly obtain estimates of transport processes.

At a hillslope scale, the mechanistic style of sediment transport can be distinguished in hillslope form. For example, at topographic steady state, a nonlinear formulation for the hillslope sediment flux results in a straighter profile than linear diffusion (*Roering et al.*, 1999). Likewise, nonlocal transport can produce relatively straight profiles, depending on the formulation (*Foufoula-Georgiou et al.*, 2010; *Tucker and Bradley*, 2010; *Furbish and Haff*, 2010). Whereas these geometric qualities are helpful and clearly stated, they rely on a characteristic being 'more' or 'less' than another configuration. Furthermore, topographic steady state is a rare condition. Nonetheless, the recognition that slopes become uniform with distance downslope under certain geomorphic conditions highlights the idea that the details of the land surface contain evidence of the mechanistic style of sediment transport. This work explores the evolution of the details of the land surface in a transient setting and identifies clear diagnostic behaviors.

To observe the details of the land surface, it is helpful to transform it into the wavenumber representation via the Fourier transform. Previous authors have demonstrated the value of using the Fourier transform for earth surface applications to identify characteristic length scales (*Perron et al.*, 2008), evaluate the surface roughness (*Booth et al.*, 2017), and solve

advection-diffusion equations (*Schumer et al.*, 2009; *Ganti et al.*, 2010). Here, we use the Fourier transform of landforms to identify the high and low-order structure – terms that we clarify here. Consider a hillslope that is Gaussian in form which is similar to the form of some hillslopes and landforms such as old lateral moraines. Now consider fitting the Gaussian hillslope with a simple triangle such that the mismatch between the two is minimized. We note that there is a clear mismatch; however, a triangle can explain much of the variance of a Gaussian profile (Figure 3.1 A). That the two functions largely share how variance is distributed illustrates what we mean by low-order structure. This becomes particularly clear when the functions are viewed in wavenumber domain, which describes how variance is distributed among scales. The transforms of both the Gaussian and triangle are similar at low wavenumber, and the spectral amplitude within this low wavenumber band makes up most of the variance. However, distinct differences are observed in the high wavenumbers which highlight the high-order structure. Whereas the bulk of the variance is contained in the low order structure of the land-surface profile, there is a disproportionate amount of information contained in the high order structure, which is the difference between a Gaussian and a triangle (Figure 3.1 B). Here we wish to emphasize an important point. We note that the transform of a Gaussian contains vanishingly small amplitude in its high-order structure. This is not to say that it does not have high order structure, but that the infinitesimal amplitudes are a signature of the Gaussian form. We suggest that clues to the physics of sediment transport are contained in the evolution of a small portion of the variance that is represented by the higher-order structure.

We identify two distinct behaviors of linear and nonlinear processes that are apparent in the evolution of high-order structure. In wavenumber domain, theory shows that linear diffusion leads to vertical destruction of spectral amplitude at rates that scale with wavenumber (*Schumer et al.*, 2009). We show here that nonlinear processes tend to compress the spectrum into lower wavenumbers, and in doing so, the spectrum tends towards longer wavelength features. In this paper, these styles of spectral evolution represent two

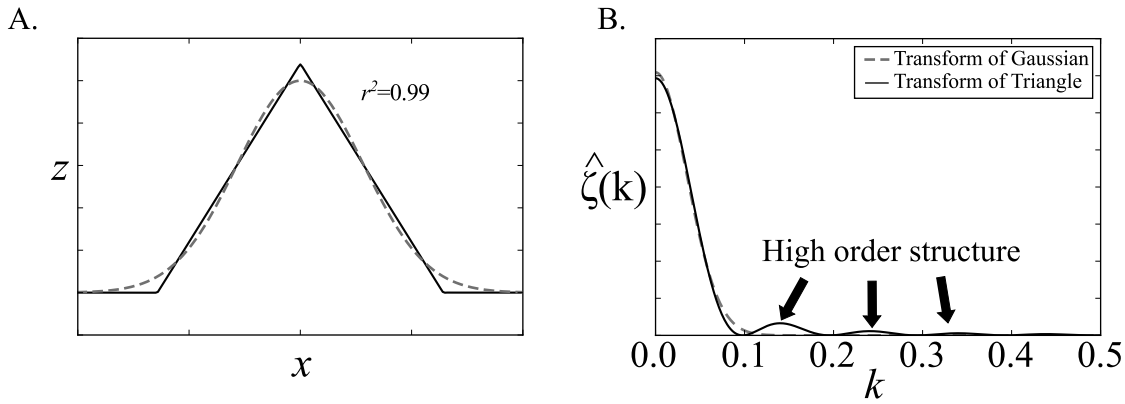

Figure 3.1: A. Profile of a Gaussian approximation of a hillslope and a triangular fit where z is elevation and x is horizontal position. B. Transforms of a Gaussian profile and its triangular fit where $\hat{\zeta}$ is the transform of the land surface and k is wavenumber.

end-member styles to destroy topographic variance. We present theory that explains the spectral evolution according to linear, nonlinear, and nonlocal processes and address the idea of using the spectra as a tool to identify linear, nonlinear, and nonlocal processes. Spectral evolution styles are more diagnostic for certain topographic configurations and we identify topographic characteristics that result in clearly diagnostic behaviors. This is significant in efforts to characterize landscapes as being steep or low-angle, which has implications for the suite of transport processes degrading the landscape.

This paper is outlined as follows. In section 2, we briefly review the theoretical development of local linear, nonlinear, and nonlocal transport. This is covered in previous work (*Culling*, 1963; *Fernandes and Dietrich*, 1997; *Roering et al.*, 1999; *Furbish and Haff*, 2010; *Furbish and Roering*, 2013), so we cover the basic principles here. Section 3 introduces the Fourier transform and applies the theory of land-surface evolution in wavenumber domain. In section 4 we present case studies of examples from the natural landscapes with simple topographic configurations. Last, we present an experimental analogue involving acoustically stimulated simulation of land-surface evolution that highlights the spectral evolution in wavenumber domain.

3.2 Sediment Transport Theory

3.2.1 Linear Diffusion

Linear diffusion has a long legacy in geomorphology (*Culling*, 1965; *Carson and Kirkby*, 1972; *Fernandes and Dietrich*, 1997; *Jyotsna and Haff*, 1997; *Furbish and Fagherazzi*, 2001; *Putkonen et al.*, 2008). Culling (1963) suggested that the quasi-random creation and collapse of pore-space within a soil column drives bulk down-slope motion. The rate of bulk motion scales linearly with land-surface slope as the lofting motions are, on average, normal to the land-surface slope and settling motions are, on average, down (*Furbish et al.*, 2009a). The volumetric hillslope sediment flux, $q(x)$ [$\mathrm{L}^2\ \mathrm{T}^{-1}$], is often described as

$$q(x) = -D\frac{d\zeta}{dx}\,, \tag{3.1}$$

where D [$\mathrm{L}^2\ \mathrm{T}^{-1}$] is a diffusivity-like rate constant, ζ [L] is the land-surface elevation, and x [L] is a horizontal position. Placing (3.1) into the Exner equation returns the familiar diffusion equation

$$\frac{\partial\zeta}{\partial t} = D\frac{\partial^2\zeta}{\partial x^2}\,. \tag{3.2}$$

The form of (3.2) is mathematically homologous to Darcy's Law for flow through a porous medium, Fick's law for molecular diffusion, and Fourier's law of heat diffusion. Mathematical treatment of this equation is extensive (*Carslaw and Jaeger*, 1959; *Hornberger and Wiberg*, 2013; *Schumer et al.*, 2009).

3.2.2 Nonlinear Diffusion

Whereas (3.1) captures the basic idea that sediment flux varies with slope, there is evidence that the relationship between land-surface slope and sediment flux is nonlinear (*Roering et al.*, 1999). For example, landscapes such as the Oregon Coast Range that are in an approximate steady-state condition contain hillslopes whose profiles become increas-

ingly linear with distance from the divide (*Roering et al.*, 2001a). This condition suggests that with increasing slope, the hillslope sediment flux must increase nonlinearly such that the divergence of the flux remains constant to satisfy the steady state condition.

Treatment of frictional and gravitational forces acting on soil as a function of slope (*Roering et al.*, 1999) leads to a nonlinear functional form for the sediment flux

$$q(x) = -D\frac{S}{1-\left(\frac{|S|}{S_c}\right)^2}, \tag{3.3}$$

where S is the land-surface slope and S_c is a critical slope related to the friction slope. This formulation suggests that as slopes steepen friction is increasingly ineffective and surface processes such as dry ravel and small land-slides occur more frequently. Equation 3.3 effectively accounts for observed topographic and erosion rate data that show a nonlinear relationship between slope and hillslope sediment flux (*Roering et al.*, 1999; *Gabet et al.*, 2000; *Gabet*, 2003; *Roering et al.*, 2007).

3.2.3 Nonlocal Transport

The class of nonlocal models is largely motivated by the success of nonlinear diffusion. Whereas (3.3) is able to simulate topographic evolution with high fidelity, it is an incomplete treatment of sediment transport. To generate large fluxes, nonlinear flux formulations appeal to increased pace of particle motions (e.g. tree-throw, dry ravel, and shallow land-slides), yet it does not include a description of particle travel distances. Travel distances associated with these motions can be on the order of meters if not tens of meters (*Gabet and Mendoza*, 2012; *DiBiase et al.*, 2017), yet (3.3) is a local function of x. That the expression is local but invokes nonlocal motions implies that (3.3) is an incomplete treatment of transport (*Doane et al.*, 2018). Nonlocal models explicitly address this concern. Furthermore, local nonlinear models are inherently scale-dependent and applicable at resolutions greater than the roughness scale (i.e. scales associated with biogeomorphic roughness) whereas

nonlocal models can be scale-independent (*Ganti et al.*, 2012).

Three general models incorporate nonlocality. Fractional calculus models take advantage of a non-integer derivative of a quantity, which produces a nonlocal dependence (*Foufoula-Georgiou et al.*, 2010). A rule-based model that evaluates the probability of continued motion for a parcel of sediment based on the local topographic conditions leads to long-distance motions (*Tucker and Bradley*, 2010). Last, a probabilistic model involves the convolution of a volume of sediment set in motion around x with the probability that the sediment passes through x (*Furbish and Haff*, 2010; *Furbish and Roering*, 2013). Here we will focus on a convolution integral form because the ingredients, a volumetric entrainment rate and particle travel distance are well-defined quantities that are, in principle, measurable (*Kirkby and Statham*, 1975; *Gabet and Mendoza*, 2012; *DiBiase et al.*, 2017).

A convolution integral formulation for nonlocal hillslope sediment transport is (*Furbish and Haff*, 2010; *Furbish and Roering*, 2013; *Doane et al.*, 2018),

$$q(x) = \int_0^x E(x')R(x-x',x')\mathrm{d}x', \tag{3.4}$$

where $x = 0$ is the ridge-top location, x' is an upslope position, E [$\mathrm{L}^3\ \mathrm{L}^{-2}\ \mathrm{T}^{-1}$] is a volumetric entrainment rate, and R is like a kernel and it is the survival function of particle travel distance. This is not a true convolution because the parameters of the survival function of travel distance, $R(x-x',x')$ are allowed to change with x' as the slope changes. That is, the mean travel distance increases with slope such that probability is shifted towards the tail. This property precludes it from being a true convolution (*Gilad and Von Hardenberg*, 2006), although we will refer to it as one here. The survival function describes the probability that particles travel at least a distance $x-x'$, which implies that they contribute to the flux. There may be different functional forms for both $E(x')$ and $R(x-x',x')$ that depend on the suite of processes that occur in a given region. Land-surface slope, however, is often a central variable in both functions, which provides a linear or nonlinear slope-dependency.

Therefore, behaviors of a nonlocal formulation can be similar to both linear and nonlinear transport depending on how the entrainment rate and survival function are formulated (*Doane et al.*, 2018).

3.3 Land-surface evolution in wavenumber domain

To illustrate distinctive behaviors of transport formulae in wavenumber space, we rely on the identities of the Fourier transform. By definition, the Fourier transform of a function $f(x)$ (i.e. land-surface elevation) of position x is

$$\hat{f}(k) = \int_{-\infty}^{\infty} f(x) e^{-ikx} \mathrm{d}x \,, \tag{3.5}$$

where $\hat{f}(k)$ is spectral amplitude [L^2] and k [L^{-1}] is wavenumber ($k = 2\pi/l$, radians per unit distance where l is wavelength). Fourier transforms have a convenient property that states that a convolution of two functions in arithmetic space is multiplicative in wavenumber domain,

$$\int_{-\infty}^{\infty} f(x') g(x - x') e^{-ikx'} \mathrm{d}x' = f(x) * g(x) = \frac{1}{2\pi} \hat{f}(k) \hat{g}(k) \,, \tag{3.6}$$

where the asterisk denotes a convolution. Additionally, the representation of a derivative (using Einstein notation $\frac{df}{dx} = f_x$) in linear space is straightforward in wavenumber domain,

$$\hat{f}_x(k) = ik \hat{f}(k) \,. \tag{3.7}$$

The Fourier transforms of higher order derivatives are simply ik raised to the integer order of the derivative. For example, the transform of a second derivative with respect to position is

$$\hat{f}_{xx}(k) = (ik)^2 \hat{f}(k) \,. \tag{3.8}$$

Einstein notation is used in this manuscript only when referring to derivatives in wavenumber domain; otherwise, Leibniz notation for derivatives is adopted.

In this section we explore the impacts of different transport formulations on the evolution of the elevation spectra. We conduct the analysis in the context of simple topographic configurations to illustrate the behavior. To simplify the analysis in wavenumber domain, we reflect landforms about the origin such that their graphical representation is an even function (symmetric about the origin), and therefore the transform is all real. The rules presented above allow for (3.2), (3.3), and (3.4) to be recast as their transforms, and land-surface evolution can be described in wavenumber domain for a set of topographic configurations. From this analysis, different behaviors emerge that highlight the evolution of high-order topographic structure. These analyses, although strictly applicable to the set of landforms tested, broadly identify land-surface behaviors that correspond with linear, nonlinear, and nonlocal formulations.

3.3.1 Linear Diffusion

Mathematical treatment of partial differential equations like (3.2) is extensive and previous work has identified an analytical expression for the time-evolution of a quantity undergoing linear diffusion (*Carslaw and Jaeger*, 1959; *Schumer et al.*, 2009). Using (3.8),

$$\hat{\zeta}_t(k) = -Dk^2\hat{\zeta}(k)\,. \tag{3.9}$$

This result is particularly significant, as it indicates that spectral amplitude in all wavenumbers must decay with time. The rate of decay scales with wavenumber such that low wavenumber (long wavelength) features persist longer than large wavenumber (short wavelength) features. Separating variables and integrating with respect to t yields an analytical solution for the transient evolution of the Fourier transform of the land-surface elevation

(*Carslaw and Jaeger*, 1959; *Schumer et al.*, 2009; *Mudd and Furbish*, 2007)

$$\hat{\zeta}(k,t) = \hat{\zeta}(k)e^{-k^2Dt}\,. \tag{3.10}$$

That topography decays exponentially in the absence of external forcing (i.e. tectonics) has been exploited for various applications (*Booth et al.*, 2017; *Mudd and Furbish*, 2007) and is a well-known behavior.

3.3.2 Nonlinear Diffusion

In contrast to (3.9), there is no simple expression for the time-evolution of the Fourier transform of a profile evolving according to nonlinear diffusion. To investigate the influence of nonlinear terms, we add a nonlinear term to (3.1). For illustration, we consider a single nonlinear term that has slope raised to a power of three,

$$q(x) = -D_1\left(\frac{d\zeta}{dx}\right)^3 - D_0\frac{d\zeta}{dx}, \tag{3.11}$$

where D_0 and D_1 [$\mathrm{L}^2\ \mathrm{T}^{-1}$] are diffusivity-like rate constants. We write the flux this way for two reasons. First, an odd power on slope maintains the correct dependence on the sign of the slope such that negative slopes have positive fluxes. Second, when $D_0 = D_1$, the expression is equal to the first two terms in the Taylor expansion of (3.3) (*Ganti et al.*, 2012; *Doane et al.*, 2018) and therefore is capable of capturing the basic behavior of a physically-based nonlinear formulation. Placing (3.11) into the Exner equation,

$$\frac{\partial\zeta}{\partial t} = 3D_1\left(\frac{\partial\zeta}{\partial x}\right)^2\frac{\partial^2\zeta}{\partial x^2} + D_0\frac{\partial^2\zeta}{\partial x^2}\,. \tag{3.12}$$

Note that in the absence of the second term on the right-hand side of (3.12) there is no change in elevation at ridges which have zero slope but finite concavity. This result would be unrealistic, and therefore a linear diffusion term is required.

The Exner equation in the form of (3.12) can be recast in wavenumber domain using the properties of Fourier transforms presented above. In particular, we take advantage of the inverse of the convolution theorem for Fourier transforms so that

$$\hat{\zeta}_t(k) = \frac{3D_1}{4\pi^2}\hat{\zeta}_{xx}(k) * [\hat{\zeta}_x(k) * \hat{\zeta}_x(k)] - D_0 k^2 \hat{\zeta}(k)\,, \tag{3.13}$$

where the asterisk denotes a convolution and subscripts on the transforms indicate a transform of a derivative. The form of (3.13) can be summarized mathematically as a convolution of the Fourier transform of slope with itself, which is then convolved with the transform of concavity. That the time derivative involves a convolution immediately suggests that the evolution of the elevation spectra of any k depends on the spectral evolution at surrounding wavenumbers. Note that the exponent on slope in (3.11) can be any positive odd integer for this analysis. For exponents, α, greater than three, the spectral evolution will involve $\alpha - 2$ convolutions of the transform of slope, thereby strengthening the nonlinear behavior in wavenumber domain.

To illustrate the nonlinear behavior, we place (3.13) into the context of an evolving triangle with no channel at the base. This is similar to the initial condition of a lateral moraine (*Doane et al.*, 2018). The Fourier transform $\hat{\zeta}(k)$ is itself a periodic function whose period is related to the width of the triangle. Using the rules of Fourier transforms we obtain $\hat{\zeta}_t(k)$ according to (3.13) which is also a periodic function with a similar wavelength but different phase. Wavenumbers that grow are associated with peaks of $\hat{\zeta}(k)$ but are at slightly lower wavenumber (Figure 3.2). This trend continues throughout the evolution of the moraine which means that spectral peaks migrate towards lower wavenumber. Physically this implies that the variance of the land-surface elevation is consistently transferred to lower wavenumber (longer wavelength), which is a way of degrading the land surface although it is distinctly different from the style in which linear diffusion operates.

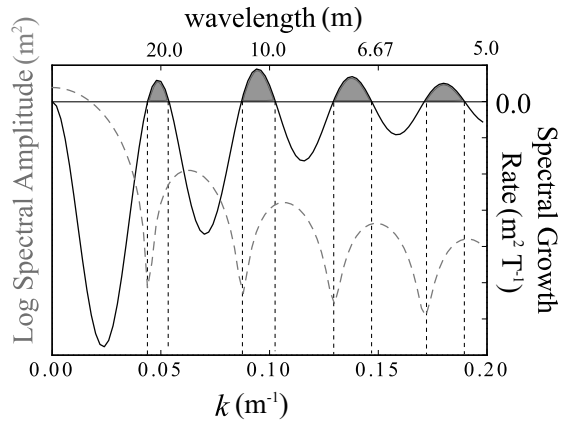

Figure 3.2: Plots of the spectral amplitude of a triangle (dashed gray line), $\hat{\zeta}(k)$, and the spectral growth rate (black line) which results from a local nonlinear flux formulation. Regions of positive growth rates are highlighted in gray and are offset from the peaks in the elevation spectrum.

3.3.3 Nonlocal Transport

The convolution integral in nonlocal formulations is the principle element distinguishing it from local linear or nonlinear diffusion. Here we highlight the impact of a convolution integral on the evolution of elevation spectra. To do so, we must consider a simplified topography for which the flux is positive everywhere and has a relatively linear slope (e.g., river terrace riser). The linear slope is important here because we cannot allow the survival function, $R(x-x',x')$, to vary with position. This is so that the dependency on x' is removed and the kernel is consistent across space which allows for the convolution theorem for Fourier transforms to be applied. With these assumptions in place, we can use the properties of the Fourier transform to illuminate the essential effect of a convolution.

Using the convolution theorem for Fourier transforms and the rules for derivatives, we write the Exner equation in wavenumber domain as

$$\hat{\zeta}_t = -ik\hat{E}\hat{R}, \tag{3.14}$$

where $\hat{E}$ is the transform of the volumetric entrainment rate, $E(x')$, and $\hat{R}$ is the transform

of the survival function, $R(x-x')$, of travel distance. Previous work has suggested that we expect most particles to travel short distances while fewer travel far which is a characteristic of exponential distributions (*Furbish and Haff*, 2010; *Furbish and Roering*, 2013; *Doane et al.*, 2018). For an exponential distribution $R(x-x')$,

$$\hat{\zeta}_t = -ik\hat{E}\frac{\mu_x}{1+ik\mu_x}, \tag{3.15}$$

where μ_x is the mean travel distance on the given slope. Note that $\hat{R}$ contains real and imaginary parts which, when expanded, have opposite signs (Figure 3.3) and the global minimum of the imaginary part occurs at $k = 1/\mu_x$. So long as the probability function of travel distance is characterized by zero mode (i.e. exponential or power-law distributions), then most particles travel short distances. A nonlocal formulation is a convolution integral which weights the impact of x' on the flux at x based on the distance, $x-x'$, with generally more weight applied to nearby locations. This is like a low-pass filter applied to the entrainment rate, which is a function of topography. By definition, low-pass filters effectively remove high-wavenumber features so that nonlinearity in the relation of mean travel distance and with slope has a subtle signature in topography. As such, nonlinearity in nonlocal formulations most likely reflects the slope-dependency of the entrainment rate. There is no single behavior that we can deduce from the form of (3.15) because the behavior depends on the form of $\hat{E}$. However, analysis using a simple topographic configuration, such as a river terrace, reveals the impact of values of μ_x.

Imagine a terrace, with the mid-point of the slope centered at the origin (Figure 3.4). The slope of the land surface is then a boxcar function centered at the origin. This condition satisfies our requirement that $R(r,x')$ be invariant with x'. Let us suggest that $E = E_1 S$, such that E is an even function and $\hat{E}(k)$ contains only real parts. In this case, spectral amplitude in all wavenumbers decay, but at a rate that differs from that of linear diffusion. In particular, the magnitude of μ_x largely determines the rate of spectral decay (Figure 3.4).

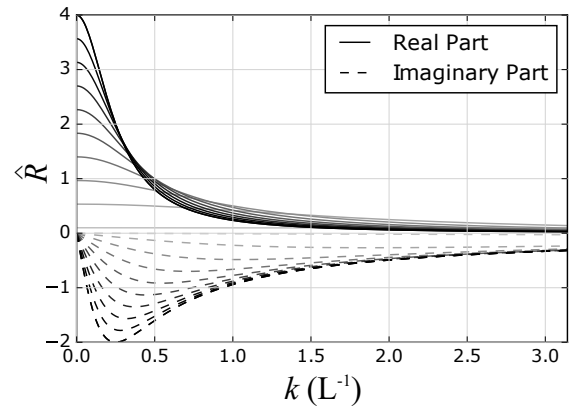

Figure 3.3: Plot of real and imaginary parts of $\hat{R}(k) = \frac{\mu_x}{1+ik\mu_x}$ for $\mu_x = 0.1$ to $\mu_x = 4.0$. Lighter colors correspond with smaller values of μ_x.

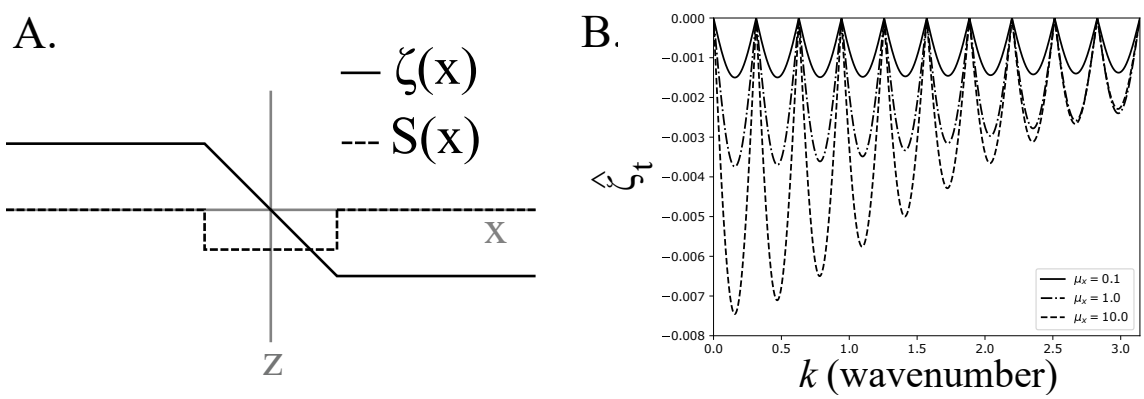

Figure 3.4: A. Plots of land-surface elevation and land-surface slope for a terrace centered on the origin. B. Plots of $\hat{\zeta}(k,0)$ (gray) and spectral growth rates for different values of μ_x.

This is a special case, but it effectively illustrates the behavior of the land-surface spectra as a result of convolution. There is inherent complexity; however, in general, we observe that long travel distances more rapidly diminish the low-order structure (Figure 3.4B).

3.3.4 Summary of Behaviors

We review the three basic behaviors for linear and nonlinear diffusion and nonlocal transport in wavenumber domain. First, linear diffusion results in spectral evolution in which spectral amplitudes at all wavenumbers, k, decay at a rate proportional to the amplitude and k^2. We classify this as vertical spectral decay because it diminishes spectra

locally. Second, nonlinear processes involve convolutions of functions related to the land-surface spectrum. We note that this operation tends to migrate spectral amplitude to lower wavenumber, which we classify as compressional spectral decay. Spectral compression temporarily results in amplitude growth in certain bands of wavenumbers, which is interpreted as a signal of nonlinear processes. Last, the presence of the convolution integral in a nonlocal formulation highlights the impact of the length-scales of the kernel, $R(x-x')$. Spectral migration or vertical decay is determined by the slope-dependency of the entrainment rate, but is then modified by the survival function of particle travel distance. Therefore, nonlocal formulations can display linear or nonlinear behavior of the entrainment rate, but it differs from local formulations according to the form of the survival function of travel distance. As such, distinguishing nonlocal behavior in land-surface evolution from local nonlinear or linear diffusion may be challenging and require field observations, as described next.

3.4 Applications: natural landforms

In this section we apply the theory developed in section 4 to three different topographic configurations: a lateral moraine, an incised lateral moraine, and a river terrace. Topographic data from all examples were collected using either a self-leveling transit or a Laser Range-Finder™, with horizontal spacing of 1-3 meters. We use these landforms because they have well-known and simple initial conditions. This allows us to compare the transform of the initial condition with that of the observed form to reveal the style of spectral evolution. However, in natural conditions, we must acknowledge that biogeomorphic processes tend to roughen the surface, and therefore are expected to add spectral amplitude (*Jyotsna and Haff*, 1997; *Booth et al.*, 2017). If enough variance is added to the land surface through roughness elements, then we run the risk of misinterpreting apparent added variance as a signature of nonlinear processes. Before we present natural examples, we show that, so long as the landform in question is much larger than the biogeomorphic

roughness, the roughness signal is negligible.

We begin with a statistical representation of topographic noise. At a horizontal resolution of a meter or less, topographic elevation at any point is likely to have a value similar to the value of points around it. We represent this idea statistically by suggesting that topographic noise is an autoregressive process of order one, "AR(1)". Mathematically we write this as,

$$\zeta_B(j+1) = \phi_B \zeta(j) + w(\sigma_w^2), \tag{3.16}$$

where ζ_B is the land-surface elevation due to roughness, j refers to a node, ϕ_B is the AR(1) parameter, and $w(\sigma_w^2)$ is white noise with variance σ_w^2. The amplitude spectrum of a profile generated by (3.16) has an analytical form (*Box et al.*, 1976) (Figure 3.5),

$$\hat{\zeta_B} = \sigma_\zeta^2 \left[\frac{(1-\phi_B^2)}{1-2\phi_B cos(2\pi k) + \phi_B^2} \right]^{1/2}. \tag{3.17}$$

For the semi-arid environments considered in this paper, land-surface variance due to biogeomorphic roughness, σ_ζ^2, is on the order of decimeters (*Jyotsna and Haff*, 1997), and so $\hat{\zeta}(k)$ is at most ~ 1 m^2. Spectral amplitudes of landforms considered in this paper are much greater than 1 m^2 and over geomorphically-relevant timescales, spectral decay due to linear diffusion is much greater that the magnitude added by roughness. That is, we expect the degree of spectral decay to be much greater than 1 m^2 over timescales of 1 ka-10 ka in most wavenumbers. Therefore, the risk of misinterpreting apparent spectral growth due to noise is minimal for relatively large and old landforms (10s of meters and ka). With this in place, we continue with natural examples and interpret any positive spectral growth rates as a result of the style of sediment transport.

3.4.1 Initial Conditions

The initial conditions for all landforms that we consider are assumed to be at or near angles of repose for the particular material. For glacial material this is a slope of 0.63–

0.67 (*Putkonen et al.*, 2008). We assume negligible losses to chemical weathering so that conservation of mass demands that the integrals of the initial and observed conditions are equal. These two constraints allow for a mass-conserving estimate of the initial condition.

The initial conditions are a series of planar surfaces that abruptly change slope. There is the possibility that actual initial conditions contain more rounded corners. Rounding corners, however, reduces the overall topographic variance, which, in wavenumber domain, is manifest as a reduction in spectral amplitude. Therefore, the spectral growth that is apparent in the examples below cannot be explained by errors in the initial condition. We formally show this in Appendix 0.1.

3.4.2 Lateral Moraine, Bloody Canyon, CA

Lateral moraines have been the subject of several previous papers that document the degradation of topography (*Putkonen et al.*, 2008; *Madoff and Putkonen*, 2016; *Doane et al.*, 2018) because we know their initial condition and have reasonable estimates of their age. Here we focus on a lateral moraine that emerges from Bloody Canyon in the eastern Sierra Nevada. There are a suite of glacial advances recorded in the nested moraines of Bloody Canyon. However, we present the analysis for a single lateral moraine that is 40 - 50 ka (*Kaufman et al.*, 2003; *Rood et al.*, 2011; *Schaefer et al.*, 2006; *Phillips et al.*, 2009). The specific age of the moraine is unimportant for our purposes because we are simply identifying a style of evolution, not rates of evolution. The general post-glacial evolution of a lateral moraine is as follows. While the glacier is active, the interior sides are supported by the glacier and are therefore oversteepened. Following recession, the side-slopes rapidly adjust to the angle of repose, which for glacial till is ~ 0.67. Meanwhile, the exterior slope remains at approximately the angle of repose during glaciation such that the initial condition is a triangle (*Putkonen et al.*, 2008). When the glacier recedes, hillslope transport then alters the form of the moraine. For this analysis, we determined the initial condition by finding a triangle with slopes of 0.67 that integrates to the area under the

observed profile. Comparing the transform of the initial condition and that of the observed, we see that certain spectral bands have grown (Figure 3.6). The location of spectral peaks in the observed transform are offset to lower wavenumber from those in the initial spectrum. Such a behavior is consistent with the analysis for nonlinear processes.

Previous work shows that both nonlinear and nonlocal models are capable of producing profiles that closely match the observed profiles in this location. Therefore, both models exhibit spectral growth (*Doane et al.*, 2018). Field evidence supports the presence of nonlocal processes and, in this case, the entrainment rate for nonlocal transport contains a nonlinear term, which is responsible for spectral growth and compression to lower wavenumbers. To illustrate this point, we numerically simulated the evolution of a moraine using a nonlocal model with a nonlinear entrainment rate (Figure 3.7). Numerical results show spectral compression, in which amplitude is advected to lower wavenumber. However, the spectrum also becomes smoother, which highlights the modifying effect of the kernel. That is, the linearity or nonlinearity of the entrainment rate, $E(x')$, determines the basic behavior, which is then modified by the kernel.

3.4.3 Fluvial Terraces, Jackson Hole, Wyoming

The iconic terraces that flank the Snake River east of the Tetons are particularly well-suited for this type of analysis (Figure 3.8). Since the LGM, the Snake River has incised into the glacial outwash plain (*Love*, 2000), leaving a series of fluvial terraces. Similar terraces have been the subject of previous work which suggests that linear diffusion does not accurately describe the evolution of fluvial terraces or fault scarps of the region (*Nash and Beaujon*, 2006). This work also suggests that hillslope diffusivities scale with landform size, and therefore the flux increases with height. That the flux scales with landform size suggests that nonlocal processes are significant in this setting because longer slopes allow for greater upslope contributions to downslope fluxes with nonlocal formulations like (3.4).

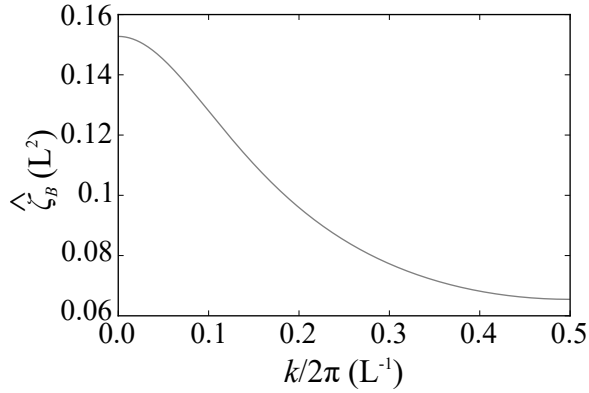

Figure 3.5: Spectrum of an AR(1) process for $\sigma_\zeta^2 = 0.1$ and $\phi_B = 0.4$.

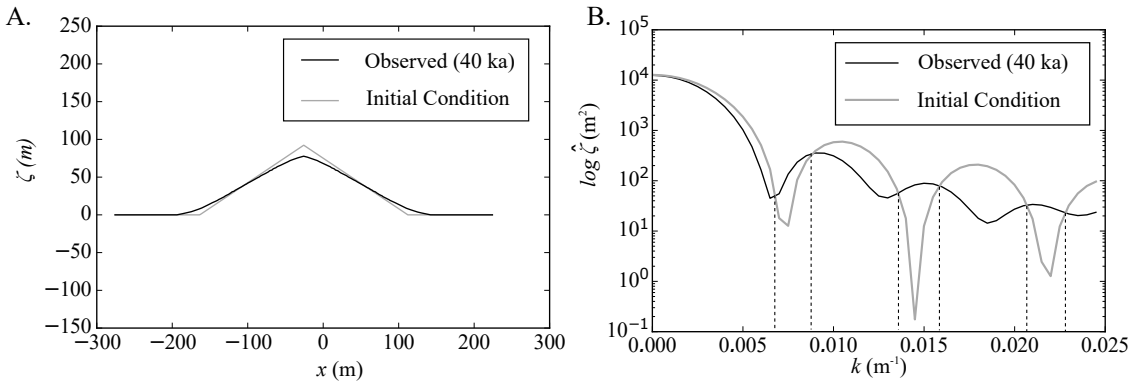

Figure 3.6: A. Initial and observed profiles of a lateral moraine B. Transforms of initial and observed profiles. Dashed lines denote the boundary of narrow bands that have spectral growth.

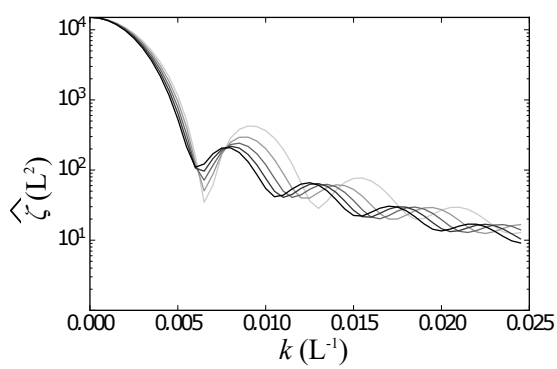

Figure 3.7: Amplitude spectra of a nonlinear and nonlocal numerical simulation of an evolving moraine. Lines represent 20ka intervals with lightest lines representing the oldest profiles.

Figure 3.8: A. Image of the riser between T2 and T3. In order to highlight the terrace, the T2 is shaded in gray, and the surface of the terrace slope is highlighted in the white dashed line. B. Sediment grain sizes appear to be clustered together and compose a sediment capacitor behind shrubs.

We surveyed a flight of two terraces, T3 and T2. T3 is higher than T2 and therefore must be older and post-date Pinedale glaciation (∼15 ka) (*Love*, 2000). Like the moraine, these features are capable of illuminating the details of sediment transport because the initial condition is relatively well constrained. We assume an initial condition with slope of 0.65 which corresponds with the angle of repose for glacial material (*Putkonen et al.*, 2008). On the face of terraces, boulders tend to accumulate behind shrubs. We interpret this observation as evidence of capacitor-style sediment transport, where boulders roll downslope until motion is impeded by a shrub (*Lamb et al.*, 2011, 2013; *DiBiase and Lamb*, 2013). This process continues and the area immediately upslope of the shrub gathers more boulders creating a small boulder field. The boulder field serves to capture more boulders setting up a positive feedback. If the boulder field becomes unstable by either a shrub dying or another event, then these boulders are available for transport. Larger grain sizes tend to travel further as they roll over surface roughness elements without losing as much momentum as smaller particles (*DiBiase et al.*, 2017). Therefore, such boulder fields represent a likely source for nonlocal transport. This is just one source of nonlocality and there may be other mechanisms for long-distance transport, for example, those involving motions initiated by

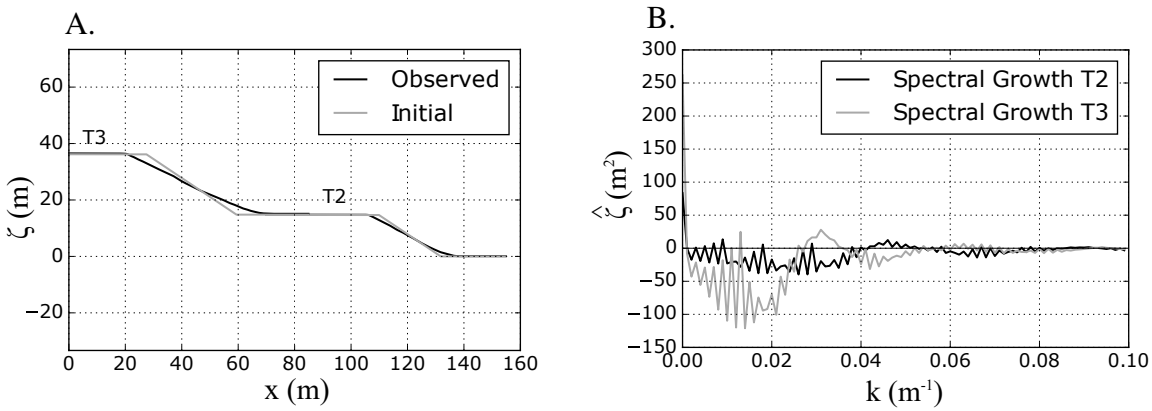

Figure 3.9: A. Profile of a flight of terraces flanking the Snake River with gray profile being an idealized initial condition. B. Spectral growth of T2 and T3 over their respective ages. Note that we have done the analysis for each terrace individually, but plotted them together in their natural configuration.

snow or large animals (i.e. elk, moose, bear).

We generated spectra for each terrace individually over the same domain length. We plot spectral growth, $\Delta\hat{\zeta} = \hat{\zeta}_T - \hat{\zeta}_0$ (Figure 3.4), because the transforms of terraces are well-defined but quite messy. There is more growth in T3; however, T2 also shows definitive growth. Wavenumbers that grow correspond with the width of the terrace riser and its harmonics. Spectral growth in this style is consistent with the style from moraine evolution and suggests that sediment transport contains a nonlinearity with slope. Given the evidence for nonlocal transport by temporary storage and release of boulders among other nonlocal processes, we suggest that a nonlinearity with respect to slope is present in either the entrainment rate, E, the pdf of travel distance, or both.

3.4.4 Incision into a plain

The two previous examples represent topographic configurations that lack a channel boundary. In order to explore the impact of a moving boundary condition, we consider a plain that is incised by a channel. Let us suggest that the channel incises at a uniform rate. Mathematically, we represent incision as a unit step function of magnitude v [L T^{-1}], which

has a transform that is a uniform function with value v (*Poularikas*, 1998). In the absence of hillslope processes, pure incision would cut a canyon with vertical walls, whose transform is a uniform function with value vT, where T is the duration of incision. Adding hillslope processes to this scenario relaxes the side-slopes and alters the uniform transform. The style in which side-slopes relax according to linear and nonlinear transport are expected to be different and highlighted in wavenumber domain.

We begin with linear diffusion. With reference to (3.9), we note that over every interval of time for which $v\Delta t$ is added to the spectrum by pure incision, this signal is counteracted by linear diffusion which retards the growth of the spectrum at high wavenumbers. The evolution of the spectrum is

$$\hat{\zeta}_t(k) = v\Delta t - k^2 D\left(v\Delta t + \hat{\zeta}(k)\right) . \tag{3.18}$$

Consider the initial incision into a plain. After Δt, the transform of the land surface is

$$\hat{\zeta}(k,\Delta t) = v\Delta t\left(1 - k^2 D\right), \tag{3.19}$$

which is a monotonically decreasing function of k. With continued evolution, this basic form remains, but the magnitude changes. In this case, continued incision drives wholesale addition of variance to the system, so spectral amplitude is expected to grow and growth is not a signature of nonlinear processes. However, the adjustment of side-slopes will reveal different behaviors in wavenumber domain.

To compare models, we numerically simulate this condition. In all cases, continued land-surface evolution leads to transforms that share the low order structure. That is, broadly, all spectra decay approximately exponentially with k. However, elevation spectra for nonlinear and nonlinear nonlocal models have a periodic signal that changes the high-order structure (Figure 3.10 B & C). In the spatial domain, the high order structure reflects the relatively sharp concavity that is maintained at the knuckle of the facet (Figure 3.11).

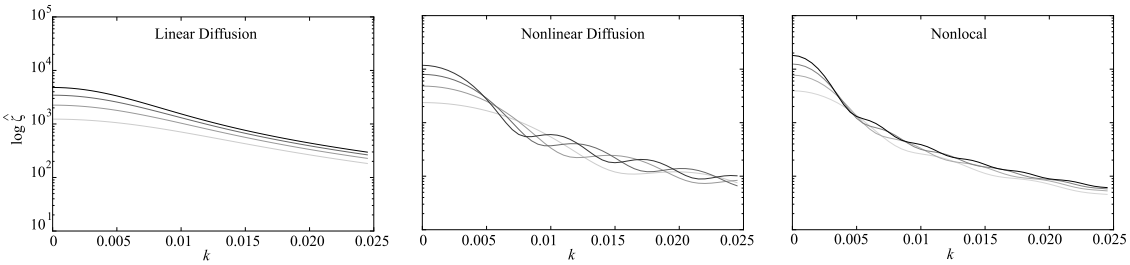

Figure 3.10: Amplitude spectra of land-surface elevation from numerical models simulating channel incision and hillslope relaxation. The older profiles correspond to lighter colors. Field data of untransformed profiles for this scenario are presented in figure 3.12A.

We test this idea with a natural example by looking at a buttressed LGM lateral moraine near Twin Lakes, CA, that has been incised since deposition. While the glacier is active, the lateral moraine is buttressed by the valley walls and sediment is supplied by the hillslope and the active glacier, such that the lateral moraine becomes a flat bench (Figure 3.11A). When the glacier recedes, sediment supply diminishes and the extant channel can begin to incise through the flat moraine (Figure 3.11B). As incision continues, hillslope processes act on the facet that is created and the facet geometry reflects the mechanics of sediment transport. Incision begins at the edge of the bench, where it drops to the valley floor, and works back to the extant channel. As such, the portion of the facet nearest the valley has the longest incision history. We surveyed two profiles along one facet, one close to the edge of the bench and one closer to the buttressing hillslope. The profiles are of different lengths and have been associated with active incision for different timespans or rates.

Profiles along a facet of the incised moraine are relatively straight and high concavity characterizes the knuckle of the facet (Figure 3.12A). In wavenumber domain, both profiles exhibit a non-monotonically decreasing spectra with quasi-periodic peaks and troughs. Such behavior is mirrored in nonlinear simulations of this scenario where the spectrum is a decaying periodic function with $|k|$ (Figure 3.10). In our natural example, we observe strongly nonlinear behavior with the spectrum periodically approaching zero (Figure 3.12 B). The higher-order structure contained in this transform reflects the high concavity con-

tained in the knuckle of the facet and is a signature of nonlinearity of transport. In this case, field evidence for nonlocal transport is not readily evident although it is likely that nonlocal processes occur here as they do for the example of the lateral moraine.

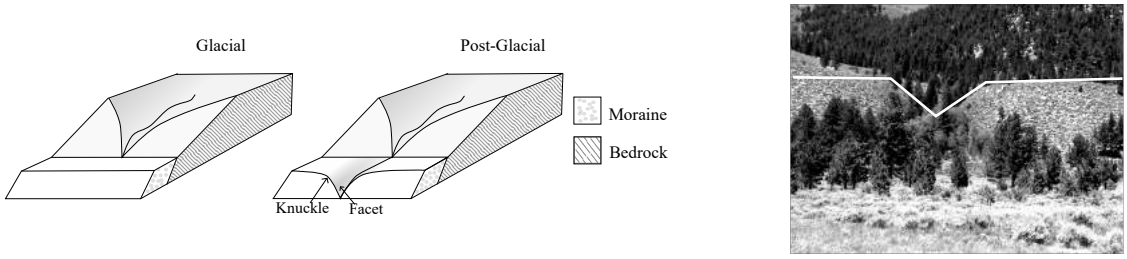

Figure 3.11: (A) Block diagram showing the evolution of a buttressed moraine. The facet is the surface that forms from post-glacial incision through the lateral moraine. The knuckle of the facet is the location at the top of the slope where the surface rolls over to horizontal. (B) Photograph of the facet surveyed at Twin Lakes, CA. The white line outlines the land surface. In both figures, the moraine is 50 meters tall.

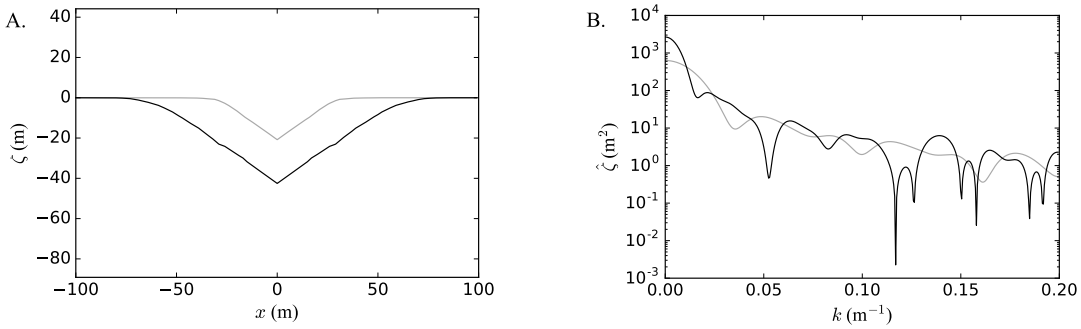

Figure 3.12: A. Land-surface profiles of incised moraine. B. Fourier transforms of profiles. Line colors correlate between A and B. Note the semi-periodic structure of the spectra that is present, suggesting a nonlinearity in the transport process. Refer for Figure (3.10) for the behaviors associated with different models.

3.5 Application: acoustic hillslope experiments

To further illustrate spectral behavior of land-surface evolution associated with nonlinear transport, we conducted experiments of a simulated hillslope on an acoustic table (*Roering et al.*, 2001b). This experiment generates a nonlinear particle flux with slope (Figure

3.13A) and we expect to observe behaviors laid out above. The hillslope is a quasi-one-dimensional pile of unconsolidated spherical silica beads with relatively uniform grainsize from 0.5 mm - 0.75 mm. The pile is constrained between two plexiglass walls that are about 15cm apart. We sculpted an initial condition at or near the angle of repose and flanked by a long flat run-out - similar to the initial condition of a lateral moraine. The entire experiment is placed on top of a large speaker which transmits acoustic waves of white noise through the experiment. The acoustic waves break particle force chains which allows for particles to move downslope in a manner that exhibits glassy or creep-like behavior.

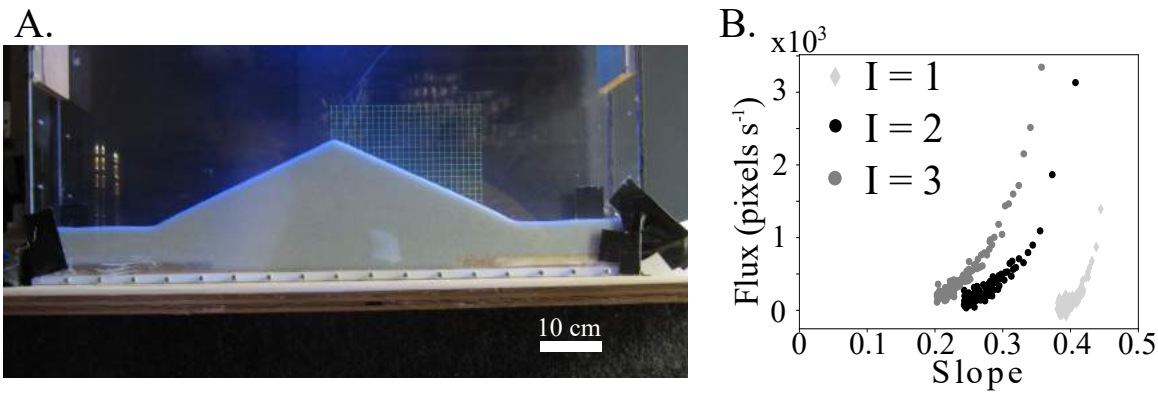

Figure 3.13: A. Photo showing the experimental set-up. B. A plot of the volumetric flux versus slope. The flux here was calculated by integrating the difference between successive profiles. The noise in these plots are due to errors in profile extraction, averaging slope over long distances, and averaging slopes between successive photos. Photos were taken every five seconds and three volumes are represented by different intensities as I. Compare with Figure 1A of *Roering et al.,* 2001.

We track the evolution of the surface to observe the behavior of nonlinear transport processes. To do so, we placed the experiment in a dark room and highlighted the surface with a black light. Highlighting allows for a simple image analysis to determine the elevation of the surface (Figure 3.13). However, the light penetrates several glass bead diameters deep so a filter algorithm is not entirely smooth, which produces artificial roughness. The magnitude of these artifacts are small compared to the profile and they have negligible impact on the relevant parts of the spectra because the variance added by this noise is significantly smaller than the total variance of the landform (Figure 3.14). Each experiment was run

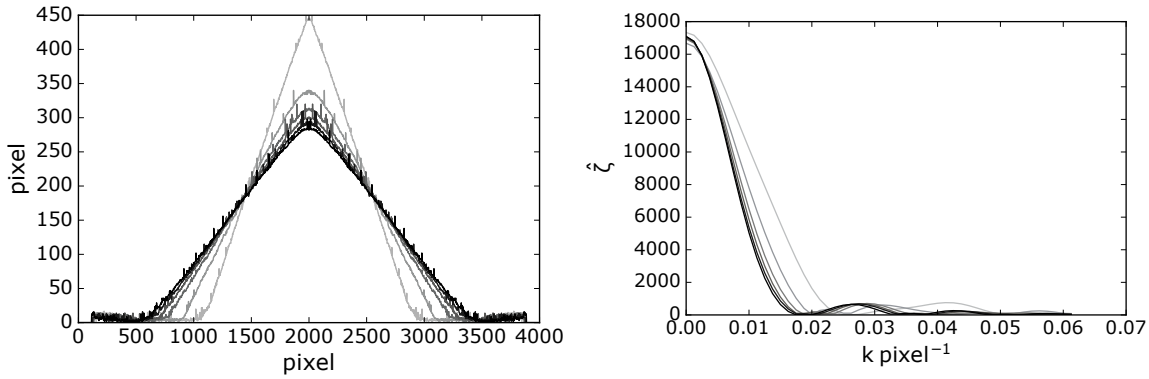

Figure 3.14: A. Profiles of the surface elevation in pixels B. Transform of the surface elevations through time. In both plots, lighter colors correspond with older profiles. These results are from an experimental trial with intensity 2.

until the flux became negligibly small – typically several hours.

Results from this experiment reveal that as the surface evolves, the profile maintains sharp concavities, which is consistent with a nonlinear flux formulation. In wavenumber domain, the profiles maintain the high order structure throughout the evolution. However, over the experimental time, the high order structure consistently migrates to lower wavenumber. Observation of the evolution of this profile in arithmetic and wavenumber domain in concert provides an illustration of a central point of this paper. Note that in the spatial domain, the evolution of the profile is essentially elastic (*Schumer et al.*, 2017). In wavenumber domain, basic elastic behavior is captured as the total spectral amplitude is reduced. However, for nonlinear systems, spectral amplitude migrates to lower wavenumbers to produce a smoother profile, whereas linear systems are characterized by vertical reduction of the spectrum. Therefore, the fate of this profile is qualitatively the same as would be under linear diffusion. We argue that this is an effective illustration that linear and nonlinear processes qualitatively result in similar spatial domain evolution although fundamentally different styles of spectral evolution.

3.6 Discussion

3.6.1 Two end-members for the destruction of variance

At this point, we consider two fundamentally different paths by which the land surface can evolve – straightening and lengthening. Straightening refers to rounding sharp concavities, which tends to degrade topographic highs and fill in hollows for conditions that lack external control on the boundary conditions (channel incision, uplift). Lengthening implies that topographic forms become wider, but meanwhile maintain sharp concavity. Both methods are mass-conserving and result in a reduction of topographic variance. As such, they are reasonable descriptions of topographic evolution. We associate straightening with linear diffusion, as it effectively diminishes sharp concavities. On observation of Figures 3.6A and 3.14A, we note that nonlinear processes are effective at lengthening topographic forms. With these distinctions in place, we question which topographic forms display nonlinear behavior and which ones might obscure it.

In the examples presented above, topographic lengthening in the spatial domain is represented by compression in wavenumber domain. For illustration, consider the transform of a triangle,

$$\hat{\zeta} = LH \left(\frac{\sin(\frac{kL}{2})}{\frac{kL}{2}} \right)^2, \tag{3.20}$$

where L [L] is one half the triangle width, and H [L] is the triangle height. When a triangle is stretched in a mass-conserving way, the lengthening is accommodated by flattening. In the wavenumber domain, this results in a translation of the transform to lower wavenumbers. We mathematically describe compression as advection to lower wavenumbers; however, to maintain periodicity, the magnitude of advection, c, must increase linearly such that $c(k) = -\gamma k$, where γ [T^{-1}] is a rate constant that reflects the rate of stretching (Appendix 0.2).

Imagine a triangle that is lengthened by increasing L and decreasing H. Conservation

of mass demands that $A = HL$ remains constant as stretching occurs. Placing $c(k)$ into an advection equation,

$$\frac{\partial \hat{\zeta}}{\partial t} = -\gamma k \frac{\partial \hat{\zeta}}{\partial k} + W(k), \tag{3.21}$$

where $W(k)$ is a sink term. We use Leibniz notation for derivatives here to be consistent with typical representation of advection equations. Insofar as topographic stretching results from nonlinear transport processes, we suggest that the advective component of (3.21) results from the nonlinear transport and $W(k)$ represents the loss of spectral amplitude due to linear diffusion,

$$W(k) = -k^2 D \hat{\zeta}. \tag{3.22}$$

Recall that a nonlinear formulation for sediment transport contains a linear term as in (3.11) so this formulation can effectively represent a nonlinear model in wavenumber domain. We note that spectral compression is only a kinematic description of the evolution of the spectra and is a simplification of the actual process. However, casting nonlinear systems this way provides a simple way to investigate which topographic configurations highlight distinctive behaviors between linear and nonlinear processes.

We suggest that a combination of topographic stretching (spectral compression) and straightening (spectral decay) that corresponds with the relative magnitude of nonlinear and linear processes accounts for landform evolution. However, because the first-order control on sediment transport is slope, the rate of stretching must decline as slope reduces. We add a modulating term, $m(t)$ to c (Appendix 0.2), which is a dimensionless coefficient that relates the dependency of c to the land-surface slope. We represent the impact of m by plotting the rates of spectral advection (stretching), $c(k,t)$, with that of vertical spectral decay (straightening), $W(k)$. With continued evolution, the magnitude of spectral celerity continues to slow whereas the ability for linear diffusion to destroy variance remains constant (Figure 3.15). Therefore, certain topographic configurations may initially exhibit nonlinear behavior that gives way to linear diffusion. Indeed we observe this pattern in

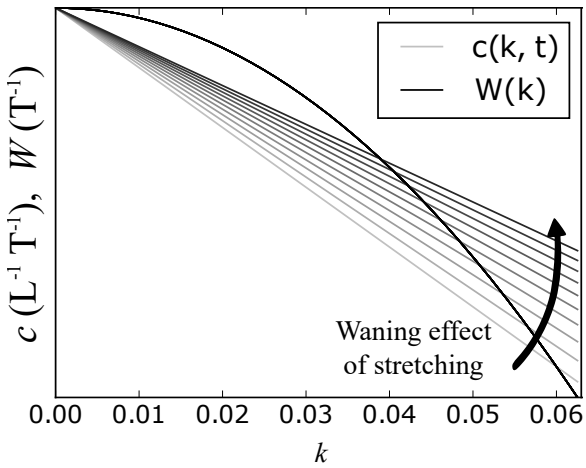

Figure 3.15: Spectral celerity from nonlinear processes (grayscale lines) and spectral decay rates from linear diffusion through time. Although not directly comparable due to different units, the spectral celerity, c decays with time whereas the rate constant associated with spectral decay for linear diffusion remains constant. Lighter lines represent celerities at earlier times in topographic evolution.

numerical simulations of an evolving moraine, where early spectral growth is rapid and contained in high wavenumbers but gives way to slower growth rates in lower wavenumbers. Eventually, spectral compression becomes negligible and evolution approaches linear behavior (*Doane et al.*, 2018).

Certain topographic configurations are likely to exhibit nonlinear behavior more clearly than others. We have identified that positive spectral growth can be a signature of nonlinear processes. This occurs because nonlinear processes drive compression in the wavenumber domain. Therefore, any spectra with a positive gradient with respect to k will temporarily grow as spectral amplitude is advected towards the origin. A positive gradient in wavenumber domain often implies a spectra that contains finite amplitude in its high-order structure, which typically reflects sharp concavities in the spatial domain. Most topographic features for which we have reasonable estimates of the initial condition contain sharp concavities (i.e. lateral moraines, terraces, incised plains), and therefore these features are effective tools for identifying the style of sediment transport that occurs on them.

Whereas certain topographic configurations will highlight nonlinear and nonlocal trans-

port, there are others that may obscure such behavior in wavenumber domain. If nonlinear processes are most clearly observed in spectra that have positive gradients with respect to k, then those that lack positive gradients will not highlight nonlinear processes. Spectra with only negative gradients can only show spectral decay by both nonlinear and linear diffusion, obscuring the distinguishing behavior. To be clear, spectra with only negative gradients may still evolve differently according to the three transport models, but the differences will be subtle. A spectrum for which nonlinear behavior is completely matched by linear diffusion does exist. By rearranging (3.21) to set the advection and sink terms equal to each other

$$-Dk^2\hat{\zeta} = \gamma k\frac{d\hat{\zeta}}{dk}. \tag{3.23}$$

Separating variables and integrating then reveals that a spectrum with a form

$$\hat{\zeta}(k) = e^{-\frac{Dk^2}{2\gamma}} \tag{3.24}$$

will momentarily evolve identically according to linear and nonlinear processes. The inverse transform of (3.24) is itself a Gaussian function and the land-surface profile is

$$\zeta(x) = \sqrt{\frac{\gamma}{D}}e^{-\frac{\gamma x^2}{2D}}. \tag{3.25}$$

In contrast to triangles or terraces, Gaussian functions effectively distribute concavity over the entire function such that no single point is characterized by high concavity values. Although the form presented in (3.25) completely obscures the distinction between nonlinear and linear diffusion, forms that share the characteristic of having relatively small concavity will effectively obscure diagnostic behavior.

This analysis returns us to the comparison between a triangle and a Gaussian (Figure 3.1). We have noted that despite clear differences between the functions, a triangle can explain much of the variance of a Gaussian, which is noted in the shared low-order structure.

Insofar as we can suggest that sediment transport is slope-dependent then linear diffusion is a first order description of land-surface evolution. Gaussian profiles have the unique property that the functional form remains the same throughout evolution according to linear diffusion. An initial Gaussian form remains a Gaussian during diffusion, but the amplitude is reduced. Therefore, although a rigid definition for low order structure is difficult to determine, we suggest that the best-fit Gaussian form is the low-order structure for a given landform. The high-order structure then is contained in the part of the spectrum that deviates from that Gaussian form. This is a working definition and there are perhaps other equally satisfying definitions.

3.7 Conclusion

We have shown that linear and nonlinear processes are associated with different spectral behaviors. Linear diffusion unambiguously shows spectral decay in every wavenumber. Nonlinear diffusion drives a compression of the spectrum to lower wavenumbers which can result in growing spectral amplitudes. Nonlocal transport can display linear or nonlinear behavior – depending on the form of the entrainment rate. The effect of the probability function of travel distance, however, is to modify the linear or nonlinear behavior (Figure 3.3), although it may be subtle. For example, the evolution of a hillslope formed by incision into a plain shows similar spectral evolution for nonlinear diffusion and nonlocal transport (Figure 3.10).

These signatures are readily distinguished for land-surface configurations that have an initial or previously known condition. We recognize we can only know this for a small portion of the landscape, but if such a feature can be identified, the mechanistic style may be applicable to the entire region. For example, even in the quasi-steady state landscape of the Oregon Coast Range, there are fluvial terraces preserved (*Almond et al.*, 2007), which may offer some clues to the mechanistic style of sediment transport. Furthermore, whereas concavity can be used to identify nonlinear versus linear diffusion in steady state hillslopes,

the spectral evolution is applicable to transient scenarios.

We have demonstrated that the three common transport models are elastic (*Schumer et al.*, 2017) as they contain slope as a central ingredient. As such, they tend to degrade topography and, in the absence of tectonic forcing, the land surface evolves towards zero variance. In wavenumber domain, we see that there are two distinct ways to do this. Linear diffusion drives a vertical variance destruction, which decays spectral amplitude in place. Nonlinear processes tend to compress all of the variance into consistently lower wavenumbers. Ultimately, when all spectral amplitude is contained in the zero wavenumber, the land surface has reached zero variance.

Chapter 4

Hillslope sediment particle rest times and the influence of capacitors

4.1 Introduction

Sediment transport is the dynamic centerpiece of geomorphology. At grand scales sediment transport drives landscape evolution and at small scales it results in the formation and translation of bedforms. Across all scales, any given particle can occupy one of two states: motion or rest. Relating the underlying physics of sediment transport to the motions of all particles and the durations of periods of rest is complex – obscured by the effects of turbulence (*Fathel et al.*, 2015), psuedo-random external perturbations such as rainsplash (*Furbish et al.*, 2009a), and a the effects of a variety of grainsizes (*Hill et al.*, 2010) among other properties. To overcome the challenges of complexity, one way researchers learn about the dynamics of sediment transport is to study the behavior of a cohort of tracer particles.

A tracer particle is one that is tagged either naturally or unnaturally and whose motion is tracked through time. By tracking these particles, researchers are able to characterize the periods of rest and motion. Painted stones (*Einstein*, 1937), radioactively tagged particles (*Sayre and Hubbell*, 1965), and radio frequency identification particles (*Nichols*, 2004) are unnatural tracers. Recently, high-speed imaging has allowed for a great number of particles to be tracked in a flume (*Fathel et al.*, 2015, 2016; *Furbish et al.*, 2017). Natural tracers are cosmogenic radionuclide concentrations (*Lal*, 1991; *Gosse and Phillips*, 2001; *Granger et al.*, 2013), optically stimulated luminescence (*Heimsath et al.*, 2002), or fallout nuclide concentrations (*Kaste et al.*, 2006; *Ritchie et al.*, 2005) of a particle which all accumulate and/or degrade depending on the path of a particle (*Furbish et al.*, 2018). The trajectories of a great number of tracer particles provide information regarding the distributions of particle

travel distances and rest times and so they are the subject of many studies (*Einstein*, 1937; *Sayre and Hubbell*, 1965; *Nikora et al.*, 2001; *Schumer et al.*, 2009; *Voepel et al.*, 2013; *Fathel et al.*, 2015; *Bradley*, 2017; *Martin et al.*, 2012; *Phillips et al.*, 2013).

Rest is the dominant state for particles at Earth's surface. In channels however, the dynamics are fast enough that a great number of periods of transport occur over timescales that are suitable for human observation (*Fathel et al.*, 2015). This is not true for particles on hillslopes. We rarely have the luxury of observing a natural particle 'hop' and therefore human observation is an unproductive approach to characterizing periods of rest and motion. However, in the past decade a new class of models has been developed that explicitly includes a theoretical description of the particle travel distance probability distribution (*Furbish and Haff*, 2010; *Foufoula-Georgiou et al.*, 2010; *Tucker and Bradley*, 2010). These models, collectively known as nonlocal models, have been the subject of a modest number of papers aimed at characterizing travel distances by dropping stones and measuring how far they travel (*Gabet and Mendoza*, 2012; *DiBiase et al.*, 2017). Whereas there are relatively simple methods to simulate and measure particle travel distances, there is no way to do the same for particle rest times. Therefore, a full treatment of tracer particle behavior on hillslopes must appeal to a theoretical foundation for particle rest times.

In this paper, we develop the first hillslope-specific theoretical treatment of particle rest times. We have two goals. First, we highlight the essential characteristics of a distribution of particle rest times on hillslopes. Second, because there is a legacy of probabilistic descriptions of rest times in fluvial settings, we address the similarities and differences. The treatment is not comprehensive and is most applicable to steep hillslopes in arid to semi-arid settings. This specificity is only because the sparse vegetation and rapid particle movement makes the process simplest to visualize, but the mathematics would be similar in other settings.

Distributions of rest times and travel distances are of interest because previous work has recognized the relationship between these distributions and the dispersion of a cohort

of tracer particles (*Schumer et al.*, 2009; *Martin et al.*, 2012; *Phillips et al.*, 2013; *Voepel et al.*, 2013; *Bradley*, 2017). Three behaviors characterize the variance of particle positions, $\sigma_x^2(t) \sim t^\alpha$ [L^2], through time: subdiffusion, normal diffusion, and super-diffusion. For normal diffusion, the exponent $\alpha = 1$, sub- ($0 < \alpha < 1$) and superdiffusion ($1 < \alpha < 2$) are examples of anomalous diffusion. When distributions of rest times or particle travel distances are heavy-tailed (i.e. they decay slower than an exponential distribution) particle dispersion can be anomalous (*Bradley*, 2017; *Weeks and Swinney*, 1998). If both of these distributions decay at least as fast as an exponential, then the central limit theorem applies and $\alpha = 1$ (*Bradley*, 2017). These behaviors are well-defined and have a legacy of exploration in physics (*Weeks and Swinney*, 1998) and geosciences (*Einstein*, 1937; *Sayre and Hubbell*, 1965; *Nikora et al.*, 2001).

Quantifying the rate of sediment transport is a common goal in geomorphology. Techniques to do so involve sampling sediment on the surface and measuring the concentration of naturally occurring nuclides that accumulate in grains with time. A mass-balance considering the production and decay of nuclides along with the transport of sediment allows quantitative measurement of the pace of sediment transport over geomorphic timescales. However, although we infer rates of sediment transport from the concentrations of nuclides in tracers, the problem of the actual behavior of tracer particles on hillslopes has not yet been addressed. This is particularly relevant for the ^{137}Cs tracer, which is a fallout nuclide that spiked during the mid-twentieth century due to nuclear weapons testing. Between 1955 and 1967, the majority of the world's ^{137}Cs was deposited evenly around the Earth's surface (*Ritchie et al.*, 2005). Spatial patterns of ^{137}Cs concentrations then inform the pace of sediment transport. The spatial distribution and interpretation of rates may vary if particles disperse normally or anomalously. The work below is a contribution towards perhaps refining the interpretations of natural tracers. There may be similar applications for other naturally occurring meteoric tracers such as ^{7}Be and ^{10}Be.

This paper addresses several important items that affect particle rest time distributions,

each of which builds off of the previous item. We begin with a treatment of rest times that occur on a barren sediment surface where particles are entrained randomly. We then add hillslope capacitors which form temporary dams on hillslopes behind which sediment wedges accumulate. Previous work explores the geometry of these wedges (*Lamb et al.*, 2013) and they have been shown to be major stochastic sources of sediment to channels (*Lamb et al.*, 2011; *DiBiase and Lamb*, 2013). We define a slightly different geometry for the wedges than *Lamb et al.* (2013) and we expect that the details of the geometry are not central to the interpretations of the results. Sediment wedges bury otherwise mobile particles thereby extending their rest times until the dam fails, at which point all particles contained within the wedge are entrained. The distribution of rest times within a single wedge behind a capacitor reflect the growth rates, which we can determine with some reasonable assumptions. Finally, we extend the analysis to an entire hillslope and identify a range of rest time distributions for different distributions of capacitor ages and spatial areal concentrations.

4.2 Probabilistic Model

We begin with a definition of an active layer for hillslope particles. We borrow from theory of rest times in fluvial settings in which *Voepel et al.,* (2013) define an active layer as the thickness of unconsolidated sediment. Beneath this layer of sediment is a rigid bed, which periodically coincides with the surface. On hillslopes, although the soil mantle has a finite thickness, the land surface rarely visits the bedrock, but particles in the soil mantle do move by creep-like processes (*Culling*, 1963; *Fernandes and Dietrich*, 1997; *Furbish et al.*, 2009a). Therefore defining an active layer on hillslopes is challenging. Although motions do occur throughout the soil mantle, the pace of particle motion is much greater at shallower depths. Here, we are concerned only with particles that move due to surface disturbances. An active layer for these particles is like the definition for a fluvial setting, although there is not a rigid bed that provides a lower limit for surface excursions. We

define an analogous active layer here.

The active layer of thickness L [L] is the layer that is entrainable by surface disturbances – or the range of elevations that the land surface can occupy. During a random walk, a particle is deposited at a position x and elevation ζ [L]. That particle may remain at the surface, become buried, or become re-entrained. Regardless of the series of events, as the surface returns to below the location of a particle from above, the particle becomes entrained and its rest time has ended. To entrain a particle, the surface must move below the particle. When the land surface is at the elevation of a particle, that particle can be at rest on the surface. This condition is similar to that considered in *Voepel et al.,* (2013) wherein they highlight that particle rest-time distributions are tempered power laws for finite bed thicknesses. The finite thickness of an active layer imposes limits on the longest rest times which are a function of L. We begin by showing how the basic model of rest times ought to be similar between fluvial and hillslope settings.

4.2.1 Unaltered Particle Rest Times

We first identify the distribution of particle rest times that emerges for a uniform surface. Imagine a line with N discrete positions. Entrainment events are equally likely to occur at each position over a specified time inteval dt which is similar to entrainment by rain-splash (*Furbish et al.*, 2009b). We define a wait time, w [T] as the time between two successive entrainment events at a given location. For a random entrainment process, the distribution of wait times is

$$f_w = \frac{1}{r_w} e^{-\frac{\tau}{r_w}} , \tag{4.1}$$

where r_w is the mean wait time and $\mathrm{d}t/r_w$ is the probability of entrainment. Wait times are a particle-independent quantity and can be used to calculate the hillslope sediment flux. For a position sufficiently far downslope from the ridge, the sediment flux is related to the wait time distribution by (*Furbish and Haff*, 2010; *Furbish and Roering*, 2013; *Doane et al.*,

2018)

$$q(x) = \frac{V_b}{r_w} \int_0^x R(x-x')\mathrm{d}x' \approx \frac{V_b \mu_\lambda}{r_w}\,, \tag{4.2}$$

for an exponential distribution of particle travel distances, where $x = 0$ is the ridge top location, μ_λ is the mean travel distance, and V_b [L] is the volume entrained per unit area and $R(x-x')$ is the probability that a particle travels at least a distance $r = x - x'$ to contribute to the flux at x. For $x \gg \mu_\lambda$ and uniform $1/r_w$, (4.2) holds.

Rest times, in contrast to wait times, are particle-dependent quantities that require keeping track of individual particles. For particles that only move when they are entrained from the surface, rest times emerge from the time series of land-surface elevation at a point (*Voepel et al.*, 2013). The rest time for a particle is the time that the land surface has spent above the elevation of the particle. Let us again imagine a land surface with a uniform probability of entrainment at any given location. Once entrained, particles are then distributed randomly according to the probability function of travel distance. This results in a random walk of the land surface and suggests then that particle rest time is governed by theory for first-return processes (*Redner*, 2001). Although the random-walk model is appealing, it can lead to unrealistic surfaces. For example, under a true random walk, a possible configuration is for all particles to occupy the same position, x, making a surface that is flat except for an unreasonably tall and narrow bump. We intuitively understand that such a configuration is unrealistic. Previous work addresses this with a stochastic differential equation, the Edwards-Wilkinson equation (*Pelletier et al.*, 1997; *Turcotte*, 2007; *Schumer et al.*, 2017),

$$\frac{\partial \zeta}{\partial t} = D\frac{\partial^2 \zeta}{\partial x^2} + \sigma_w\,, \tag{4.3}$$

where ζ [L] is the land-surface elevation, x [L] is horizontal position, D [$\mathrm{L}^2\ \mathrm{T}^{-1}$] is a diffusivity, and σ_w is a white noise with zero mean. The surface evolution is driven by random shocks from the white noise and is subsequently smoothed by diffusion. The impact of this smoothing term is that the bed elevations typically fall within a given range, λ [L],

for non-aggrading or degrading conditions (*Voepel et al.*, 2013) and large excursions are prevented.

The distribution of return times for a surface evolving by (4.3) to all elevations within λ has no closed form expression although a tempered Pareto approximates the form (*Voepel et al.*, 2013). A tempered Pareto decays as a power-law to a cross-over time, $T_C = L^2/D$ [T], after which the distribution is approximately exponential. If the scope of a study is much longer than T_C, then an exponential distribution captures the long-timescale behavior. Otherwise, analysis requires the tempered Pareto. Here, we adopt an exponential distribution for the rest times within the active layer. We use a numerical model to illustrate and justify this choice.

In the model, particles occupy every location in an annular configuration with uniform depth. Particles at the surface are then entrained with uniform probability and transported counter clock-wise according to a distribution function of travel distance. This allows us to demonstrate the dynamics of many particles on an effectively infinitely long hillslope so that we are not limited by the domain length. The surface evolves as a random walk that is limited by the rigid boundary beneath the particles. We do this for several initial particle depths and calculate particle rest time distributions. The model, although simplified, shows power law decay that shifts to an exponential form after a cross-over period, T_C (Figure 4.1). The mean and cross-over time depend on the thickness of the active layer, L; however, the simulations here all show a shift from a power-law to exponential distribution (Figure 4.1). In order to move forward with a theoretical exploration of particle rest times, we simplify the distribution to an exponential form,

$$f_r(\tau) = \frac{1}{r} e^{-\frac{\tau}{r}}, \tag{4.4}$$

where τ [T] is rest time and r [T] the mean rest time.

The tempered Pareto distribution which we approximate with (4.4) represents the rest

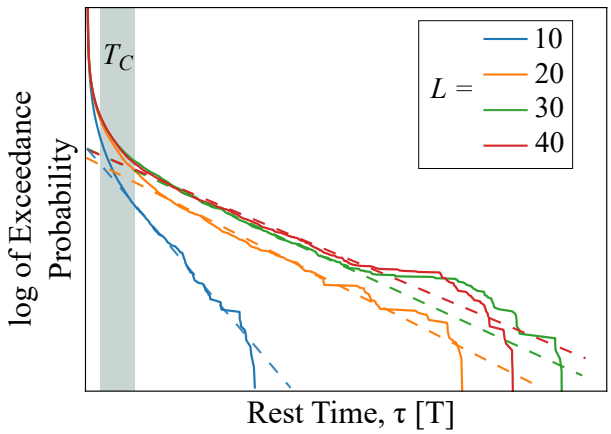

Figure 4.1: Exceedance probability for particle rest times in an annular flume of varying initial active layer thicknesses. Tails of the distributions are exponential. Dashed lines visual references for exponential functions.

times for particles on a surface with uniform probability for entrainment. Now consider this scenario on a sloped surface where most sediment moves downslope. When physical impediments are on the hillslope, sediment gets trapped and a wedge of sediment accumulates behind the dams. Previous work refers to these wedges as capacitors as they tend to fill and then catastrophically fail and release the wedge of sediment (*Lamb et al.*, 2011, 2013; *DiBiase and Lamb*, 2013). Capacitors can be major sources of sediment in steep

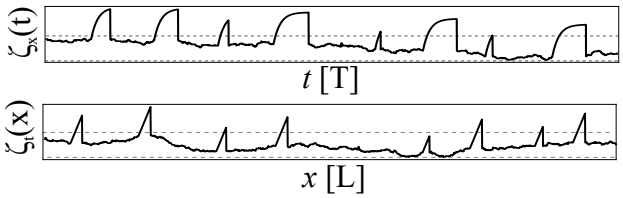

Figure 4.2: Time series of ζ at position x over the growth and failure of several capacitors, and a spatial series at time t over all positions. The dashed lines highlight the range of elevations in the absence of capacitors. The axes are vertically exaggerated.

settings and can have a central role in setting the pace of sediment motion (*Doane et al.*, 2018). We also expect them to have a significant impact on the distributions of rest times. In the absence of capacitors, the expected distribution of rest times is as described above – a tempered Pareto. However, the growth of capacitors is not driven by a white noise and there is some correlation in the time-series of elevation (Figure 4.2). The following

sections demonstrate how the departure from a white noise or Edwards-Wilkinson-type evolution alters the distribution of particle rest times.

We highlight three components of the problem that are central to the altered distribution of particle rest times. First, as the wedge grows, it buries particles that would have otherwise been in the active layer. Therefore, these particles are protected from entrainment during the longevity of the particular capacitor. Second, as capacitors build, more particles become a part of the wedge and are removed from the active layer. These first two components can be combined to illustrate the distribution of rest times within a single capacitor. The composite distribution of all rest times on a hillslope then involves the distribution of capacitor ages and the areal concentration that they occupy. We develop these components below.

4.2.2 Wedge Geometry

The geometry of capacitors has been explored in previous work for steep settings (*Lamb et al.*, 2013; *Doane et al.*, 2018). *Lamb et al.* (2013), focused on the geometry of wedges that form on slopes steeper than a critical slope – which is associated with mixed bedrock-colluvial surfaces. These authors suggest that the wedge of sediment is like a prism. The capacitors we consider are on slopes below a cricital slope, although we follow *Lamb et al.* (2013) and consider a prism-like geometry her. We recognize that this is a simplification and actual wedges likely lack sharp boundaries. So long as a prism captures the essential relationship between basal area of a wedge and volume of a wedge, the particular geometrical form will not significantly influence the distribution of rest times. The geometry of a prism on a hillslope is

$$\begin{aligned} h(x) &= H_0 - Sx \\ w(x) &= \tfrac{H_0 - Sx}{\theta}, \end{aligned} \tag{4.5}$$

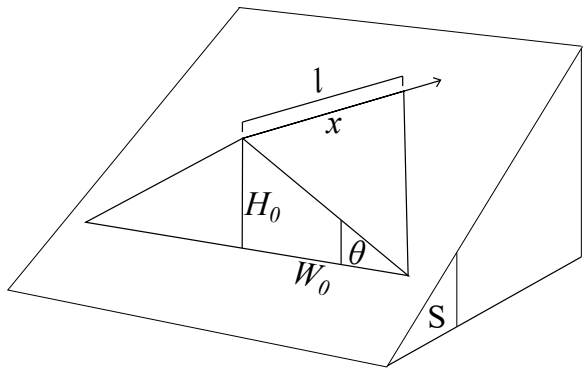

Figure 4.3: Definition diagram showing the geometry of simplified capacitors.

where h [L] is the height, w [L] is the half-width, S is the land-surface slope, θ is the side-slope, and x [L] is position upslope of the dam. The area of a vertical slice through the wedge at any x is $A_v = h(x)w(x)$. The two relevant characteristics of the wedge are the basal area of buried particles and the volume within the wedge. The volume, V [L^3], and basal area, A_B [L^2], for a given H_0 is

$$\begin{aligned} V &= \int_0^l h(x)w(x)\mathrm{d}x = \tfrac{H_0^3}{3\theta S}\,, \\ A_B &= \tfrac{H_0^2}{2\theta S}\,, \\ V &= \tfrac{2}{3}A_B^{3/2}\,. \end{aligned} \tag{4.6}$$

Growth rates of A_B and V are necessarily related to the hillslope sediment flux. We now turn to the distribution of rest times within a single wedge.

4.2.3 Buried Rest Times

As the wedge grows, particles that were recently in the active layer are buried and remain so for the duration of the capacitor. These buried particles are a sample from the underlying unaltered distribution of rest times (4.4). The sample ages to longer rest times as the capacitor ages and continued growth of the wedge buries more particles at rates that coincide with the growth rate. We suggest that the area covered by a single wedge

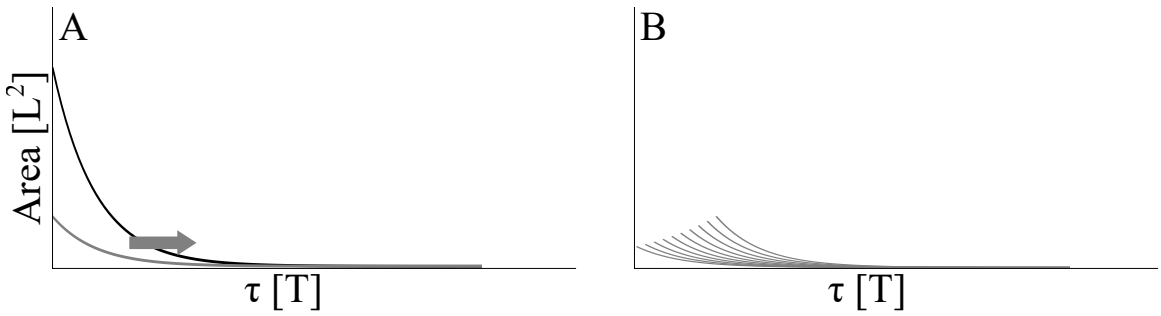

Figure 4.4: A) Figure illustrating the initial distribution of particle rest times and a sample representing the buried portion. (B) The rest times get advected towards longer times and exponentially declining samples are subsequently taken from the underlying distribution.

asymptotically approaches a maximum area, a_0 [L^2],

$$a(t_0) = a_0 \left(1 - e^{-\frac{t_0}{r_a}}\right), \tag{4.7}$$

where a [L^2] is an area and r_a [T] is a rate constant that describes the areal growth rate of the wedge and is, in principle, related to the flux and the land-surface slope. This leads to an exponentially declining growth rate for each wedge area. The distribution of buried rest times involves combining the growth rates with the distribution of sampled rest times in a convolution-like operation

$$f_a(\tau;t_0) = \frac{a_0}{r_a r}\int_0^{\tau} e^{-\frac{t_0-t'}{r}} e^{-\frac{\tau-t'}{r_a}}\,\mathrm{d}t' + \frac{a_0}{r_a r}\int_0^{t_0} e^{-\frac{t_0-t'}{r_a}} e^{-\frac{\tau-t'}{r}}\,\mathrm{d}t', \tag{4.8}$$

where t_0 is the age of the given capacitor. Carrying out the integration in (4.8) leads to an asymmetric double exponential function for the distribution of buried particle rest times. The analytical form is

$$f_a(\tau;t_0) = \frac{a_0}{r+r_a}\left(e^{\frac{\tau-t_0}{r_a}} - e^{-\frac{t_0}{r_a}} e^{-\frac{\tau}{r}}\right)_{[0,t_0]} + \frac{a_0}{r+r_a}\left(e^{\frac{t_0-\tau}{r}} - e^{-\frac{t_0}{r_a}} e^{-\frac{\tau}{r}}\right)_{[t_0,\infty)}, \tag{4.9}$$

which is a distribution with finite mode at t_0 that decays at different exponential rates to the left and right (Figure 4.5).

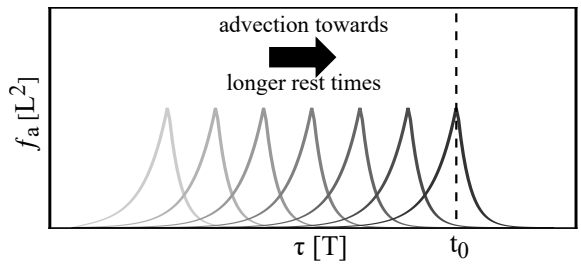

Figure 4.5: Laplace distribution of rest times for buried particles as they remain buried. Colors correspond to time.

We now turn to the particles within the wedge itself. A particle that becomes part of the wedge volume was necessarily just previously entrained and therefore begins with a rest time of zero. Once a particle is a part of a wedge, the rest time increases until the capacitor fails. The distribution of ages within a single wedge reflects the arrival times of particles, which is informed by the time series of volumetric growth rate. The distribution evolves as the advection of rest times

$$\frac{\partial f_V}{\partial t} = -\frac{\partial f_V}{\partial \tau} \tag{4.10}$$

and has boundary conditions at $\tau = 0$ for all times t that reflect the growth of the capacitor

$$V(t) = \frac{2}{3} a(t)^{3/2} \,. \tag{4.11}$$

Placing (4.7) into (4.11) and taking the time derivative yields the boundary condition for (4.10) and the distribution of ages within a single wedge of age t_0 is

$$f_V(\tau; t_0) = \frac{3a_0^{3/2}}{2} \left(1 - e^{-\frac{t_0-\tau}{r_a}}\right)^{1/2} \left(\frac{1}{r_a} e^{-\frac{t_0-\tau}{r_a}}\right) \qquad \tau \leq t_0 \tag{4.12}$$

where t_0 [T] is the age of a given capacitor. The volume function advects at the same rate

as (4.9). The total volume within a wedge is the sum of (4.9) and (4.12)

$$f_{\tau,t_0}(\tau,t_0) = \frac{a_0 L}{r+r_a}\left(e^{\frac{\tau-t_0}{r_a}} - e^{-\frac{t_0}{r_a}}e^{-\frac{\tau}{r}}\right)_{[0,t_0]} + \frac{a_0 L}{r+r_a}\left(e^{\frac{t_0-\tau}{r}} - e^{-\frac{t_0}{r_a}}e^{-\frac{\tau}{r}}\right)_{[t_0,\infty)} + \frac{3a_0^{3/2}}{2}\left(1-e^{-\frac{t_0-\tau}{r_a}}\right)^{1/2}\left(\frac{1}{r_a}e^{-\frac{t_0-\tau}{r_a}}\right)_{[0,t)]}, \tag{4.13}$$

where L [L] is the thickness of the active layer. The distribution of ages within the wedge is definitively skewed left (Figure 4.6). So long as $L < \frac{2}{3}a_0^{1/2}$ there are more particles in the

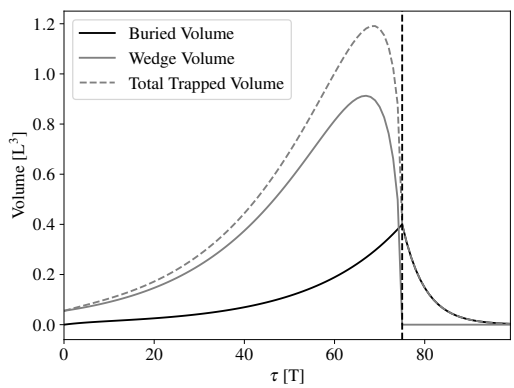

Figure 4.6: Distribution of rest times of all trapped particles for a single wedge. Dashed vertical line is t_0, and with increasing time t_0 continues to grow, leading to advection of trapped rest times.

wedge than those that are buried and the third term of (4.13) dominates f_{τ,t_0}.

We recognize that the exponential growth rates that we have used may not completely capture the time-series of wedge evolution. However, we are confident that growth rates asymptotically approach a steady value. It is possible that the growth rates are better represented by power laws or other functional forms; however, the mathematical steps would remain the same and the overall forms would be similar. We do not intend for the reader to assume that the distributions presented above are the exact form for rest times within a capacitor, but as an illustration of how capacitors add probability towards the tail of rest-time distribution.

4.3 Capacitor ages

We broadly define capacitors as any temporary blockage on a hillslope that builds up a wedge of sediment behind it. In natural systems, this includes shrubs (*Lamb et al.*, 2013; *Doane et al.*, 2018), trees, and boulders (*Glade et al.*, 2017). In disturbed areas, capacitors can be anthropogenic objects including fences, retaining walls, trails, and roads. A potentially interesting avenue for future research might be the behavior of tracer particles in an human-dominated environment. Here, we will focus on a natural system that is composed of a single species and might reflect a desert ecological community.

Imagine a desert shrub community at steady state. Under such a condition, the number of shrubs, N_0, recruited over any interval of time, $\mathrm{d}t$, is exactly balanced by the number of shrubs that die over that same interval. We can define a failure rate, $s(t)$ [T^{-1}] which uniquely determines the form of the distribution of shrub life spans. Three possibilities are common in ecological population dynamics. Type I failure rates increase with time which concentrates mortality, or failure, towards the tail of possible life spans. Type II populations have a uniform failure rate, which leads to an exponential distribution of life spans. Last, type III populations have high failure rate at young ages that slows as the organisms age. This type of population dynamic is relevant for groups like fish that produce far more eggs than survive to adulthood, but once they do, they enjoy a relatively lower mortality rate (*Begon et al.*, 2009). The form of the distribution of life spans, f_l [T^{-1}] is uniquely determined by the failure rate, $s(\tau)$ [T^{-1}], through its relation to the survival function,

$$R(\tau) = e^{-\int_0^\tau s(t)\mathrm{d}t}. \tag{4.14}$$

From the survival function, we can determine the distribution for longevity of a single cohort by the relation $-\frac{dR}{dt_0} = f_l$. If the population is at steady state, then f_l is constant through time.

It is important that we distinguish between the fixed single cohort distribution of longevity,

f_l, and the static distribution of ages, f_{t_0} (*Begon et al.*, 2009). The latter is the probability distribution of ages of a population at any moment, whereas the former is the life spans experienced by a single cohort. The two are related and are identical in the case of a type II failure rate. However, we generalize their form here.

On a given hillslope a number of new shrubs are recruited per time, $N_0(t)$ [T^{-1}], at time $t-\tau$. The number of shrubs that have survived after τ years is $N_0(t-\tau)R_l(\tau)$, and they therefore have age τ (Figure 4.7). Therefore the static distribution of ages is

$$f_{t_0}(\tau;t) = \frac{N_0(t-\tau)R_l(\tau)}{\int_0^\infty N_0(t-\tau)R_l(\tau)\mathrm{d}\tau}\,. \tag{4.15}$$

As written, (4.15) allows for N_0 to vary with time. If recruitment and failure rates are steady through time,

$$f_{t_0}(t_0) = \frac{R_l(t_0)}{\int_0^\infty R_l(t_0)\mathrm{d}t_0}\,. \tag{4.16}$$

By definition, $R_l(\tau)$ converges so the denominator is always a finite value. Furthermore, we note that for uniform recruitment rate, the distribution of capacitor ages must monotonically decline. That is, there can never be a cohort of older shrubs that outnumber a younger cohort. This condition is satisfied by the survival function, which also by definition, must monotonically decline. That f_{t_0} involves only R_l suggests that it shares properties with f_l. In particular, the properties of the tail are shared between age and longevity distributions and the failure rate, $s(t_0)$, determines both.

The distribution of capacitor ages and single-capacitor rest times combine to form a joint probability distribution, $f_{t_0,\tau}(t_0,\tau)$. The distribution of capacitor ages, $f_{t_0}(t_0)$, is one of the marginal distributions and the particle rest time distribution within a single capacitor is the conditional probability, $f_{\tau|t_0}(\tau|t_0)$, from the joint distribution (Figure 4.8). The remaining marginal distribution is the distribution of particle rest times from all capacitors,

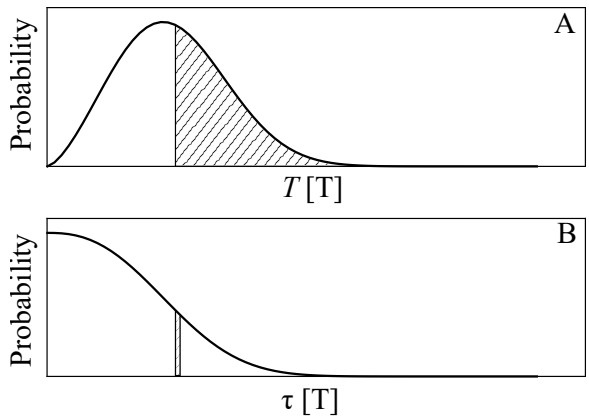

Figure 4.7: A) Distribution of shrub life spans according to a Weibull distribution with a shape parameter $k = 2.5$. B) Distribution of shrub ages at any given moment for a steady-state condition. The distribution of shrub ages must be monotonically decreasing at steady state. Hatched areas illustrate that those shrubs of a cohort of age t_0 that will live longer than t_0 contribute to the distribution of ages that are t_0 to $t_0 + \mathrm{d}T$.

$f_\tau(\tau)$, which remains unknown. By definition,

$$f_{t_0,\tau}(t_0,\tau) = f_{t_0}(t_0) f_{\tau|t_0}(\tau|t_0)\,,$$

and the remaining marginal distribution is

$$f_\tau(\tau)\mathrm{d}\tau = \int_\tau^\infty f_{t_0,\tau}(t_0,\tau)\mathrm{d}t_0\,. \tag{4.17}$$

Placing (4.13) and (4.16) in (4.17) retrieves the composite rest time distribution for particles contained in all capacitors. Moving forward therefore requires knowledge of the distribution of capacitor ages.

Consider for a moment a type II (uniform mortality rate) shrub community that is at steady state. There is a range of survivorship curves for various herbaceous species and the assumption a type II survivorship curve is intended as an illustration here – although certain species do exhibit type II or similar behaviors (*Watkinson*, 1992). According to (4.16), a uniform rate of mortality and steady recruitment rate leads to an exponential distribution of

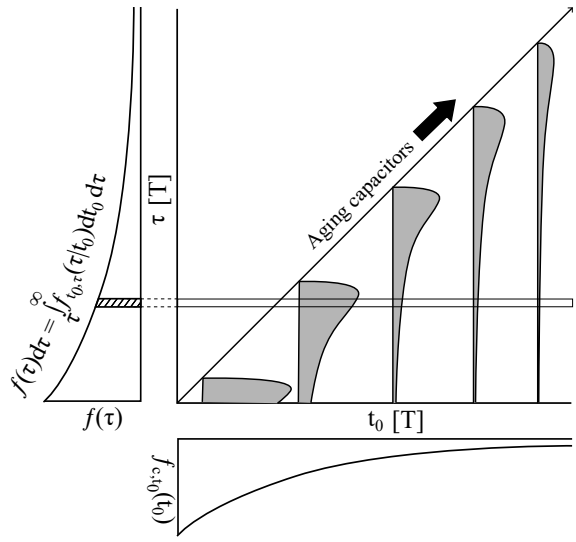

Figure 4.8: Joint and marginal distributions of shrub age and particle rest time. The monotonically decaying marginal distribution of shrub ages, $f_{c,t_0}(t_0)$, results a monotonically decreasing distribution of particle rest times, $f(\tau)$.

capacitor ages,

$$f_c(t_0) = \frac{1}{r_c} e^{-\frac{t_0}{r_c}}, \tag{4.18}$$

where r_c is the mean capacitor age. Placing (4.12) and (4.18) in (4.15) reveals that the distribution of rest times within all capacitors on a hillslope involves a convolution-like operation of f_V and f_c with appropriate limits of integration. To carry out the integration, we expand the first term of (4.12) as a binomial series to three terms which makes the problem tractable. The non-normalized marginal distribution is approximately

$$\begin{aligned} f(\tau) = \frac{a_0 h r_a}{(r_a+r)(r_a+r_c)}\left(e^{-\frac{\tau}{r_c}} - e^{\frac{-\tau}{r}}\right) + \frac{a_0 h r_a}{(r_a+r)(r_c-r)}\left(e^{-\frac{\tau}{r_c}} - e^{-\frac{\tau}{r}}\right) + \\ \frac{3a_0^{3/2} e^{-\frac{\tau}{r_c}}}{2}\left(\frac{1}{r_c+r_a} - \frac{1}{2(2r_c+r_a)} - \frac{1}{8(3r_c+r_a)}\right). \end{aligned} \tag{4.19}$$

For large capacitors, we can neglect the first two terms and normalizing (4.19) returns f_{t_0}. However, this result after normalization only occurs when both the filling rates and the distribution of capacitor ages f_{t_0} are exponential.

When the filling rate and f_{t_0} do not share the same form, the resulting form of f_τ is non-

trivial. To illustrate this, we maintain the filling rate as an exponential-like function (4.12) and investigate the resulting composite distribution when the age distribution is Weibull or Pareto. A Weibull distribution yields

$$f_{t_0}(t_0) = \frac{e^{-\left(\frac{t_0}{r_c}\right)^{k_w}}}{C}, \tag{4.20}$$

where $C = \int_0^\infty R_l(t_0)\mathrm{d}t_0$ is a normalization factor and r_c is a rate-constant. A Weibull is a general distribution that can capture all three survivorship types depending on the value of the shape parameter, k_w. When $0 < k_w < 1$, the distribution reflects a decreasing failure rate. When $k_1 > 1$ the failure rate increases with age, resulting in a thin-tailed distribution. For the special case when $k_w = 1$, the Weibull reduces to an exponential distribution.

A Pareto distribution is a general, two-parameter power-law distribution that gives

$$f_{t_0}(t_0) = \frac{\left(1 + \frac{t_0}{t_c}\right)^{-k_p}}{C}, \tag{4.21}$$

where k_p and t_c [T] are shape and scale parameters respectively. When $k_p < 2$, the variance of the distribution is undefined and the distribution decays slower than an exponential and is said to be 'heavy-tailed' (*Bradley*, 2017). When $k_p < 1$, the mean is undefined. We note that there is a range of definitions for what constitutes a heavy tail. Here we limit the definition to those distributions that have undefined second moments. This definition is consistent with previous work which suggests that such conditions lead to anomalous diffusion.

Combining the non-exponential forms of f_{t_0} and the exponential-like $f_{\tau|t_0}(\tau|t_0)$ yields distributions that are of neither form. Plots of $f_{t_0}(t_0)$ against $f_\tau(\tau)$ reveal differences and where they occur (Figure 4.9). In particular, when a Weibull for f_{t_0} is combined with an exponential-like $f_{\tau|t_0}$, the tail of f_τ remains equal to that of f_{t_0}, but they differ near the origin. When capacitor age is distributed as a Pareto, f_τ differs in both the tail and at the

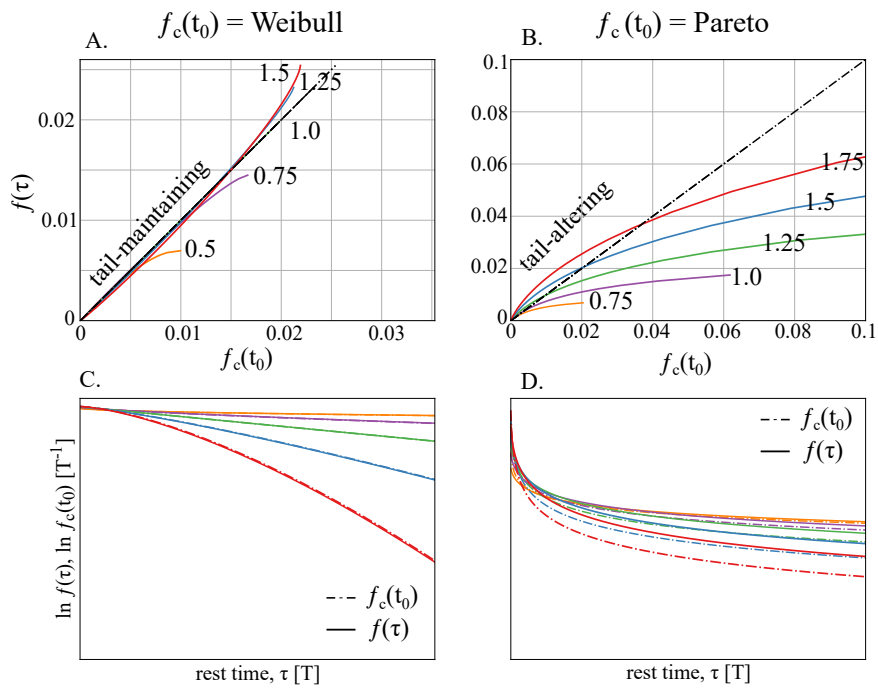

Figure 4.9: Plots of the distribution of capacitor ages, $f_c(t_0)$, against the composite distribution of particle rest times, $f(\tau)$, within all capacitors when t_0 is distributed as a Weibull (A) and Pareto (B). Numbers labeling lines refer to the values for the shape parameter of the distribution. (C) and (D) show $f_c(t_0)$ and $f(\tau)$ on the same plots.

origin. For all values of k_p, the composite distribution is more heavy-tailed; however, the effect is greater for larger values of k_p. To be clear, this only makes the tail heavier than that of f_{t_0}. If the shape parameter is 2 or greater, f_τ will shift probability to the tail, but it will not alter the properties of the tail (i.e. heavy- versus thin-tailed). That is, if f_{t_0} has finite moments, then so too will f_τ.

4.4 Discussion

We have demonstrated the mathematical operations that describe rest time distributions on hillslopes that include the impact of capacitors. Simple assumptions and approximations allow us to use primarily exponential functions to describe land surface and particle behaviors for this problem. This was a conscious choice as exponential functions are convenient to work with and can provide closed form expressions for the convolution-like operations

above. However, they also conveniently provide a set of comparable timescales. We have introduced four: r, the average rest time, r_w, the average wait time, r_a, the characteristic timescale of capacitor growth, and r_c, the mean age of capacitors. Their relationships are worth summarizing:

$$r_w < r, r_a$$

$$0 < r_c < \infty \tag{4.22}$$

$$\tag{4.23}$$

The most basic timescale, r_w, is a component in the volumetric entrainment rate and is therefore involved in calculations of the hillslope sediment flux. Second, r is necessarily greater than r_w when L is greater than one particle diameter. The growth rate of the basal area of the wedge, r_a, must be larger than r_w as it is a function of the flux, but it does not need to be larger than r. The mean age of capacitors can have any value. When the value is less than r, there is no impact on the distribution of particle rest times. With increasing r_c, f_τ becomes increasingly broader with more probability shifted towards the tail. The clear interpretation of the characteristic timescale in the exponential function is not shared for parameters of, say, a Pareto distribution. However, we stress that the same limits and relationships must apply to a mixture of functional forms for each component.

The aggregate distribution of particle rest times involves appropriately weighting the distributions of unaltered rest times and the rest times within capacitors. We imagine that the spatial areal concentration of capacitors and wedges must be far less than one in order to prevent capacitors from interfering with one another and so that the timescales presented above are uniform for each capacitor. Such a condition is similar to the spatial arrangement of desert shrubs such as sage brush observed on a moraine in eastern California (*Doane et al.*, 2018). For illustration we consider a proportion of the hillslope area, $0 \leq A \leq 0.5$, that is occupied by the basal area of all capacitors. As A increases, the aggregate distribution

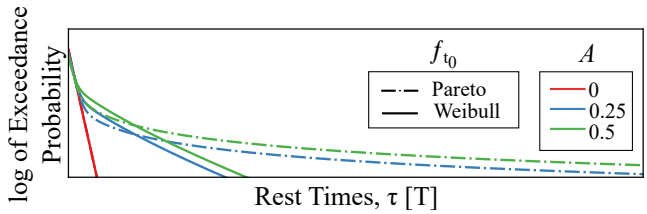

Figure 4.10: Aggregate exceedance probabilities for various densities of shrubs. For increasing concentration of capacitors, the aggregate distribution approaches the distribution of capacitor ages. In this case, $k_w = 0.75$ and $k_p = 1.5$, which are both Type III failure rates that create mildly heavier than exponential tails.

resembles the distribution of capacitors (Figure 4.10). For a heavy-tailed distribution of capacitor ages, f_τ, has an exponential form over short rest times that transitions to a heavy tail at the long rest times. With values of A well below 0.5, if the distribution of capacitor ages is heavy-tailed, so too will be the aggregate distribution of particle rest times across the hillslope. Therefore, a relatively sparsely populated surface with reasonably heavy-tailed ages of capacitors can have a heavy-tailed distribution of rest times.

We purposefully did not address the particle travel distance component of sediment transport to avoid introducing too much heuristic theory. We assume that if particles are entrainable, then once entrained, they move according to a distribution of particle travel distance. However, the style of motion accompanying capacitor failure and, say, motion due to rainsplash are likely to differ. This will pose a problem when capacitor-style release of a granular flow influences the growth rate of a downslope capacitor. If capacitors are spaced sufficiently far apart, the results are qualitatively more applicable.

There is a growing recognition that the distribution of particle travel distances on hillslopes are thin-tailed (*Gabet and Mendoza*, 2012; *DiBiase et al.*, 2017). Insofar as the travel distance distributions have finite statistical moments, then any source of anomalous diffusion would come from rest time distributions (*Weeks and Swinney*, 1998; *Martin et al.*, 2012; *Phillips et al.*, 2013). We have shown that it is possible to obtain heavy-tailed distributions of particle rest time, which depends mostly on the parameters of the capacitor age distribution. A heavy-tailed distribution of particle rest times does not imply either sub-

or superdiffusion, but it does allow for the possibility of anomalous diffusion. The designation of sub-or super diffusion depends on the symmetry or asymmetry (downslope and upslope versus downslope only) of transport. With a heavy-tailed distribution of rest times and weak asymmetry or symmetric transport, spreading behavior is subdiffusive. However, for the same scenario with strong asymmetry, spreading behavior becomes superdiffusive. This distinction is particularly relevant for hillslopes and contrasts with the fluvial setting, for which transport is strongly asymmetric. On hillslopes, transport occurs on all slopes, and on steeper slopes it becomes increasingly asymmetric (*Furbish et al.*, 2009b; *Furbish and Haff*, 2010). Therefore, a given form for the rest time distribution may result in a range of behaviors from sub-diffusive on low slopes to super diffusive on steep slopes. It is also possible for normal diffusion to result despite a heavy-tailed distribution of rest times.

As stated earlier, field testing and observation of natural particle rest times is exceedingly difficult. There are some possible avenues for progress. Optically stimulated luminescence (OSL) could potentially reveal the distribution of particle rest times within a wedge. Very briefly, OSL is an analytical technique that takes advantage of electrons that get trapped in the defects of a crystal. Over time, these traps accumulate more electrons until they are subjected to high enough energy to clear the traps. In many cases, sunlight is high enough energy to accomplish this, so the number of electrons that are trapped is, in principle, related to the burial time of a particle. Particles within a wedge were necessarily at the surface prior to burial, and so the OSL signal should reflect the burial time of that particle. A well-mixed sample from the wedge then would have OSL ages that form a censored distribution of particle rest times. The distribution is censored because the rest times have not been completed (*Fathel et al.*, 2015). However, for very old capacitors, the wedge is expected to be near steady-state so that the form of the distribution could be inferred. This, however, is likely a highly labor-intensive study as it requires OSL ages from many grains and the timescales may be too short for optimal OSL applications.

The spatial concentrations of ^{137}Cs is perhaps the most promising avenue for study-

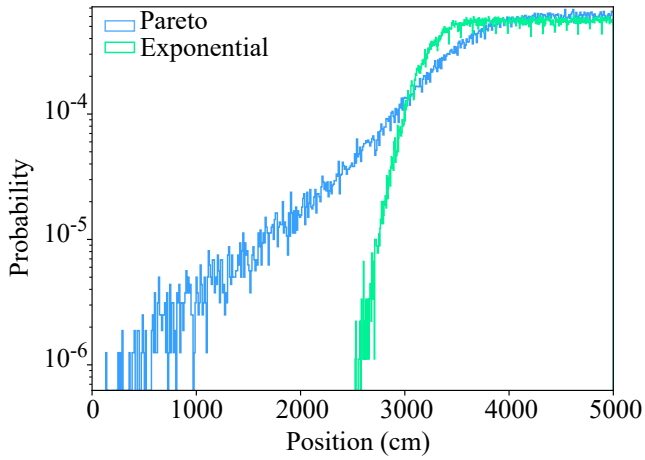

Figure 4.11: Profile of ^{137}Cs particles on a hillslope after some time. The falling limb of the distribution of Cs-containing particles for exponentially-distributed rest times decays parabolically in semi-logarithmic space – indicating a normal distribution. The falling limb for Cs-containing particles with heavy-tailed Pareto-distributed rest times decays slower than a normal and indicates super-diffusion.

ing particle rest times on hillslopes. The spatial pattern of ^{137}Cs reflects transport since the mid-twentieth century when nearly all of the worlds ^{137} was deposited. On an idealized, planar and straight hillslope the concentration of Cs-containing particles will increase downslope to a maximum value. The increasing limb of the concentration profile for Cs is like the falling limb of a break-through curve. For normal diffusion, the falling limb of the breakthrough curve will decay as a normal distribution. For anomalous diffusion, the limb will not decay as a normal distribution. To illustrate this, we numerically simulate the Cs profile for exponentially- and Pareto-distributed rest times that have the same means. A hillslope with exponentially-distributed particle rest times has a falling limb that decays as a normal distribution – indicative of normal diffusion. However, when there is a mild heavy tail in the distribution of rest times as there is for a Pareto with a shape parameter of 1.5, the falling limb decays slower than a normal distribution and indicates anomalous, and in this case, super-diffusion (Figure 4.11). We recognize that this simple numerical model avoids the nuances of Cs dynamics, and measurement may not be straightforward. But the

forms of the profiles are diagnostic and may be worth exploring further.

Two field settings for Cs concentrations have potential. The first scenario is the distribution of Cs-containing particles on the slope of a lateral moraine. In this case, slopes are generally steep so transport is highly assymetric and slopes are relatively uniform so rate constants will also be relatively uniform. Such a setting would be a particularly valuable one for simply identifying normal versus anomalous diffusion on hillslopes. The second interesting setting would be a fluvial terrace where slopes range from 0 to steep and transport goes from symmetric to highly assymetric. Such a setting may demonstrate the transition from sub- to superdiffusion for heavy-tailed rest times as transport goes from symmetric to assymetric (*Weeks and Swinney*, 1998). There are likely other interesting field settings that will highlight a range of behaviors as well.

We have taken an approach that tracks the volumetric growth of wedges associated with temporary blockages on hillslopes. An alternative approach to this problem that may be more general lies solely in the properties of the time series of elevation at a point, $\zeta(t)$ (Figure 4.2). There may be value in exploring the first returns for a time-series that is partially governed by a Edwards-Wilkinson equation (4.3) and partially by periods that have more correlation, which indicate the presence of a capacitor. The properties of a Edwards-Wilkinson-dominated time series is well known (*Voepel et al.*, 2013), and the statistics of the correlated portions would provide the deviation. This approach should produce similar results to what we have already demonstrated, but may be a more general way to study particle rest times.

4.5 Conclusions

We have conducted a preliminary study of the distribution of rest times on hillslopes. On a barren surface, the expected distribution of particle rest times for those particles entrainable by surface disturbances is a tempered Pareto as it is in fluvial settings. When natural hillslope elements are added to a hillslope, they tend to impede particle motion and

therefore lengthen particle rest times. The form of the rest times within a wedge of sediment stored behind a capacitor monotonically increases to the age of the capacitor. This property of rest times behind dams then places a great amount of significance on the distribution of capacitor ages for the aggregate distribution of rest times for an entire hillslope. In particular, we have demonstrated that the form of the distribution of capacitor ages largely determines the tail properties of the aggregate distribution.

Observation of heavy tails in particle transport on hillslopes remains remarkably difficult. However, the spatial distribution certain tracers on hillslopes may be able to suggest heavy- or thin-tailed distributions of rest times. In particular, ^{137}Cs is a potentially promising signal. Because ^{137}Cs was evenly deposited across the landscape as a sustained impulse, the downslope profile of Cs-containing particle concentration is similar to the falling limb of a break-through curve. A falling limb that decays as a normal distribution reflects normal diffusion whereas one that does not implies anomalous diffusion.

Chapter 5

Synthesis

The primary goal of this dissertation was to demonstrate nonlocal transport in a natural setting. In pursuing this goal, the above chapters identify and address several ancillary questions with regard to nonlocal, linear, and nonlinear models. Here, I review the major conclusions from each chapter and comment on future avenues for progress.

The first chapter demonstrated nonlocal transport by numerically simulating the evolution of several lateral moraines over their post-glacial durations. Several important items came out of this chapter. First, we were able to provide the first numerical estimates for relevant nonlocal transport parameters. Second, we show that the parameter that most likely controls the magnitude of the hillslope sediment flux is the volumetric entrainment rate. This conclusion suggests that a promising avenue for future research is in the measurement of the volumetric entrainment rate. Third, for systems that evolve by linear diffusion, the land-surface form only reflects the time-averaged diffusivity and contains no information about the order or history of past values. This is significant as the hillslope diffusivity is commonly linked to climate and some effort has been aimed at linking the hillslope diffusivity with climatic shifts. Last, we suggested that signatures of nonlocal transport might be contained in the wavenumber representation of land-surface evolution.

The second chapter expands on the signatures of nonlocal, linear, and nonlinear transport models. This chapter demonstrates theory that transforms these three models into Fourier wavenumber domain which highlights details of land-surface evolution. Although we had anticipated observing a signature of nonlocal processes in wavenumber domain, the dominant signal reflects the linearity or nonlinearity of the slope terms in the transport model. In particular, we recognize that nonlinear transport is characterized by compression of the land-surface spectrum whereas linear diffusion is represented by vertical decay of

the spectrum. Some combination of linear and nonlinear processes can represent a suite of transport processes, and so we envision that some combination of spectral compression and vertical decay may be another way to represent transport processes. The theory and signatures discussed in this chapter may be relevant for numerical modeling, dating cinder-cones, and for planetary science where nonlinear versus linear transport may point to the presence of fluids.

The third chapter explores the particle-dependent quantity of particle rest time distributions. It is worth noting that such an inquiry is not possible with local models and we require elements such as a volumetric entrainment rate and particle travel distance to even begin to conceptualize the rest times of particles. Rest time distributions are central to the study of tracer particles, which is common in fluvial settings, but had not previously been done for a hillslope setting. This is largely because we cannot observe natural rest times on hillslopes as we can in channels. In particular, this chapter is aimed at exploring the possibility of heavy-tailed rest times as a source for anomalous diffusion of tracer particles. The theory we present suggests that if temporary blockages on hillslopes have heavy-tailed age distributions then so too will the distribution of rest times on hillslopes. The theory for this work relies on several assumptions, the most important of which is our definition of an active layer. Future work might be well guided to demonstrate a relevant active layer on hillslopes. Furthermore, certain meteoric tracers offer particularly appealing methods for testing and observing the effects of particle rest time distributions.

The central theme of this dissertation is nonlocal transport. The term "nonlocal" is somewhat of a misnomer, because, as stated in the introduction, it does not necessarily imply that sediment must travel a very long distance. It simply recognizes that sediment travels a finite distance and therefore involves particle motions that are of all lengths. We see a lot of potential in the application and continued study of nonlocal transport because the mathematical formulation has clear and physically well-defined components that are potentially measurable. We do not think that measurement will be easy, but as our com-

munity becomes increasingly clever with theory and our use of tracers, direct measurement may not be that far off and could offer great value to research.

Appendices

.1 Why the Land surface only records time-averaged conditions for linear diffusion

The Fourier transform of a one-dimensional signal (e.g., land surface) undergoing linear diffusion has the solution

$$Z(k,T_1) = Z(k,0)e^{-k^2 D_0 T_0}\,, \tag{1}$$

where $Z(k,0)$ is the initial transform and D_0 is the diffusivity over the time interval T_0 ending at the start of the next interval T_1. The Fourier transform after successive time intervals with different values of D are

$$Z(k,T_2) = Z(k,T_1)e^{-k^2 D_1 T_1} \tag{2}$$

$$Z(k,T_3) = Z(k,T_2)e^{-k^2 D_2 T_2} \qquad \text{etc.} \tag{3}$$

Using these definitions, we can recursively substitute expressions for $Z(k,T_n)$ to give, for example,

$$\begin{aligned} Z(k,T_3) &= Z(k,0)e^{-k^2 D_0 T_0}e^{-k^2 D_1 T_1}e^{-k^2 D_2 T_2} \\ &= Z(k,0)e^{-k^2(D_0 T_0 + D_1 T_1 + D_2 T_2)}\,. \end{aligned} \tag{4}$$

In general we may choose $\Delta T = T_0 = T_1 = T_2 = \ldots$ so that the total time $T = n\Delta T$ and $D_0 T_0 + D_1 T_1 + D_2 T_2 + \ldots = (D_0 + D_2 + D_3 + \ldots)\Delta T = (D_0 + D_2 + D_3 + \ldots)T/n = \overline{D}T$, where $\overline{D} = (D_0 + D_2 + D_3 + \ldots)/n$ is the time-averaged diffusivity. Then,

$$Z(k,T) = Z(k,0)e^{-k^2 \overline{D} T}\,. \tag{5}$$

Note that because (4) is additive, the order in which the values of D appear is unimportant. In the limit of $\Delta T \to 0$, the formulation represents the outcome of a smooth (rather than discrete) variation in D (e.g., Box and Jenkins, 1976 p.355-362).

.2 Initial Condition

We recognize that the initial conditions for landforms may contain rounded knuckles whereas we have used sharp boundaries. We show here that more rounded initial conditions can not result in the observed bands of spectral growth for the landforms used in this paper. To do so, we imagine smoothing our chosen initial conditions.

A common method of smoothing a function is by implementing a moving average. Such an operation is a convolution of the function with a weighting function – which is commonly a Gaussian function that integrates to unity. The transform of this Gaussian is itself a Gaussian. A convolution in the spatial domain is multiplication in wavenumber domain so a smoothed initial condition would be

$$\hat{\zeta}_i(k) = a\hat{\zeta}(k,0)e^{-l^2k^2}, \tag{6}$$

where l is a characteristic length of the averaging window and a is the amplitude of the transform of the weighting function. The transform of the smoothing window is everywhere less than one, so the only possibility is for spectral amplitudes to be less than an initial condition with sharp corners and thus spectral growth is not attributable to more rounded initial conditions.

.3 Rate of spectral compression as a function of time and k

Here we illustrate that compressing a spectral function, as related to stretching in the spatial domain, can be accomplished by advection with a linearly varying celerity. We illustrate this with an example of spectral compression of a triangle. The transform of a triangle is

$$\hat{\zeta}(k) = HL\left[\frac{\sin(kL/2)}{kL/2}\right]^2, \tag{7}$$

where H is height and L is the half-width. Note that stretching (7) in a mass-conserving way demands that as L lengthens H decreases such that $A = HL$ remains constant. Lengthening is represented by

$$\frac{\partial \hat{\zeta}}{\partial t} = \frac{\partial \hat{\zeta}}{\partial L}\frac{dL}{dt}. \tag{8}$$

The derivative with respect to L,

$$\frac{d\hat{\zeta}}{dL} = 2A\left[\frac{\sin(kL/2)}{kL/2}\right]\left[\frac{\frac{k^2L}{4}\cos(kL/2) - \frac{2L}{4}\sin(kL/2)}{(kL/2)^2}\right], \tag{9}$$

and we specify $\frac{dL}{dt} = m$. According to the advection equation,

$$\frac{\partial \hat{\zeta}}{\partial L}\frac{dL}{dt} = -c(k)\frac{\partial \hat{\zeta}}{\partial k}, \tag{10}$$

where $c(k)$ is a spectral celerity ($\mathrm{L}^{-1}\ \mathrm{T}^{-1}$). The derivative with respect to k

$$\frac{d\hat{\zeta}}{dk} = 2A\left[\frac{\sin(kL/2)}{kL/2}\right]\left[\frac{\frac{kL^2}{4}\cos(kL/2) - \frac{2k}{4}\sin(kL/2)}{(kL/2)^2}\right]. \tag{11}$$

Solving for $c(k)$

$$c(k) = -m\left[\frac{k^2L\cos(kL/2) - 2k\sin(kL/2)}{kL^2\cos(kL/2) - 2L\sin(kL/2)}\right] = -m\frac{k}{L}, \tag{12}$$

which, despite the form, is a linear function of k. We can also relate γ from equations (3.21 - 3.25) to $c(k)$ and discover that $\gamma = \frac{m}{L}$ in this case.

As written, (12) describes the spectral evolution of a triangle that stretches by a constant dL/dt. We heuristically imagine that the rate of stretching scales with slope, H/L. If we specify that $\frac{dL}{dt} = m\frac{H}{L}$, we can solve for $L(t)$,

$$\frac{dL}{dt} = m\frac{H}{L} = m\frac{A}{L^2}. \tag{13}$$

Separating variables and integrating

$$L(t) = (3mAt)^{1/3} + L_0, \tag{14}$$

where L_0 [L] is an initial length. Note that although we suggest the rate of stretching varies linearly with slope, this does not suggest that the flux varies linearly with slope. Indeed the slope-dependency of stretching could be nonlinear where

$$\frac{dL}{dt} = m\left[\frac{H}{L}\right]^{\beta}, \tag{15}$$

which leads to

$$L(t) = [(2\beta+1)mA^{\beta}t]^{\left(\frac{1}{2\beta+1}\right)} + L_0 \tag{16}$$

and is valid for $\beta > 0$. In these cases, $c(k,L)$, such that the advective velocity decreases with time. As $\beta \to 0$, the rate of stretching becomes increasingly insensitive to the slope.

BIBLIOGRAPHY

Almond, P., J. Roering, and T. Hales (2007), Using soil residence time to delineate spatial and temporal patterns of transient landscape response, *Journal of Geophysical Research: Earth Surface*, *112*(F3).

Ancey, C. (2010), Stochastic modeling in sediment dynamics: Exner equation for planar bed incipient bed load transport conditions, *Journal of Geophysical Research: Earth Surface*, *115*(F2).

Ancey, C., A. Davison, T. Böhm, M. Jodeau, and P. Frey (2008), Entrainment and motion of coarse particles in a shallow water stream down a steep slope, *Journal of Fluid Mechanics*, *595*, 83–114.

Anderson, R. S. (2002), Modeling the tor-dotted crests, bedrock edges, and parabolic profiles of high alpine surfaces of the wind river range, wyoming, *Geomorphology*, *46*(1), 35–58.

Anderson, R. S. (2015), Particle trajectories on hillslopes: Implications for particle age and 10be structure, *Journal of Geophysical Research: Earth Surface*, *120*(9), 1626–1644.

Begon, M., M. Mortimer, and D. J. Thompson (2009), *Population ecology: a unified study of animals and plants*, John Wiley & Sons.

Booth, A. M., S. R. LaHusen, A. R. Duvall, and D. R. Montgomery (2017), Holocene history of deep-seated landsliding in the north fork stillaguamish river valley from surface roughness analysis, radiocarbon dating, and numerical landscape evolution modeling, *Journal of Geophysical Research: Earth Surface*, *122*(2), 456–472.

Box, G. E., G. M. Jenkins, G. C. Reinsel, and G. M. Ljung (1976), *Time series analysis: forecasting and control*, John Wiley & Sons.

Bradley, N. D. (2017), Direct observation of heavytailed storage times of bed load tracer particles causing anomalous superdiffusion, *Geophysical Research Letters*, *44*(24), 12,227–12,235, doi:10.1002/2017GL075045.

Brantley, S. L., A. F. White, and M. Hodson (1999), *Growth, dissolution and pattern formation in geosystems*, 291–326 pp., Springer.

Carretier, S., P. Martinod, M. Reich, and Y. Godderis (2016), Modelling sediment clasts transport during landscape evolution, *Earth Surface Dynamics*, *4*(1), 237–251, doi:10.5194/esurf-4-237-2016.

Carslaw, H. S., and J. C. Jaeger (1959), Conduction of heat in solids, *Oxford: Clarendon Press*.

Carson, M. A., and M. J. Kirkby (1972), *Hillslope form and process*, vol. 475, Cambridge University Press Cambridge.

Culling, W. (1963), Soil creep and the development of hillside slopes, *J. Geol*, *71*(2), 127–161.

Culling, W. (1965), Theory of erosion on soil-covered slopes, *The Journal of Geology*, pp. 230–254.

DiBiase, R. A., and M. P. Lamb (2013), Vegetation and wildfire controls on sediment yield in bedrock landscapes, *Geophysical Research Letters*, *40*(6), 1093–1097.

DiBiase, R. A., K. X. Whipple, A. M. Heimsath, and W. B. Ouimet (2010), Landscape form and millennial erosion rates in the san gabriel mountains, ca, *Earth and Planetary Science Letters*, *289*(1), 134–144.

DiBiase, R. A., M. P. Lamb, V. Ganti, and A. M. Booth (2017), Slope, grain size, and roughness controls on dry sediment transport and storage on steep hillslopes, *Journal of Geophysical Research: Earth Surface*, doi:10.1002/2016JF003970.

Doane, T. H., D. J. Furbish, J. J. Roering, R. Schumer, and D. J. Morgan (2018), Nonlocal sediment transport on steep lateral moraines, eastern sierra nevada, california, usa, *Journal of Geophysical Research: Earth Surface*, doi:10.1002/2017JF004325.

Domaradzki, J. A., and R. S. Rogallo (1990), Local energy transfer and nonlocal interactions in homogeneous, isotropic turbulence, *Physics of Fluids A: Fluid Dynamics (1989-1993)*, *2*(3), 413–426.

Dunne, T., D. V. Malmon, and S. M. Mudd (2010), A rain splash transport equation assimilating field and laboratory measurements, *Journal of Geophysical Research: Earth Surface*, *115*(F1).

Einstein, H. (1937), Bedload transport as a probability problem, *Sedimentation (reprinted in 1972). Water Resources Publications, Colorado*, pp. 105–108.

Fathel, S., D. Furbish, and M. Schmeeckle (2016), Parsing anomalous versus normal diffusive behavior of bedload sediment particles, *Earth Surface Processes and Landforms*, *41*(12), 1797–1803.

Fathel, S. L., D. J. Furbish, and M. W. Schmeeckle (2015), Experimental evidence of statistical ensemble behavior in bed load sediment transport, *Journal of Geophysical Research: Earth Surface*, *120*(11), 2298–2317, doi:10.1002/2015JF003552, 2015JF003552.

Ferdowsi, B., C. P. Ortiz, and D. J. Jerolmack (2018), Glassy dynamics of landscape evolution, *Proceedings of the National Academy of Sciences*, *115*(19), 4827–4832, doi: 10.1073/pnas.1715250115.

Fernandes, N. F., and W. E. Dietrich (1997), Hillslope evolution by diffusive processes: The timescale for equilibrium adjustments, *Water Resources Research*, *33*(6), 1307–1318.

Foufoula-Georgiou, E., V. Ganti, and W. Dietrich (2010), A nonlocal theory of sediment transport on hillslopes, *Journal of Geophysical Research: Earth Surface (2003–2012)*, *115*(F2).

Furbish, D. J. (2003), Using the dynamically coupled behavior of land-surface geometry and soil thickness in developing and testing hillslope evolution models, *Prediction in Geomorphology*, pp. 169–181.

Furbish, D. J., and S. Fagherazzi (2001), Stability of creeping soil and implications for hillslope evolution, *Water Resources Research*, *37*(10), 2607–2618.

Furbish, D. J., and P. K. Haff (2010), From divots to swales: Hillslope sediment transport across divers length scales, *Journal of Geophysical Research: Earth Surface (2003–2012)*, *115*(F3).

Furbish, D. J., and J. J. Roering (2013), Sediment disentrainment and the concept of local versus nonlocal transport on hillslopes, *Journal of Geophysical Research: Earth Surface*, doi:10.1002/jgrf.20071.

Furbish, D. J., P. K. Haff, W. E. Dietrich, and A. M. Heimsath (2009a), Statistical description of slope-dependent soil transport and the diffusion-like coefficient, *J.of Geophys. Res.: Earth Surf. (2003–2012)*, *114*(F3).

Furbish, D. J., E. M. Childs, P. K. Haff, and M. W. Schmeeckle (2009b), Rain splash of soil grains as a stochastic advection-dispersion process, with implications for desert plant-soil interactions and land-surface evolution, *Journal of Geophysical Research: Earth Surface (2003–2012)*, *114*(F3).

Furbish, D. J., P. K. Haff, J. C. Roseberry, and M. W. Schmeeckle (2012), A probabilistic description of the bed load sediment flux: 1. theory, *Journal of Geophysical Research: Earth Surface (2003–2012)*, *117*(F3).

Furbish, D. J., S. L. Fathel, M. W. Schmeeckle, D. J. Jerolmack, and R. Schumer (2017), The elements and richness of particle diffusion during sediment transport at small timescales, *Earth Surface Processes and Landforms*, *42*(1), 214–237.

Furbish, D. J., J. J. Roering, A. KeenZebert, P. Almond, T. H. Doane, and R. Schumer (2018), Soil particle transport and mixing near a hillslope crest: 2. cosmogenic nuclide and optically stimulated luminescence tracers, *Journal of Geophysical Research: Earth Surface*, doi:10.1029/2017JF004316.

Gabet, E. J. (2003), Sediment transport by dry ravel, *Journal of Geophysical Research: Solid Earth*, *108*(B1), doi:10.1029/2001JB001686.

Gabet, E. J., and M. K. Mendoza (2012), Particle transport over rough hillslope surfaces by dry ravel: Experiments and simulations with implications for nonlocal sediment flux, *Journal of Geophysical Research: Earth Surface*, *117*(F1), doi:10.1029/2011JF002229.

Gabet, E. J., O. Reichman, and E. W. Seabloom (2003), The effects of bioturbation on soil processes and sediment transport, *Annual Review of Earth and Planetary Sciences*, *31*(1), 249–273.

Gabet, E. J., et al. (2000), Gopher bioturbation: Field evidence for non-linear hillslope diffusion, *Earth Surface Processes and Landforms*, *25*(13), 1419–1428.

Ganti, V., M. M. Meerschaert, E. Foufoula-Georgiou, E. Viparelli, and G. Parker (2010), Normal and anomalous diffusion of gravel tracer particles in rivers, *Journal of Geophysical Research: Earth Surface*, *115*(F2), doi:10.1029/2008JF001222.

Ganti, V., P. Passalacqua, and E. Foufoula-Georgiou (2012), A sub-grid scale closure for nonlinear hillslope sediment transport models, *Journal of Geophysical Research: Earth Surface*, *117*(F2), doi:10.1029/2011JF002181.

Gilad, E., and J. Von Hardenberg (2006), A fast algorithm for convolution integrals with space and time variant kernels, *Journal of Computational Physics*, *216*(1), 326–336.

Glade, R. C., R. S. Anderson, and G. E. Tucker (2017), Block-controlled hillslope form and persistence of topography in rocky landscapes, *Geology*, *45*(4), 311, doi:10.1130/G38665.1.

Gosse, J. C., and F. M. Phillips (2001), Terrestrial in situ cosmogenic nuclides: theory and application, *Quaternary Science Reviews*, *20*(14), 1475–1560.

Granger, D. E., N. A. Lifton, and J. K. Willenbring (2013), A cosmic trip: 25 years of cosmogenic nuclides in geology, *GSA Bulletin*, *125*(9-10), 1379–1402.

Hales, T., K. Scharer, and R. Wooten (2012), Southern appalachian hillslope erosion rates measured by soil and detrital radiocarbon in hollows, *Geomorphology*, *138*(1), 121–129.

Heimsath, A. M., J. Chappell, N. A. Spooner, and D. G. Questiaux (2002), Creeping soil, *Geology*, *30*(2), 111–114.

Hellmer, M. C., B. A. Rios, W. B. Ouimet, and T. R. Sibley (2015), Ice storms, tree throw, and hillslope sediment transport in northern hardwood forests, *Earth Surface Processes and Landforms*, doi:10.1002/esp.3690.

Heyman, J., P. Bohorquez, and C. Ancey (2016), Entrainment, motion and deposition of coarse particles transported by water over a sloping mobile bed, *Journal of Geophysical Research: Earth Surface*, pp. n/a–n/a, doi:10.1002/2015JF003672, 2015JF003672.

Hill, K., L. DellAngelo, and M. M. Meerschaert (2010), Heavy-tailed travel distance in gravel bed transport: An exploratory enquiry, *Journal of Geophysical Research: Earth Surface*, *115*(F2), doi:10.1029/2009JF001276.

Hornberger, G., and P. Wiberg (2013), *Numerical Methods in the Hydrological Sciences*, 1–20 pp., American Geophysical Union, doi:10.1002/9781118709528.ch8.

Hughes, M. W., P. C. Almond, and J. J. Roering (2009), Increased sediment transport via bioturbation at the last glacial-interglacial transition, *Geology*, *37*(10), 919–922.

Hurst, M. D., S. M. Mudd, R. Walcott, M. Attal, and K. Yoo (2012), Using hilltop curvature to derive the spatial distribution of erosion rates, *Journal of Geophysical Research: Earth Surface*, *117*(F2), doi:10.1029/2011JF002057.

Istanbulluoglu, E., and R. L. Bras (2005), Vegetation-modulated landscape evolution: Effects of vegetation on landscape processes, drainage density, and topography, *Journal of Geophysical Research: Earth Surface*, *110*(F2), doi:10.1029/2004JF000249.

Johnson, M. O., S. M. Mudd, B. Pillans, N. A. Spooner, L. Keith Fifield, M. J. Kirkby, and M. Gloor (2014), Quantifying the rate and depth dependence of bioturbation based on optically-stimulated luminescence (osl) dates and meteoric 10be, *Earth Surface Processes and Landforms*, *39*(9), 1188–1196, doi:10.1002/esp.3520.

Jyotsna, R., and P. Haff (1997), Microtopography as an indicator of modern hillslope diffusivity in arid terrain, *Geology*, *25*(8), 695–698.

Kaste, J. M., A. M. Heimsath, and M. Hohmann (2006), Quantifying sediment transport across an undisturbed prairie landscape using cesium-137 and high resolution topography, *Geomorphology*, *76*(3-4), 430–440.

Kaufman, D. S., S. C. Porter, and A. R. Gillespie (2003), Quaternary alpine glaciation in alaska, the pacific northwest, sierra nevada, and hawaii, *Dev. Quat. Sci*, *1*, 77–103.

Kirkby, M., and I. Statham (1975), Surface stone movement and scree formation, *The Journal of Geology*, *83*(3), 349–362.

Lal, D. (1991), Cosmic ray labeling of erosion surfaces: in situ nuclide production rates and erosion models, *Earth and Planetary Science Letters*, *104*(2-4), 424–439.

Lamb, M. P., J. S. Scheingross, W. H. Amidon, E. Swanson, and A. Limaye (2011), A model for fire-induced sediment yield by dry ravel in steep landscapes, *Journal of Geophysical Research: Earth Surface*, *116*(F3), doi:10.1029/2010JF001878.

Lamb, M. P., M. Levina, R. A. DiBiase, and B. M. Fuller (2013), Sediment storage by vegetation in steep bedrock landscapes: Theory, experiments, and implications for postfire sediment yield, *Journal of Geophysical Research: Earth Surface*, *118*(2), 1147–1160.

Love, J. (2000), Geologic map of the teton village quadrangle, teton county, wy, *Wyoming State Geological Survey*.

Madoff, R. D., and J. Putkonen (2016), Climate and hillslope degradation vary in concert; 85ka to present, eastern sierra nevada, ca, usa, *Geomorphology*, *266*, 33–40.

Martin, R. L., D. J. Jerolmack, and R. Schumer (2012), The physical basis for anomalous diffusion in bed load transport, *Journal of Geophysical Research: Earth Surface*, *117*(F1), doi:10.1029/2011JF002075.

McGuire, L. A., J. D. Pelletier, and J. J. Roering (2014), Development of topographic asymmetry: Insights from dated cinder cones in the western united states, *Journal of Geophysical Research: Earth Surface*, *119*(8), 1725–1750.

Mensing, S. A. (2001), Late-glacial and early holocene vegetation and climate change near owens lake, eastern california, *Quaternary Research*, *55*(1), 57–65.

Michaelides, K., and G. J. Martin (2012), Sediment transport by runoff on debris-mantled dryland hillslopes, *Journal of Geophysical Research: Earth Surface*, *117*(F3).

Michaelides, K., I. Ibraim, G. Nord, and M. Esteves (2010), Tracing sediment redistribution across a break in slope using rare earth elements, *Earth Surface Processes and Landforms*, *35*(5), 575–587, doi:10.1002/esp.1956.

Morgan, D., and J. Putkonen (2012), Moraine degradation rates quantified with cosmogenic be-10 from soil profiles in bloody canyon, geological Society of America Annual Meeting.

Mudd, S. M., and D. J. Furbish (2007), Responses of soil-mantled hillslopes to transient channel incision rates, *Journal of Geophysical Research: Earth Surface*, *112*(F3).

Nash, D. B., and J. S. Beaujon (2006), Modeling degradation of terrace scarps in grand teton national park, usa, *Geomorphology*, *75*(3), 400–407.

Nichols, M. (2004), A radio frequency identification system for monitoring coarse sediment particle displacement, *Applied Engineering in Agriculture*, *20*(6), 783.

Nikora, V., J. Heald, D. Goring, and I. McEwan (2001), Diffusion of saltating particles in unidirectional water flow over a rough granular bed, *Journal of Physics A: Mathematical and General*, *34*(50), L743.

Ouimet, W. B., K. X. Whipple, and D. E. Granger (2009), Beyond threshold hillslopes: Channel adjustment to base-level fall in tectonically active mountain ranges, *Geology*, *37*(7), 579–582.

Parker, G., C. Paola, and S. Leclair (2000), Probabilistic exner sediment continuity equation for mixtures with no active layer, *Journal of Hydraulic Engineering*, *126*(11), 818–826.

Pelletier, J. D., B. D. Malamud, T. Blodgett, and D. L. Turcotte (1997), Scale-invariance of soil moisture variability and its implications for the frequency-size distribution of landslides, *Engineering Geology*, *48*(3-4), 255–268.

Pelletier, J. D., M. H. Nichols, and M. A. Nearing (2016), The influence of holocene vegetation changes on topography and erosion rates: a case study at walnut gulch experimental watershed, arizona, *Earth Surface Dynamics*, *4*(2), 471–488, doi:10.5194/esurf-4-471-2016.

Perron, J. T., J. W. Kirchner, and W. E. Dietrich (2008), Spectral signatures of characteristic spatial scales and nonfractal structure in landscapes, *Journal of Geophysical Research: Earth Surface*, *113*(F4), doi:10.1029/2007JF000866.

Perron, J. T., P. W. Richardson, K. L. Ferrier, and M. Lapôtre (2012), The root of branching river networks, *Nature*, *492*(7427), 100–103.

Phillips, C. B., R. L. Martin, and D. J. Jerolmack (2013), Impulse framework for unsteady flows reveals superdiffusive bed load transport, *Geophysical Research Letters*, *40*(7), 1328–1333.

Phillips, F. M., M. G. Zreda, S. S. Smith, D. Elmore, P. W. Kubik, and P. Sharma (1990), Cosmogenic chlorine-36 chronology for glacial deposits at bloody canyon, eastern sierra nevada, *Science*, *248*(4962), 1529–1532.

Phillips, F. M., M. Zreda, M. A. Plummer, D. Elmore, and D. H. Clark (2009), Glacial geology and chronology of bishop creek and vicinity, eastern sierra nevada, california, *Geological Society of America Bulletin*, *121*(7-8), 1013–1033.

Poularikas, A. D. (1998), *Handbook of formulas and tables for signal processing*, vol. 13, CRC Press.

Putkonen, J., J. Connolly, and T. Orloff (2008), Landscape evolution degrades the geologic signature of past glaciations, *Geomorphology*, *97*(1), 208–217.

Putkonen, J., D. J. Morgan, and G. Balco (2012), Regolith transport quantified by braking block, mcmurdo dry valleys, antarctica, *Geomorphology*, *155*, 80–87.

Radice, A., F. Ballio, and V. Nikora (2009), On statistical properties of bed load sediment concentration, *Water resources research*, *45*(6), doi:10.1029/2008WR007192.

Redner, S. (2001), *A guide to first-passage processes*, Cambridge University Press.

Reneau, S. L., and W. E. Dietrich (1991), Erosion rates in the southern oregon coast range: Evidence for an equilibrium between hillslope erosion and sediment yield, *Earth Surface Processes and Landforms*, *16*(4), 307–322.

Ritchie, J. C., M. A. Nearing, M. H. Nichols, and C. A. Ritchie (2005), Patterns of soil erosion and redeposition on lucky hills watershed, walnut gulch experimental watershed, arizona, *Catena*, *61*(2-3), 122–130.

Roering, J. J., J. W. Kirchner, and W. E. Dietrich (1999), Evidence for nonlinear, diffusive sediment transport on hillslopes and implications for landscape morphology, *Water Resources Research*, *35*(3), 853–870.

Roering, J. J., J. W. Kirchner, and W. E. Dietrich (2001a), Hillslope evolution by nonlinear, slope-dependent transport: Steady state morphology and equilibrium adjustment timescales, *Journal of Geophysical Research: Solid Earth (1978–2012)*, *106*(B8), 16,499–16,513.

Roering, J. J., J. W. Kirchner, L. S. Sklar, and W. E. Dietrich (2001b), Hillslope evolution by nonlinear creep and landsliding: An experimental study, *Geology*, *29*(2), 143–146.

Roering, J. J., P. Almond, P. Tonkin, and J. McKean (2004), Constraining climatic controls on hillslope dynamics using a coupled model for the transport of soil and tracers: Application to loess-mantled hillslopes, south island, new zealand, *Journal of Geophysical Research: Earth Surface*, *109*(F1), doi:10.1029/2003JF000034.

Roering, J. J., J. T. Perron, and J. W. Kirchner (2007), Functional relationships between denudation and hillslope form and relief, *Earth and Planetary Science Letters*, *264*(1), 245–258.

Roering, J. J., J. Marshall, A. M. Booth, M. Mort, and Q. Jin (2010), Evidence for biotic controls on topography and soil production, *Earth and Planetary Science Letters*, *298*(1), 183–190.

Rood, D. H., D. W. Burbank, and R. C. Finkel (2011), Chronology of glaciations in the sierra nevada, california, from 10 be surface exposure dating, *Quaternary Science Reviews*, *30*(5), 646–661.

Roseberry, J. C., M. W. Schmeeckle, and D. J. Furbish (2012), A probabilistic description of the bed load sediment flux: 2. particle activity and motions, *Journal of Geophysical Research: Earth Surface*, *117*(F3), doi:10.1029/2012JF002353.

Sayre, W. W., and D. W. Hubbell (1965), *Transport and dispersion of labeled bed material, North Loup River, Nebraska*, US Government Printing Office.

Schaefer, J. M., G. H. Denton, D. J. Barrell, S. Ivy-Ochs, P. W. Kubik, B. G. Andersen, F. M. Phillips, T. V. Lowell, and C. Schlüchter (2006), Near-synchronous interhemispheric termination of the last glacial maximum in mid-latitudes, *Science*, *312*(5779), 1510–1513.

Schumer, R., M. M. Meerschaert, and B. Baeumer (2009), Fractional advection-dispersion equations for modeling transport at the earth surface, *Journal of Geophysical Research: Earth Surface*, *114*(F4).

Schumer, R., A. Taloni, and D. J. Furbish (2017), Theory connecting nonlocal sediment transport, earth surface roughness, and the sadler effect, *Geophysical Research Letters*, *44*(5), 2281–2289.

Shelef, E., and G. E. Hilley (2016), A unified framework for modeling landscape evolution by discrete flows, *Journal of Geophysical Research: Earth Surface*, doi:10.1002/2015JF003693.

Tucker, G. E., and D. N. Bradley (2010), Trouble with diffusion: Reassessing hillslope erosion laws with a particle-based model, *Journal of Geophysical Research*, *115*, F00A10, doi:10.1029/2009JF001264.

Tucker, G. E., and R. L. Bras (1998), Hillslope processes, drainage density, and landscape morphology, *Water Resources Research*, *34*(10), 2751–2764.

Turcotte, D. L. (2007), Self-organized complexity in geomorphology: Observations and models, *Geomorphology*, *91*(3), 302–310.

Voepel, H., R. Schumer, and M. A. Hassan (2013), Sediment residence time distributions: Theory and application from bed elevation measurements, *Journal of Geophysical Research: Earth Surface*, *118*(4), 2557–2567.

Watkinson, A. (1992), Plant senescence, *Trends in ecology & evolution*, *7*(12), 417–420.

Weeks, E. R., and H. L. Swinney (1998), Anomalous diffusion resulting from strongly asymmetric random walks, *Physical Review E*, *57*(5), 4915.